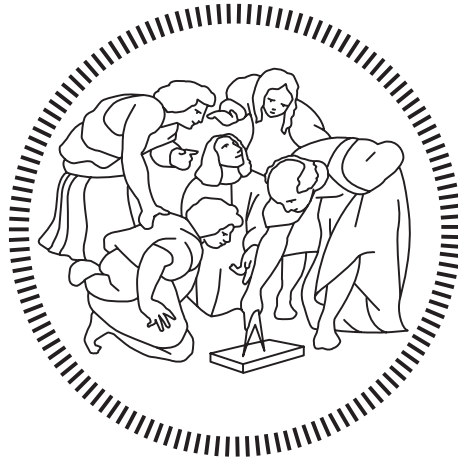


Politecnico di Milano

SCHOOL OF INDUSTRIAL AND INFORMATION ENGINEERING

Master of Science – Electrical Engineering



**Multi-component concentration
measurement from restricted TDLAS
spectral lines and neural network**

Supervisor

Flavia GRASSI

Candidate

Yaru YANG – 10673010

Academic Year 2018 – 2021

Acknowledgements

So far, it means that my master's career has come to a curtain call. Looking back on my three-year master's life, I have mixed feelings and feelings for a while. Before I stop writing, I want to express my gratitude to the teachers, parents, classmates, relatives and friends who have accompanied me through my youth.

First of all, I would like to thank my tutors from Beihang University and the Politecnico di Milano for their help in my studies and life. The teachers are rigorous in academic studies and are the mentors of my life. They are always able to answer my questions with ease and give me new inspirations when I encountered a bottleneck.

Here, I would like to thank Professor Xu Lijun and Professor Cao Zhang from Beihang University for their hard work in advancing the research tasks of the research group. The good research atmosphere and advanced equipment in the laboratory make the students' scientific research tasks smooth. I would also like to thank Professor Flavia Grasii, thanks for her hard work in the dual degree program of Beihang University and Politecnico di Milano. In the face of our kinds of problems, she always answers patiently and solves efficiently. Thanks to every teacher at the Politecnico di Milano for their prechihng, which benefits me a lot.

Learning alone without friends is lonely and ignorant. I would also like to thank all my fellows in the laboratory, for their meticulous and patient answers to each of my questions, and for giving me new inspirations in experimental schemes and data processing. Like grinding, the joy is endless.

Finally, I would like to thank my parents, relatives and friends who have been unconditionally supporting and accompanying me. Thank my parents for their selfless love, encouragement and teaching, and thank my friends for their comfort and comfort every time I complain about depression. Enlightenment and companionship every time I am happy and happy, thank you for giving me the motivation to regain my confidence and the courage to face setbacks time and time again.

At this point, the life of graduate students has come to an end. Again, I would like to express my gratitude to every teacher, classmate, friend, and family member who cares about me. It is you who taught me to be brave to love, to pursue and to persist in my dreams. Thank you for your continuous care and encouragement to accompany me in my continuous progress and growth.

Sommario

La combustione converte direttamente i combustibili in energia efficace e coinvolge varie complicate reazioni fisiche e chimiche. In un processo di combustione di combustibili carboniosi come il metano, le concentrazioni spaziali di metano e vapore acqueo rispettivamente come reagente e prodotto sono essenziali per la verifica del modello di combustione e la regolazione della fiamma. La tecnologia di spettroscopia di assorbimento laser a diodi sintonizzabili (TDLAS) è adatta per il monitoraggio della fiamma per la sua calibrazione gratuita, risposta rapida e alta precisione e rilevamento di parametri multipli. Tuttavia, l'aliasing dello spettro di assorbimento adiacente, la complicata messa a punto del laser e la configurazione sperimentale ne limitano le applicazioni nella misurazione multiparametrica. In questo lavoro, vengono utilizzati modelli di simulazione numerica di fiamme tipiche e una rete neurale per stimare le concentrazioni multicomponenti dai dati spettrali di diverse righe di assorbimento e i contenuti principali sono organizzati come segue.

In primo luogo, vengono introdotti principi e metodi, nonché lo stato dell'arte delle tecniche TDLAS. Le sfide della tradizionale misurazione in tempo reale per più componenti vengono analizzate in aspetti di complessità sistematica e computazionale.

In secondo luogo, la fluidodinamica computazionale viene applicata con un meccanismo di reazione semplificato, per simulare fiamme di combustione premiscelate di metano e aria in casi di rapporti di equivalenza diversi. Due linee spettrali vicino a 7185 cm^{-1} e 7444 cm^{-1} vengono selezionate per generare i dati del profilo spettrale di assorbimento delle molecole di vaporizzatore d'acqua. Una rete neurale di propagazione dell'errore viene utilizzata per l'addestramento e la previsione delle concentrazioni multicomponente da queste due linee spettrali. L'algoritmo proposto prevedeva la concentrazione di metano lungo un singolo percorso laser dagli spettri di assorbimento del vapore acqueo e l'errore relativo è compreso tra lo 0,5% rispetto alla concentrazione misurata dai dati spettrali effettivi.

Infine, il metodo di previsione multicomponente proposto viene applicato alle fiamme del bruciatore McKenna. I laser centrati alle lunghezze d'onda di 1391,8 nm e 1343,4 nm vengono utilizzati per misurare gli spettri di assorbimento del vapore acqueo e calcolare la temperatura media lungo il percorso del laser. Viene selezionato un laser centrato a 1684 nm per determinare la concentrazione media di metano. Questi tre laser sono stati scansionati in una rapida cascata per misurare simultaneamente gli spettri di assorbimento del vapore acqueo e del metano. La temperatura media e le concentrazioni di vapore acqueo e metano nella fiamma sono misurate a diverse altezze assiali e altezze radiali dal metodo tradizionale di assorbimento diretto. La fattibilità del metodo proposto è preliminarmente verificata dai risultati sperimentali.

Abstract

Combustion directly converts fuels into effective energy and involves various complicated physical and chemical reactions. In a combustion process of carbonaceous fuels such as methane, spatial concentrations of methane and water vapor are essential indicators to combustion model verification and flame tuning. Tunable diode laser absorption spectroscopy technology (TDLAS) is suitable for flame monitoring for its free calibration, fast response, high accuracy and multiple parameter detection. However, the aliasing of adjacent absorption spectrum, complicated laser tuning and experimental setup limit its applications in multi-parameter measurement. In this work, numerical simulation models of typical flames and a neural network are used to estimate multi-component concentrations from the spectral data of several absorption lines main contents are organized as follows.

Firstly, principles and methods as well as the state-of-art of TDLAS techniques are introduced. The challenges of the traditional real-time measurement for multiple components are analyzed in aspects of systematical and computational complexities.

Secondly, computational fluid dynamics is applied with a simplified reaction mechanism, to simulate premixed combustion flames of methane and air in cases of different equivalence ratios. Two spectral lines near 7185 cm^{-1} and 7444 cm^{-1} are selected to generate the absorption spectral profile data of water vapor molecules. An error back propagation neural network is used for training and prediction of the multi-component concentrations from these two spectral lines. The proposed algorithm predicts the concentration of methane along a single laser path from the absorption spectra of water vapor, and the relative error is within 0.5% compared with concentration measured from the actual spectral data.

Finally, the proposed multi-component prediction method is applied in flames of the McKenna burner. Lasers centered at the wavelengths of 1391.8 nm and 1343.4 nm are used to measure the absorption spectra of water vapor and calculate the average temperature along the laser path. A laser centered at 1684nm is selected to determine the average concentration of methane. These three lasers were scanned in a fast cascade way to simultaneously measure the absorption spectra of water vapor and methane. The average temperature and concentrations of water vapor and methane in the flame are measured at different axial heights and radial heights from the traditional direct absorption method. The feasibility of the proposed method is preliminarily verified by the experimental results.

Extended Abstract

The TDLAS measurement method is widely used in combustion parameter measurement because of its fast response, high measurement accuracy, and no damage to the flow field. This work is based on the TDLAS measurement principle and the multi-angle sensor device to design a method for measuring the concentration of multiple components with fewer spectral lines by combining with the computational fluid dynamics combustion numerical simulation method and the artificial neural network method. The difference between this method and the traditional measurement method is that it uses the computational fluid dynamics (CFD) software to perform numerical simulation of typical premixed combustion, and obtains the distribution of combustion parameters when the equivalent ratio is between 1.6 and 2.5 of the flame of methane and air. Combining the average combustion parameter measurement of a single ray source and the geometric model of the parameter distribution measurement of the multi-angle sensor respectively, the characteristic absorption of water vapor in the combustion field at the selected band is forward calculated. Through the neural network algorithm, the numerical relationship between the absorption spectrum of the water vapor in the combustion field and the concentrations of the remaining components produced by the combustion is also constructed. By mining the hidden information of the limited spectrum data, the utilization value of the measured spectrum data is improved, and the problems of low content of certain components in the combustion field, weak absorption, and difficult measurement of the spectrum data are made up for.

In order to verify the feasibility of the algorithm proposed in this thesis, it is planned to measure and calculate the average concentration of the unburned methane and water vapor on the optical path in the combustion field under the oxygen-lean combustion conditions. In the experiment, the methane flow rates of the Mckenna burner are sequentially set to 2.23 L/min, 2.4 L/min, and 2.56 L/min. The air flow rate is always 10.6L/min to ensure that the corresponding equivalent ratios are 2, 2.15, and 2.3. For the combustion conditions under these three working conditions, two DFB lasers with center wavenumbers of 7185 cm^{-1} and 7444 cm^{-1} were used as the light source to obtain the absorption spectrum of water vapor in the combustion zone on a single laser path and the average temperature on the path can be calculated. At the same time, one DFB laser with a center wavenumber of 5938 cm^{-1} is used to measure the average concentration of methane molecules on the same path under the same working conditions.

This work is divided into the following chapters:

Chapter One: briefly introduces the research background and significance of the concentration measurement of various gas components in the combustion field, especially the difficulty and research significance of the measurement of pollutants such as methane,

nitrogen oxides and trace components of OH radicals. Then this chapter introduces the application, advantages, disadvantages and development status of TDLAS technology in multi-parameter measurement of combustion field. At the end of the first chapter, the research methods and content of this work are proposed.

Chapter Two: briefly describes the basic principles, specific parameters and measurement methods of TDLAS spectral measurement technology. Firstly, the Beer-Lambert law, basic principle of laser absorption spectroscopy for flow field parameter measurement is introduced. Then some specific parameters such as linear intensity $S(T)$, linear function \varnothing are introduced. At the same time, two typical measurement methods in TDLAS are briefly analyzed. The advantages and disadvantages and applicable conditions of the direct absorption method and the wavelength modulation method are compared at the end of the chapter two.

Chapter Three: in chapter three, the algorithm simulation work of multi-component concentration measurement is carried. Firstly, the CFD software and GRI 3.0 methane/air reaction mechanism are used to simulate the combustion parameters of Mckenna burners under various working conditions, and obtain the two-dimensional distribution of temperature, pressure, and concentrations of components in the combustion field, which are also the numerical basis for subsequent simulations and the sample of neural network training. Secondly, based on the simulation results, the combustion measurement environment and the parameter distribution of combustion parameters are analyzed. According to the principle of spectrum line selection, the suitable measurement spectra of CH_4 and H_2O in the combustion environment of the temperature range is from 1000 K to 2000 K, the pressure range is from 0.5 atm to 1 atm, and the equivalent ratio of 2 to 2.3 are selected from the HITRAN database. On the basis that the spectral line has been determined, combined with the single-line parameter measurement and the geometric model of the multi-angle sensor, the forward simulation of the water vapor absorption absorbance on the measured waveband is used as the input samples of the neural network, and the corresponding concentration of methane obtained by the CFD simulation is used as the output samples. Through the self-learning and training of the neural network model, the simulation of the measurement algorithm with fewer spectral lines to multiple parameters is carried out.

Chapter Four: the measurement experiment of the measurement of the absorption spectrum of water vapor, the average temperature and the average concentration of methane and water vapor in the flame are carried out. Firstly, the temperature driven control system of the laser and the data acquisition module selected in the experiment are introduced in detail. Then the data collecting and processing process are briefly analyzed. The single optical path TDLAS measurement system is used to measure the absorption spectrum of water vapor, the average temperature and concentrations of methane and water vapor on the axial and radial optical paths of the flame under various working conditions. At last, the calculation results based on the neural network algorithm and the experimental measurement results were compared and analyzed to verify the feasibility of the algorithm proposed in this thesis.

Chapter Five: in this chapter, the research contents and results are introduced, introducing the research ideas, unique innovations, existing shortcomings and prospects of this work.

Table of Contents

Acknowledgements	II
Sommario	III
Abstract	V
Extended Abstract	VII
List of Figures	XIII
List of Tables	XVI
Chapter 1 Introduction	1
1.1 Research background and significance.....	1
1.2 Main methods of multi-parameter measurement of combustion field	2
1.3 Research status and main problems of tunable laser absorption spectroscopy technology at home and abroad	4
1.3.1 TDLAS development history and research status at home and abroad.....	4
1.3.2. Application and development of TDLAS in multi-parameter measurement of combustion field.....	7
Chapter 2 Basic Principles of Tunable Laser Absorption Spectroscopy Technology 11	
2.1 Basic principles and important parameters of TDLAS technology.....	11
2.1.1 Beer-Lambert absorption law	11
2.1.2 Absorption line intensity	12
2.1.3 The linear function of absorption spectrum.....	13
2.2 Typical measurement methods of TDLAS technology	17
2.2.1 Direct absorption technology.....	17
2.2.2 Wavelength modulation technology	18
2.3 Summary of this chapter.....	19
Chapter 3 Multi-component Concentration Measurement Method Based on Neural Network 21	
3.1 Forward simulation of the absorption spectrum of water vapor based on CFD numerical simulation.....	21

3.1.1	Combustion numerical simulation based on CFD.....	22
3.1.2	The selection and analysis of the measurement spectrum line of methane and water vapor.....	27
3.1.3	Forward simulation of the absorption spectra of water vapor.....	32
3.2	Multi-component concentration prediction method based on neural network.....	35
3.2.1	Multi-component concentration prediction method based on neural network	36
3.2.2	Comparison and analysis of simulation results and original data of multi-component prediction methods.....	39
3.3	Summary of this chapter	51
Chapter 4 Multi-component Concentration Measurement Experiment and Algorithm Feasibility Verification.....		52
4.1	Measurement experiment of the average temperature and the average concentration of multiple components on a single laser path in the combustion field	52
4.1.1	Temperature and multiple component concentration measurement experimental system.....	52
4.1.2	Measurement of water vapor absorption spectrum and calculation of average temperature and analysis of measurement results.....	55
4.2	Measurement experiment and result analysis of the average concentration of methane on a single laser path in the combustion field.....	63
4.2.1	Measurement experiment of average methane concentration	63
4.2.2	Comparative analysis of the prediction results of the average methane concentration algorithm and the experimental measurement results.....	64
4.3	Measurement experiment and result analysis of two-dimensional temperature distribution in combustion field.....	65
4.4	Summary of this chapter	67
Chapter 5 Summary And Outlook.....		69
Acronyms		73
Appendix		74
Bibliography		83

List of Figures

Figure 2.1 the schematic diagram of the Beer-Lambert Law	12
Figure 2.2 Figure 2.2.3 Schematic diagram of the direct absorption method system	17
Figure 3.1 Main line mechanism of CH ₄ combustion reaction	23
Figure 3.2 Sectional view of Mckenna burner	24
Figure 3.5 Intensity of methane absorption line in the wavenumber range of 5930cm ⁻¹ to 5940cm ⁻¹	29
Figure 3.6 The absorption spectrum of water vapor, carbon dioxide and methane in the range from 5930cm ⁻¹ to 5940cm ⁻¹ (a) The absorption spectrum in the range from 5930cm ⁻¹ to 5940cm ⁻¹ (b) The absorption spectrum of methane in the range from 5937cm ⁻¹ to 5939cm ⁻¹	30
Figure 3.7The absorption spectrum of water vapor in two spectral bands (a) Absorption spectra of water vapor from 7180cm ⁻¹ to 7190cm ⁻¹ (b) Absorption spectra of water vapor from 7440cm ⁻¹ to 7450cm ⁻¹	30
Figure 3.8 Temperature measurement sensitivity and line-strength ratio in the spectral range of 7185cm ⁻¹ and 7444cm ⁻¹ (a) Temperature measurement sensitivity in the spectral range of 7185cm ⁻¹ to 7444cm ⁻¹ (b) Line intensity ratio in the spectral range from 7185cm ⁻¹ to 7444cm ⁻¹	32
Figure 3.9Simulation results of single optical path absorption spectrum (a) Absorption spectrum from 7180cm ⁻¹ to 7190cm ⁻¹ (b) Absorption spectrum from 7440cm ⁻¹ to 7450cm ⁻¹	33
Figure 3.10Optical path layout model for multi-angle absorption spectrum simulation.....	34
Figure 3.11Simulation results of integrated absorbance on 120 paths when the burner is at the center of the sensor	34
Figure3.12 Simulation results of the integrated absorption area on the 120 path when the burner is not strictly located at the center of the sensor	35
Figure3.13 Schematic diagram of three-layer neural network	36
Figure3.14 Algorithm flowchart	38
Figure3.15 Algorithmic calculation results of methane concentration in a single optical path with different axial heights.....	40
Figure3.16 Algorithmic simulation results of methane concentration in a single optical path with different radial distances	41
Figure3.17 Temperature simulation results of a single optical path at different radial positions of the flame when the measuring height is 2cm	42
Figure3.18 Temperature simulation results of a single optical path at different radial positions of the flame when the measuring height is 5cm	43
Figure3.19 Algorithmic calculation results of methane concentration distribution at the root of the flame (a) Methane concentration distribution given by CFD (b) Algorithm reconstruction result when no noise is added (c) Algorithm reconstruction results when the signal-to-noise ratio is 40dB (d) Algorithm reconstruction results when the signal-to-noise ratio is 20dB	44

Figure3.20	Algorithmic calculation results of methane concentration distribution at the top of the flame (a) Methane concentration distribution given by CFD (b) Algorithm reconstruction result when no noise is added (c) Algorithm reconstruction results when the signal-to-noise ratio is 40dB (d) Algorithm reconstruction results when the signal-to-noise ratio is 20dB	45
Figure3.21	Reconstruction error under different signal-to-noise ratio conditions	46
Figure3.22	Simulation results of methane concentration when the burner is at any position of the sensor(a) Distribution of methane concentration given by CFD (b) Algorithm reconstruction results when there is no noise(c) Distribution of methane concentration given by CFD (d) Algorithm reconstruction results when there is no noise	47
Figure3.23	The simulation results of the flame root temperature distribution algorithm(a) Temperature distribution given by CFD (b) Algorithm reconstruction result when no noise is added(c) Algorithm reconstruction results when the signal-to-noise ratio is 20dB (d) Algorithm reconstruction results when the signal-to-noise ratio is 40dB.....	47
Figure3.24	Simulation results of the temperature distribution algorithm at the top of the flame(a) Temperature distribution given by CFD (b) Algorithm reconstruction result when no noise is added(c) Algorithm reconstruction results when the signal-to-noise ratio is 20dB (d) Algorithm reconstruction results when the signal-to-noise ratio is 20dB.....	48
Figure3.25	Relative error of temperature reconstruction under different signal-to-noise ratio conditions	49
Figure3.26	Temperature simulation results when the burner is at any position of the sensor(a) Temperature distribution given by CFD (b) Algorithm reconstruction result when no noise is added(c) Temperature distribution given by CFD (d) Algorithm reconstruction result when no noise is added	50
Figure3.27	Reconstruction error of different signal-to-noise ratio.....	50
Figure4.1	Single optical path experimental system diagram.....	53
Figure4.2	Laser control module and data acquisition module.....	54
Figure4.3	Mass flow controller	55
Figure4.4	Experimental system diagram of single optical path	56
Figure4.5	Transmitted light intensity signal.....	57
Figure4.6	Light intensity signal and etalon signal in one scanning period(a) Transmitted light intensity signal (b) Etalon signal	58
Figure4.7	Sectional truncation of the light intensity signal.....	58
Figure4.8	The transmitted light intensity and baseline of the spectral band with the central wavenumber of 7185cm ⁻¹ and 7444 cm ⁻¹ (a) The transmitted light intensity and baseline of the spectral band with the central wavenumber of 7185cm ⁻¹ (b) The transmitted light intensity and baseline of the spectral band with the central wavenumber of 7444cm ⁻¹	59
Figure4.9	Absorption spectrum fitting of water vapor on the spectral band with the central wavenumber of 7185cm ⁻¹ and 7444cm ⁻¹ (a) Absorption spectrum fitting of water vapor on the spectral band with the central wavenumber of 7185cm ⁻¹ (b) Absorption spectrum fitting of water vapor on the spectral band with the central wavenumber of 7444cm ⁻¹	59
Figure4.11	Average concentration of water vapor under different working conditions	62

Figure4.12 Methane transmitted light intensity signal and linear fitting Baseline fitting on the spectral band with a central wavenumber of 5938cm^{-1} (b) Fitting the absorption spectrum on the spectral band with a central wavenumber of 5938cm^{-1} 63

Figure4.14 Algorithm reconstruction and experimental measurement results of two-dimensional distribution of temperature (a) Experimental measurement results of temperature distribution when the equivalence ratio is 0.98 (b) Algorithmic calculation results of temperature distribution when equivalence ratio is 0.98 (c) Experimental measurement results of temperature distribution when the equivalence ratio is 0.7 (d) Algorithmic calculation results of temperature distribution when equivalence ratio is 0.7..... 67

List of Tables

Table 3.1 Combustion simulation with different equivalent ratio flow settings	24
Table 3.2 Distribution diagram of temperature, water vapor volume fraction, and methane volume fraction under different working conditions.....	25
Table 3.3 Distribution diagram of temperature, water vapor volume fraction, and methane volume fraction under different working conditions.....	27
Table 3.4 Spectral parameters of methane from 5937cm-1to 5940cm ⁻¹	27
Table 3.5 Specific absorption information of water vapor absorption spectra on two spectral bands	31
Table 4.1 Average temperature measurement result of single optical path.....	60
Table 4.2 Measurement results of the average concentration of methane on a single optical path..	64

Chapter 1

Introduction

1.1 Research background and significance

For a very long time, due to the needs of industrial production activities, mankind has carried out large-scale development and utilization of fossil energy, which has destroyed the earth's carbon cycle and caused a series of environmental problems such as global warming. With the rapid development of society and economy, the demand for energy in industrial production and people's lives has increased sharply. Since 2010, although fossil fuels account for a decreasing proportion of total energy production year by year, they still occupy the core position of energy production and still are important energy sources to ensure the normal development of society [1]. The efficient use of energy and the control of pollutant emissions have become problems of the whole society and the whole mankind that need to be solved urgently. Therefore, exploring low-pollution and low-emission combustion technologies is an important development direction in combustion field 4. It plays a key role in controlling the combustion process, optimizing combustion efficiency and reducing pollutant emissions to use various methods to carry out combustion diagnosis and combustion parameter measurement. It is also an important aspect to improve the energy efficiency of industrial production and promote the development of low pollution emissions [3].

In the process of measuring combustion parameters, the parameters of temperature and concentrations of gas components are particularly important. They are not only important indicators reflecting the combustion process, but also critical means to study combustion theory and simplify combustion mechanism. In the combustion field of industrial production or experiment, there are not only the fuel and air components that participate in the combustion process, such as oxygen, nitrogen, etc., but also new products that appear in the combustion process, such as carbon oxide, water vapor, nitrogen oxide, hydrogen, intermediate product groups, sulfide and solid soot particles, etc. The detection of carbon oxides, methane, sulfides, nitrogen oxides and other pollutants in the flue gas of the combustion system can not only reflect the working efficiency of the combustion boiler energy saving and emission reduction system, but also guide the adjustment of the relevant parameters of the energy saving and emission reduction system to meet the requirements of the flue gas emission standard [4]. Meanwhile, it also contributes to control the progress of the combustion reaction and optimize the design of the combustion chamber. In many

industrial productions such as metallurgy and steelmaking, a large amount of coke oven gas and other fuels are used. Since carbon monoxide, methane, and hydrogen are the main gas components, the measurement of the distributions of gas components such as methane and carbon oxide during the fuel combustion process directly reflects the combustion process and efficiency. At the same time, the detection and measurement of carbon oxide, methane and oxygen in the industrial production is also the key to ensuring safe and efficient production [5].

In actual industrial production, it is necessary to detect a variety of parameters in the combustion products to accurately capture changes in the combustion process, and to determine the level of combustion efficiency and pollutant emissions indicators. Multi-parameter measurement means that the complexity of the detection system or the difficulty of the parameter calculation process sharply increases. At present, the commonly used combustion parameter measurement methods face the difficulty of complex experimental measurement systems and the difficulty in obtaining independent absorption spectra of each parameter in the process of multi-parameter measurement [6]. Therefore, the study of multi-parameter measurement methods based on limited measurement data has important research significance and application value for combustion process detection and the development of combustion theory.

Lorem ipsum dolor sit amet, consectetur adipiscing elit, sed eiusmod tempor incididunt ut labore et dolore magna aliqua. Ut enim ad minim veniam, quis nostrum exercitationem ullam corporis suscipit laboriosam, nisi ut aliquid ex ea commodi consequatur. Quis aute iure reprehenderit in voluptate velit esse cillum dolore eu fugiat nulla pariatur. Excepteur sint obcaecat cupiditat non proident, sunt in culpa qui officia deserunt mollit anim id est laborum.

Lorem ipsum dolor sit amet, consectetur adipiscing elit, sed eiusmod tempor incididunt ut labore et dolore magna aliqua. Ut enim ad minim veniam, quis nostrum exercitationem ullam corporis suscipit laboriosam, nisi ut aliquid ex ea commodi consequatur. Quis aute iure reprehenderit in voluptate velit esse cillum dolore eu fugiat nulla pariatur. Excepteur sint obcaecat cupiditat non proident, sunt in culpa qui officia deserunt mollit anim id est laborum.

Lorem ipsum dolor sit amet, consectetur adipiscing elit, sed eiusmod tempor incididunt ut labore et dolore magna aliqua. Ut enim ad minim veniam, quis nostrum exercitationem ullam corporis suscipit laboriosam, nisi ut aliquid ex ea commodi consequatur. Quis aute iure reprehenderit in voluptate velit esse cillum dolore eu fugiat nulla pariatur. Excepteur sint obcaecat cupiditat non proident, sunt in culpa qui officia deserunt mollit anim id est laborum.

1.2 Main methods of multi-parameter measurement of combustion field

There are two main methods for measuring combustion field parameters: contact and non-contact measurement methods. The contact temperature and gas components analysis and measurement methods mainly include the gas sampling analysis method and the

thermocouple temperature measurement method. The contact temperature measurement method requires the probe of the temperature measurement sensor to be directly placed in the combustion field, which will cause certain interference to the flow field. In addition, in harsh working environments of high temperature and high pressure, the contact temperature measurement method is unable to meet the working requirements of stable measurement [7]. However, non-contact temperature and gas component analysis and measurement methods mainly include various optical and acoustic measurement methods, such as spectroscopy temperature measurement method, acoustics, interferometry and so on. The equipment used for measurement of these methods can be completely isolated from the area to be measured, stable and real-time measurement can be achieved in high temperature and pressure working environment. In the actual measurement of combustion parameters process, the measurement results of the thermocouple and the laser absorption spectroscopy technology are relative compared, which can accurately measure the parameter information of the temperature and gas components concentration of the combustion field [8].

The principle of thermocouple temperature measurement is to use a closed circuit composed of two different conductors to directly penetrate into the temperature field to be measured. When there is a temperature difference between the two ends, a current is generated in the closed circuit, and thermoelectromotive force appears at both ends of the circuit and then temperature value can be calculated based on the measured potential difference. The thermocouple has simple structure, convenient operation, low price and can realize a wide range of temperature measurement. However, when measuring temperature, the metal couple wire needs to be exposed to the field to be measured, in which not only destroys the flow field, but also the high temperature measurement environment affects the mechanical strength of the metal couple. The thermocouple temperature measurement method cannot meet the long-term temperature measurement needs [9].

Tunable laser absorption spectroscopy (TDLAS) technology mainly uses the characteristics of the narrow linewidth and the characteristics of wavelength changing with injection current tunable semiconductor lasers to realize the measurement of single absorption line or several lines that are very close and difficult to distinguish of molecular to be measured [10]. TDLAS technology is based on the Beer-Lambert absorption law to obtain the parameters of the combustion field. Laser absorption spectroscopy technology is based on the Beer-Lambert absorption law. When measuring combustion field parameters, a single narrow-band laser frequency is used to scan an independent gas absorption line to calculate the laser incident light intensity and the transmitted light intensity after passing through the area to be measured. Therefore, the pressure, temperature and concentration of the absorbing component on the laser path can be solved. Laser absorption spectroscopy technology to measure combustion parameters puts forward higher requirements on the output linewidth of lasers. Currently, the commonly used Distributed Feedback (DFB) semiconductor laser has a linewidth of about 10MHz, which is small compared to the half-width of the gas absorption line. It is precisely because of the narrow linewidth characteristics that this laser is often used for combustion parameter measurement [11].

TDLAS technology has the advantages of high sensitivity and no need to interfere with the measured flow field, and can realize real-time and dynamic measurement. Combined with the long optical path gas absorption cell, the lower limit of TDLAS technology can reach the order of ppm or even ppb. When measuring the combustion parameters using TDLAS, the measuring device does not need to be in contact with the gas to be measured, and the measurement can be completed without destroying the flow field, which has high environmental adaptability [12]. Combustion products such as H₂O, CH₄, NO, CO and CO₂ have abundant absorption peaks in the near mid-infrared spectral band. Due to the narrow bandwidth of DFB lasers, usually one laser can only meet the needs of single component concentration measurement. In the process of measuring the concentration of multiple components, the measurement system is often complicated and the absorption spectrum lines of the several gas components overlap each other. At the same time, TDLAS technology also faces the limitation of low spatial distribution rate, single optical path measurement can only obtain the average temperature and gas concentration on the path. Combining TDLAS technology with tomographic imaging algorithms, we can reconstruct the two-dimensionally distributed parameters of the combustion field to be measured, and make up for the shortcomings of the low spatial resolution of single optical TDLAS technology, which will better reflect the spatial distribution information of the parameters to be measured [13].

Due to its unique advantages and potentially important application value in many fields, TDLAS technology is one of the most popular research fields in recent years, and it has gradually become a key technology in the field of combustion parameter measurement [14].

1.3 Research status and main problems of tunable laser absorption spectroscopy technology at home and abroad

1.3.1 TDLAS development history and research status at home and abroad

Most of the molecules of the substance have obvious characteristics of the rotation spectrum in the infrared spectrum, so they have abundant characteristic absorption lines. Beginning in the 1970s, the RK Hanson research group of Stanford University began to study the TDLAS technology, in 1977 the laser was first applied to the combustion flow field diagnosis, and successfully realized the measurement of the absorption spectra of carbon monoxide in the McKenna combustion field, which opened the door to the development of TDLAS technology applied to combustion parameter measurement [15]. The early development of TDLAS technology was mainly limited by the development of lasers. The wide-bandwidth light sources could not accurately scan the characteristic absorption lines of gas components, which brought large errors to the measurement results. With the advent of narrow bandwidth, high power, and high monochromatic laser light sources, the measurement accuracy of TDLAS technology has been greatly improved. Especially after the 1990s, due to the advantages of small size, simple structure, low price, long life, and the ability to cover the

absorption spectrum of a variety of gases in the infrared band, semiconductor lasers were quickly introduced into the combustion diagnosis process by a large number of scholars.

In 1993, the researchers of RK Hanson's team used a DFB laser with a center wavelength near 1385nm and the current modulation was used to control the laser to repeatedly scan a range of wavenumbers at a frequency of 80Hz to measure the characteristic absorption lines of water vapor. They use direct absorption spectra technology to calculate the temperature and the concentration of water vapor on the laser path. At the same time, the collision widening coefficient of water was calculated firstly [16]. In 1996, DS Baer of Stanford University used two Distributed feedback (DFB) lasers to scan the two absorption lines of water vapor near 1392 nm and 1343 nm. Which successfully measured the concentration of water vapor and the average temperature in the combustion flame hydrogen and oxygen combustion. Comparing the temperature results obtained by the thermocouple with the results obtained by the fixed wavelength calculation method, verifying the feasibility of the TDLAS technology temperature measurement system and method [17]. Subsequently, the RM Mihalcea research team selected the methane/air premixed flame of a flat flame combustion furnace as the measurement object and used three DFB lasers to scan the spectral range of 6345 cm^{-1} to 6660 cm^{-1} . In the end, they measured the absorption spectrum and calculated the concentrations of CO, CO₂ and CH₄ that were generated during the combustion process. By comparing with the pure chemical calculation results, the temperature and concentrations results are in good agreement with the results of TDLAS [18]. In 2003, X. Zhou's research team used a current-driven DFB laser to scan and measured the two absorption lines of water vapor near 1.4 μm . And measured the temperature and concentration of water vapor of the laser path. Compared with the measurement method of wavelength division multiplexing, this method of using one laser to achieve multiple absorption spectrum scanning effectively simplifies the system complexity [19].

In some small-sized burners, the concentration of some combustion products such as H₂O, CO, NO and other components is low, and the transmitted light intensity signal obtained for measurement is too weak to calculate when the direct absorption method is used. Which brings large errors to the calculations of temperature and the concentration of gas components. In order to improve the signal-to-noise ratio in the measurement process, the wavelength modulation technology is proposed based on the main noise characteristics of the TDLAS technology. The wavelength modulation technology is mainly to superimpose a high frequency sine wave on a low frequency triangle wave, thereby controlling the output wavelength and power of the laser by modulating the input current of the laser. Sub-harmonic signals are detected and analyzed [20].

In 2000, the research group of Hanson proposed to use the wavelength modulation method to detect weakly absorbed trace signals, and successfully used it in the measurement of the rapid chemical combustion reaction in the shock tube [21,22], which lay a foundation for the rapid development of wavelength modulation TDLAS technology. In 2004, JTC Liu of the Hanson's research team used the wavelength modulation method to detect the absorption lines of water vapor at 1343 nm and 1392 nm. In this research the low-frequency triangular

wave carrier frequency was 1 kHz, and the high-frequency sine wave modulation frequency was 170 kHz. The temperature and the concentration of water vapor in the combustion flow field were measured and [23] promoted the wide application of wavelength modulation technology in the combustion field.

The research on TDLAS technology in China started relatively late, and the current research is mostly at the stage of laboratory measurement and simple industrial environment application. It is worth mentioning that in recent years, the Xu Lijun research team of Beihang University has used a miniaturized multi-angle sensor system to obtain absorption spectrum information from multiple angles and multiple paths. Determining the temperature and temperature in the asymmetric flame flow field by combing with tomographic imaging algorithms [24].

The Cai Weiwei research team of Shanghai Jiaotong University has conducted a lot of research in the fields of combustion diagnosis and tomography parameter measurement [25,26]. In 2018, they combined deep learning algorithms with tomography technology and introduced them into laser absorption spectroscopy measurement technology to reconstruct the spatial distribution of temperature and H₂O concentration in the area to be measured using limited-angle laser absorption spectroscopy information, which opened up a new path for the further development of TDLAS [27]. In 2017, Zhang Lifang of Zhejiang University used laser absorption spectroscopy to measure the gas components produced in the process of biomass decomposition. During the measurement process, the three gas groups CO, CO₂, and CH₄ were measured at the same time by multiplexing. It also explored the temporal and spatial changes of the above three gas components in the process of eucalyptus cortex decomposition [28]. Wang Fei of Zhejiang University developed a fan-shaped laser beam measurement system to reconstruct the two-dimensional distribution of H₂O in the flame field by using tunable laser absorption spectroscopy technology [29]. In this research the two absorption lines of water vapor around 1937.87nm were scanned. The soot volume fraction, the concentration of water vapor and the temperature were measured simultaneously in an ethylene/air premixed flame environment [30]. Liu Wenqing and Kan Ruifeng of the Anhui Institute of Optics and Fine Mechanics of the Chinese Academy of Sciences have been engaged in the research of TDLAS technology for a long time. Based on the time-sharing scanning technology, they have studied the dual-wavelength temperature and concentration detection technology. In the experimental measurement, the centrally symmetrical flame of the methane and air premixed flat flame furnace is used as the research object. The online temperature calculation results are compared with the thermocouple measurement results to verify the feasibility of the temperature measurement algorithm. They have been engaged in the research of tunable laser absorption spectroscopy for many years, and have achieved many results in combustion diagnosis and high-sensitivity and rapid monitoring of trace gases [31].

In recent years, with the continuous development and improvement of TDLAS technology and the continuous improvement of the laser spectrum database, more and more absorption spectra of different molecules are measured and used. The detection of temperature and

temperature parameters has gradually become an important requirement in the field of combustion diagnosis. And the tunable laser absorption spectroscopy technology is more widely used to determine the concentration of multiple components in the combustion field.

1.3.2. Application and development of TDLAS in multi-parameter measurement of combustion field

A substance produces an absorption spectrum of the substance for electromagnetic radiation of a specific frequency, and different substances have different absorption in the same frequency range. As early as 1802, Wollaston firstly observed the solar spectrum and found that the colored solar spectrum was split by some black lines. Later, it was discovered that this was the absorption of certain elements of the solar spectrum when sunlight passed through the atmosphere, which was called the phenomenon of "divided rainbow". Semiconductor laser absorption spectroscopy technology was first proposed in the 1970s, and has since been widely used in environmental detection, industrial process analysis, atmospheric research, medical diagnosis, aerospace and other fields. Different from the traditional infrared absorption spectroscopy technology, the semiconductor laser light source has the characteristic of narrow bandwidth, the monochromatic light source emitted by the semiconductor is much smaller than the half-width of the gas absorption spectrum, which can accurately capture the "fingerprint" produced by molecules in a specific wavelength band. When using laser absorption spectroscopy for combustion process detection and parameters measurement, the process of combustion involves a variety of complex chemical and physical changes, multiple mixed components are interdependent in this complex process. In actual measurement requirements it is sometime necessary to distinguish or measure multiple components of complex gas mixtures. Covering the multi-component that to be measured or multiple absorption spectra of a component at the same time during the measurement process becomes very necessary [32]. The current tunable laser in the infrared band has a limited tuning range, generally on the order of 200 cm^{-1} , and the current tunable width is 1 cm^{-1} to 2 cm^{-1} . In the actual spectrum measurement, the temperature tuning laser is used to make the center wavelength emitted. The component to be measured absorbs the laser near the center of the spectrum, and the current-tuned laser is used to scan the component absorption band to ensure that at least one absorption line of the component to be measured is covered. Only when the distance between the two absorption spectra of the component is within the range of 1 cm^{-1} , multiple spectra can be detected only by using one single laser. In the actual measurement of multiple gas components, it is generally necessary to select a special laser for each component to be measured. To achieve rapid simultaneous measurement of multiple components, it is convenient to use multiplexing technology to control the work order of different lasers. At present, the multiple technologies commonly used for simultaneous measurement of multiple components mainly include time division multiplexing technology and wavelength division multiplexing technology [33].

Time-division multiplexing (TDM) technology uses time as a signal division parameter to control a series of lasers to emit light at different times to obtain absorption spectra of multiple components to be measured. The R.Kormann's research team used time division multiplexing technology to control four laser beams to pass through the same optical path at different times to successfully measure four atmospheric components [34]. The system structure of time division multiplexing technology is very simple, and there is no limit to the number of multi-channel lasers. What's more, in experimental measurement, usually only one detector is needed and the same signal processing method can be used to solve the light intensity signal of different band [35].

Frequency Division Multiplexing (FDM) technology is to directly combine and control multiple lasers to work in different measurement signal frequency bands. The combined laser signal passes through the area to be measured along the same optical path, and the transmitted light intensity signal passes through an optical spectroscopic element and then detected by different detectors at different positions of the transmitted light intensity of multiple bands. In this way, the simultaneous measurement of the concentration of multiple components will be realized. JTC Liu et al. performed frequency modulation by superimposing sinusoidal signals of different frequencies on multiple lasers. After the two lasers passed through the area to be measured, they were received by the detector. By demodulating the light intensity signal at different frequencies, the signals on different bands were obtained. Light intensity signal to obtain the concentration of multiple components [36]. Xu Lijun of Beihang University used frequency division multiplexing technology and combined the main peak scanning method to introduce into the WMS method. And at the same scanning speed, it achieves a high frame rate six times that of the traditional TDLAS sensor. For the first time, two wavelengths modulated at different frequencies were used to extract absorption in parallel along different laser paths, and it was successfully implemented on TDLAS tomography hardware to reconstruct the distribution of temperature and substance concentration at a frame rate of up to 10kHz [37]. Although the wavelength division multiplexing technology solves the problem of slow detection speed in the time division multiplexing process, the diffractive beam splitting element introduced by it may bring about the etalon effect and affect the accuracy of the measurement results.

Neither time division multiplexing technology or frequency division multiplexing technology can solve the problem of overlapping absorption spectra of the components to be measured in the measurement of multi-component concentration, and it is impossible to solve an independent single absorption spectrum from the aliased absorption spectrum. In the infrared spectrum range, some components to be tested do not have independent absorption lines with high absorption intensity. When these components are interfered by other components, their individual absorption spectra cannot be measured, which causes the spectrum measurement signal of the component to be measured to be interfered by the impurity component. It is difficult to directly calculate the concentration distribution of the component interference. Although the development of TDLAS technology is becoming more and more perfect, its concentration measurement sensitivity can reach the ppm level,

and it has been widely used in the field of trace gas detection [38]. However, in some harsh environments such as high pressure, high temperature, and high turbulence, the measurement sensitivity of TDLAS technology is limited, and the ability to capture weak absorption signals of trace gases cannot meet the sensitivity requirements of gas measurement [39]. In order to detect multi-component gases at the same time or near the same time, Zhang Zhirong and other researchers used three measurement methods to detect the mixture of H₂S at 578nm, HCl and N₂ at 1747nm in real time. They used time-sharing-sawtooth method (10kHz high frequency sine wave modulation, 30Hz low frequency sawtooth wave), optical switching method (10kHz sine wave of the same frequency, 30Hz sawtooth wave) and multi-frequency modulation (10kHz and 20kHz sine wave) to measure the concentration of those three gas components. The results show that the time-sharing scanning method has little influence on the measurement results except for changes in the light intensity range. The optical switch method will be a little unstable during the switching process, but it has little effect on the subsequent measurement results. When using frequency division multiplexing TDLAS to measure the concentration of multiple components, the signal-to-noise ratio (SNR) and anti-interference ability are improved, and the signal-to-noise ratio is increased by 0.95 and 3.17 respectively [40,41]. Based on the demand for multi-component measurement, in this work, neural network tools are introduced, and the combustion numerical simulation method is used to prepare training sets for self-learning of neural networks, so as to realize the prediction of multi-component concentration using limited absorption spectrum data. When using combustion simulation software to provide the training set of the neural network, it can cover the distribution information of the components that are difficult to capture in the experimental measurement process such as trace gas and toxic gas by simulating the combustion under various working conditions in which relatively hard to measure in a laboratory measuring environment.

Chapter 2

Basic Principles of Tunable Laser Absorption Spectroscopy Technology

Tunable semiconductor laser absorption spectroscopy technology has the advantages of non-invasive measurement, fast response speed, high sensitivity, and simultaneous measurement of multiple parameters. It is widely used in fields such as combustion diagnosis and quantitative detection of gas concentrations. TDLAS technology is mainly based on the Beer-Lambert absorption law. When a beam of laser irradiates the gas to be measured, a photodetector is used to detect the spectral signal containing parameter distribution information such as gas concentration, temperature, and pressure. The line type of the absorption spectrum is obtained by non-linear fitting, and by comparison and analysis with standard spectrum data, the temporal and spatial distribution of the gas temperature and concentration of the field to be measured can be reversed [42]. Among them, the broadening of molecular absorption lines can be divided into natural broadening, doppler broadening and collision broadening according to the broadening mechanism. Correspondingly, the broadened line types can be divided into Gauss line type, Lorentz line type and Voigt linear type according to their different proportions. Each line type has different characteristics and applications. When using laser absorption spectroscopy to measure temperature and concentration in the field to be measured, there are two typical measurement methods: direct absorption using low-frequency sawtooth scanning, and high-frequency sine wave modulation and wavelength modulation.

2.1 Basic principles and important parameters of TDLAS technology

2.1.1 Beer-Lambert absorption law

The application of laser absorption spectroscopy to measuring the parameters to is mainly based on the Beer-Lambert absorption law. Figure 2.1 shows a schematic diagram of the principle of laser absorption spectroscopy. When a laser beam with a center frequency of ν passes through the gas field to be measured, the measured molecules in the medium will

absorb photons of specific frequencies and undergo energy level transitions. Different molecules need to absorb photons of different frequencies during energy level transitions. As a result, different absorption spectra are produced, showing the characteristics of "fingerprint" absorption.

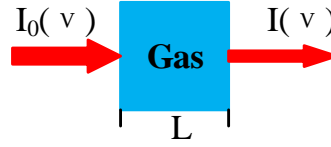


Figure 2.1-the schematic diagram of the Beer-Lambert Law

According to the absorption law, when a laser beam with a frequency of ν (cm^{-1}) passes through a gas medium with a length of L , the absorbance $\alpha(\nu)$ can be used to characterize the relationship between the incident laser light intensity and the transmitted laser light intensity can be expressed as:

$$\alpha(\nu) = -\ln\left(\frac{I_t(\nu)}{I_0(\nu)}\right) = P \int_0^L X_{abs}(x) \times S(T) \times \phi \times dx \quad (0.1)$$

where I_0 and I_t are the intensity of the incident and transmitted laser light, respectively. P [atm] is the total pressure, $T(x)$ [K] is the temperature at position x on the laser path, and $X_{abs}(x)$ is the gas concentration at x , ϕ [cm] is the linear function of the absorption spectrum, $S(T(x))$ [$\text{cm}^{-2}\text{atm}^{-1}$] is the line intensity and characterizes the strength of gas absorption, which will be described in detail in section 2.1.2. If the combustion parameter to be measured is uniformly distributed on the laser absorption path, the absorbance $\alpha(\nu)$ of the gas to be measured in the laser with frequency ν can be expressed as:

$$\alpha(\nu) = -\ln(\tau(\nu)) = PX_{abs}lS(T)\phi(\nu) \quad (0.2)$$

The linear function $\phi(\nu)$ satisfies the normalization condition on the frequency. The integral of the absorbance $\alpha(\nu)$ to the frequency ν , that is, the integrated absorption area A of the absorption rate $\alpha(\nu)$, can be expressed as:

$$A = \int_{-\infty}^{\infty} \alpha(\nu) d\nu = PX_{abs}lS(T) \quad (0.3)$$

2.1.2 Absorption line intensity

The line strength $S(T(x))$ [$\text{cm}^{-2}\text{atm}^{-1}$] indicates the absorption capacity of the selected absorption spectrum for a certain intensity of laser signal, and represents the absorption and radiation strength of gas molecules during energy level transitions. The line intensity at temperature T can be expressed as:

$$S(T) = S(T_0) \frac{Q(T_0)}{Q(T)} \exp\left[-\frac{hcE''}{k} \left(\frac{1}{T} - \frac{1}{T_0}\right)\right] * \left[\frac{1 - \exp\left(\frac{hc\nu_0}{kT}\right)}{1 - \exp\left(\frac{hc\nu_0}{kT_0}\right)} \right] \quad (0.4)$$

Where k [J/K] is Boltzmann's constant, $S(T_0)$ is the line intensity at the reference temperature (usually T_0 is room temperature, 296K). $Q(T)$ and $Q(T_0)$ are partition functions under the temperature T and the reference temperature T_0 respectively. The corresponding value can be obtained by querying the HITRAN database. h [J·s] is the Planck constant, c [cm/s] is the propagation speed of light in vacuum, ν_0 [cm⁻¹] is the center frequency of the absorption line and E'' [cm⁻¹] is the low-level energy of the absorption transition.

According to the above formula, the line intensity $S(T)$ of the spectral line is only related to temperature for the absorption spectrum of a specific gas. Among them, the partition function $Q(T)$ reflects the ratio of the number of particles at the corresponding low energy level to the total number of particles at the temperature T [K]. The approximate value of the partition function $Q(T)$ can be obtained by polynomial fitting:

$$Q(T) = a + bT + cT^2 + dT^3 \quad (0.5)$$

The coefficients a , b , c and d have different values in different temperature ranges. The selection of specific fitting parameters can be queried through the HITRAN spectrum database.

2.1.3 The linear function of absorption spectrum

In an ideal state, the transition of the energy level reflects the change of the total energy inside the molecule, and the transition of each molecular energy level corresponds to a specific frequency. In actual situations, the lifetime of the molecule at the upper energy level is limited. Many factors such as Puller broadening, collision broadening and natural broadening have a great impact on molecular transitions. The actually measured spectral lines are usually absorption curves with specific linear functions ϕ and specific frequency widths. The linear function ϕ is used to characterize the shape of the absorption spectrum of the molecule at a specific frequency. It is a symmetrical curve centered at the center frequency ν_0 , which reflects the relative change of the spectral absorption rate with frequency. The normalization conditions are met on the domain so the following formula can be written as:

$$\int_{-\infty}^{\infty} \phi(\nu) d\nu = 1 \quad (0.6)$$

The linear functions of the absorption spectrum can be divided into three categories according to the degree of influence of different broadening mechanisms. They are Gauss linear functions, Lorentz linear functions and Voigt linear functions. The following is a detailed introduction of various linear functions and their broadening mechanisms.

(1) Gauss linear function

The random thermal motion of the absorbing molecule causes the Doppler broadening of the absorption spectrum. In the natural state, the velocity distribution of the random thermal motion of the molecule obeys the Maxwell-Boltzmann law. In the thermal equilibrium state

of temperature T , the absorption is used to characterize the thermal motion speed of molecules:

$$v = \left(\frac{2kT \ln 2}{m} \right)^{\frac{1}{2}} \quad (0.7)$$

Due to the influence of the Doppler frequency shift, the half-maximum width of the absorption spectrum can be obtained from the average velocity of the molecular thermal motion, which can be expressed as:

$$\Delta v_D = 2 \times \frac{v_0}{c} \left(\frac{2kT \ln 2}{m} \right)^{\frac{1}{2}} \quad (0.8)$$

Among them, Δv_D is the Doppler half-maximum width, v_0 is the center frequency of the absorption line, c is the speed of light, k is the Boltzmann constant, and m is the molecular mass of the absorbing molecule. The linear function affected by the Doppler widening mechanism has the characteristics of Gauss distribution, and its linear function can be expressed as:

$$\phi_D(v) = \frac{2}{\Delta v_D} \left(\frac{\ln 2}{\pi} \right)^{\frac{1}{2}} \exp \left(-4 \ln 2 \left(\frac{v - v_0}{\Delta v_D} \right)^2 \right) \quad (0.9)$$

At the center frequency of v_0 , the Gaussian line shape of the gas absorption spectrum has the maximum value, which can be expressed as:

$$\phi_D(v) = \frac{2}{\Delta v_D} \left(\frac{\ln 2}{\pi} \right)^{\frac{1}{2}} \quad (0.10)$$

It can be seen from the above formula that the linear function with Gauss distribution is only affected by the ambient temperature parameter. The higher the temperature, the larger the half-width of the absorption line and the smaller the peak value. Therefore, if the ambient temperature is the main influencing factor of the measurement environment, and the environmental pressure has a relatively small effect on the spectral absorption measurement results, it is suitable to choose the Gauss line type to fit and characterize the absorption spectrum.

(2) Lorentz linear function

The uniform broadening of the absorption spectrum is caused by the collective average lifetime of the particles in the excited state. This contains two influencing factors: natural broadening and collision broadening. Among them, the natural broadening is caused by the uncertainty of the energy level of the absorption spectrum. The half-height width of the spectral line affected by the natural broadening mechanism is much less than tens of MHz, and the contribution to the overall spectral line broadening is small and can be ignored. Collision broadening is caused by the collision of photons and absorbing molecules. The more photons in the surrounding medium collide with molecules, the lifetime of the

molecules at a certain energy level will decrease, and the absorption line will be broadened. The linear function of collision broadening can be expressed as the Lorentz linear function:

$$\phi_C(\nu) = \frac{1}{2\pi} \frac{\Delta\nu_C}{(\nu - \nu_0)^2 + \left(\frac{\Delta\nu_C}{2}\right)^2} \quad (0.11)$$

Where $\phi_C(\nu)$ represents the linear function of the collision broadening spectrum, and ν_0 is the center frequency of the absorption spectrum. The Lorentz linear function has the maximum value at the center frequency, which can be expressed as:

$$\phi_C(\nu) = \frac{1}{\pi} \frac{2}{\Delta\nu_C} \quad (0.12)$$

Where $\Delta\nu_C$ is the half-width of the spectral line of the Lorentz linear function, which can be expressed as a function of pressure and temperature:

$$\Delta\nu_C = P \sum_j (X_j 2\gamma_j) \quad (0.13)$$

Where X_j is the volume fraction of the j th substance, and j is the collision broadening coefficient caused by the disturbance of the j th substance. The collision widening coefficient γ_j changes with temperature. The specific value of γ_j can be queried through the HITRAN database. The relationship between the collision widening coefficient and temperature can be expressed as:

$$\gamma_j(T) = \gamma_j(T_0) \left(\frac{T_0}{T}\right)^{n_j} \quad (0.14)$$

Where T_0 is the reference temperature, which is usually the room temperature, n_j is the influence coefficient of the temperature on the Lorentz half-width, generally a value less than one. Therefore, among the influencing factors of the entire linear function, the environmental pressure has a greater impact than other environmental parameters. Generally, when the pressure is greater than 0.1 atm, the influence of the Lorentz linear pattern on the linear absorption pattern of the entire absorption spectrum cannot be ignored.

According to the above analysis, when the influence of the ambient temperature is dominant under low pressure conditions, the Doppler broadening mechanism mainly affects the absorption spectrum of the molecular transition. Under these circumstances, the linear function is mainly affected by the Gauss linear function. When the pressure increases, the influence of environmental pressure on the absorption spectrum gradually increases. The half-maximum width of the absorption line is mainly affected by the widening of the collision. In this situation, the line function reflects more and more characteristics of the Lorentz function. Which is suitable for choosing the Lorentz function to fit the absorption line.

(3) Voigt linear function

In the actual situation, the linear function of the molecular absorption spectrum is affected by the superposition of multiple linear broadening mechanisms. At this time, the absorption

spectrum is neither a pure Gauss line nor a Lorentz line to describe it completely. In order to describe it accurately, the absorption line type is described using a hybrid of the two line types, namely the Voigt line type . The Voigt linear function is expressed as the convolution form of the Gauss linear function and the Lorentz linear function, which can be expressed as:

$$\phi_V(\nu) = \int_{-\infty}^{\infty} \phi(u)\phi(\nu-u)du \quad (0.15)$$

Defining the parameter a to characterize the relationship between Doppler broadening and impact broadening on the line shape. The specific expression is:

$$a = \frac{\sqrt{\ln 2}\Delta\nu_C}{\Delta\nu_D} \quad (0.16)$$

According to the above formula, it can be seen that the larger a is, the greater the impact of collision widening, and the smaller a is, the greater the impact of Doppler broadening. The defined dimensionless number w is the length of the spectrum from the center of the absorption spectrum, and the specific expression is as following:

$$w = \frac{2\sqrt{\ln 2}(\nu - \nu_0)}{\Delta\nu_D} \quad (0.17)$$

The integral variable y is defined as:

$$y = \frac{2u\sqrt{\ln 2}}{\Delta\nu_D} \quad (0.18)$$

Therefore, the Voigt linear function can be expressed as:

$$\phi_V(\nu) = \frac{2}{\Delta\nu_D} \sqrt{\frac{\ln 2}{\pi}} \times \frac{a}{\pi} \times \int_{-\infty}^{\infty} \frac{\exp(-y^2)}{a2 + (w^2 - y^2)} \quad (0.19)$$

Since the calculation of Voigt's linear function includes volume integrals, its analytical solution cannot be obtained by direct calculation, and can only be solved by numerical calculation. There are empirical formulas for estimating the half-height width of a line type in the literature [44,45], which can quickly obtain the absorption coefficient at the center of the Voigt spectrum and the half-height width of the line type. The empirical formula can be expressed as:

$$\Delta\nu_V = 0.5346\Delta\nu_C + \sqrt{(0.2166\Delta\nu_C^2 + \Delta\nu_D^2)} \quad (0.20)$$

Where $\Delta\nu_V$ represents the full width at half maximum of the Voigt line. According to the above formula, it can be seen that $\Delta\nu_V$ can be estimated by the Doppler broadening coefficient and collision broadening coefficient under the same calculation conditions.

2.2 Typical measurement methods of TDLAS technology

2.2.1 Direct absorption technology

Direct absorption is the simplest and most direct method of TDLAS technology. It has the advantages of simple system, high accuracy and fast speed. The system diagram of the direct absorption method is shown in Figure 2.2. When using the direct absorption method to measure combustion parameters, the laser controller is loaded with a sawtooth signal of a certain frequency to modulate the output of the laser, so that the laser continuously scans around the center frequency ν to achieve the scanning of the entire absorption line. One laser passes through the gas to be measured, and the other laser directly passes through the etalon. A photodetector is used to collect the transmitted light intensity signal. By analyzing the transmitted light intensity through the gas to be measured and the etalon, the baseline signal is obtained. Thus, the temperature and concentration can be calculated.

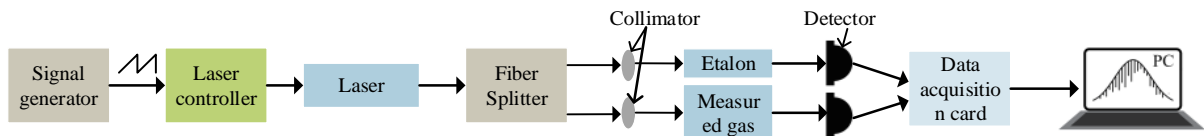


Figure 2.2-Schematic diagram of the direct absorption method system

From the introduction to the principle of laser absorption spectroscopy in section 2.1.1, it can be told that when using laser absorption spectroscopy to measure the parameter information of combustion field on a single optical path, the absorbance and integral absorption can be expressed as a correlation function of parameters such as pressure, temperature and average concentration on the path if the parameters such as temperature and pressure are uniformly distributed on the laser absorption path. When using the dual spectrum temperature measurement method to measure the average temperature T and the average gas concentration X_{abs} on the laser absorption path, the ratio of the integrated areas of the absorption rates of the two different absorption lines R_{DAS} is only a function of temperature:

$$R_{DAS} = \frac{A_1}{A_2} = \frac{PX_{abs}IS_1(T)}{PX_{abs}IS_2(T)} = \frac{S_1(T)}{S_2(T)} \quad (0.21)$$

Where A_1 and A_2 represents the integrated absorbance of the two spectral bands, respectively. On the basis of using the above formula to calculate the temperature parameters, using any of the two absorption spectrum lines, the concentration of the gas to be measured can be calculated according to the following formula:

$$X_{abs} = \frac{A}{pIS(T)} \quad (0.22)$$

When using the direct absorption spectroscopy method to measure temperature and the concentrations of gas components, it is necessary to fit the absorption baseline during data processing. But in the process of data collection and processing, the measured transmitted

light intensity signal will be affected by the background noise of the measurement system. The accuracy of linear fitting parameters selection in the data processing process cannot be guaranteed, which results in relatively large temperature and concentration measurement errors. Therefore, the direct absorption technology method cannot solve the effects of factors such as large particle concentration, laser intensity fluctuations, and spectral line overlap under high pressure situation. In addition, the direct absorption technology method can only be applied under strong absorption conditions, which also restricts its further development.

2.2.2 Wavelength modulation technology

In order to solve the measurement problem of limited measurement accuracy and sensitivity of TDLAS technology in the condition of strong background noise, high pressure, the wavelength modulation technology was introduced into the TDLAS measurement process in the 1980s. Different from the direct absorption spectroscopy method, wavelength modulation spectroscopy superimposes a high-frequency sine wave on the wavelength of the incident laser to perform high-frequency modulation. In the subsequent harmonic detection process, the interference of low-frequency background noise signals is removed. Therefore, the essence of wavelength modulation technology is to move the original absorption spectrum information to the high-frequency region, which improves the accuracy and sensitivity of TDLAS technology. Wavelength modulation technology can greatly reduce the interference of background noise in the measurement system, it is widely used in the detection of trace gases and measurements in harsh environments.

The measurement system of wavelength modulation spectroscopy is shown in Figure 2.3. A signal generator is used to superimpose a high-frequency sine wave signal on the low-frequency sawtooth wave signal, which is used to drive and modulate the output laser wavelength of the tunable laser near the peak of the absorption spectrum of the component to be measured. The transmission signal received by the photodetector contains not only the absorption spectrum information of the gas to be measured, but also the harmonic components of the absorption spectrum itself. In the process of data processing, even harmonic signals are often selected to calculate the combustion parameters because of the large signal strength and the signal-to-noise ratio. The digital lock-in amplifier is often used to extract the second harmonic components of the absorption spectrum ($2f$) to calculate the temperature and concentration of the measured gas component. Different from the data processing process of direct absorption spectroscopy method, wavelength modulation spectroscopy does not need to determine the baseline signal in the measurement process, so the measurement accuracy is higher than that of direct absorption spectroscopy.

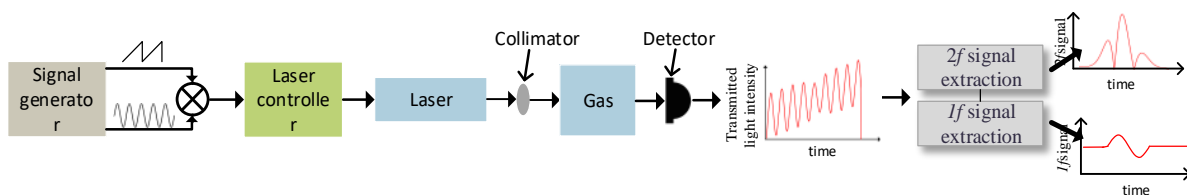


Figure 2.3-Schematic diagram of the wavelength modulation method system

At the beginning of parameter measurement using wavelength modulation spectroscopy technology, it is necessary to calibrate the high-order harmonic signals in advance. There are two main calibration methods for TDLAS based on wavelength modulation technology when measuring concentrations of gas components. One method is to use the direct absorption method to calculate the gas concentration value and calibrate the concentration result calculated using the $2f$ signal. The other is to obtain a real $2f$ signal by measuring a gas sample with a known concentration, and calibrate the $2f$ signal in the experimental measurement. In the actual measurement process, especially under the harsh measurement conditions of high temperature, high pressure, and high turbulence, it is not realistic to calibrate the $2f$ signal in advance. Therefore, using the ratio of the second harmonic signal to the first harmonic signal, that is, the normalized second harmonic signal to perform harmonic analysis has been developed. The calibration-free wavelength modulation method can eliminate the influence of the system hardware parameter settings on the measurement and reduce the error of results. The tunable semiconductor laser absorption spectroscopy technology detects and analyzes the absorption spectrum signal of the gas molecule to be measured, and uses the measured transmitted light intensity signal to perform non-contact measurement of parameters such as the temperature of the measured field and the concentrations of gas components. Therefore, laser absorption spectroscopy has the advantages of high measurement accuracy, fast response speed, and can realize simultaneous measurement of multiple parameters.

2.3 Summary of this chapter

In this chapter, the theoretical basis and related parameters of laser absorption spectroscopy technology is firstly introduced in detail. TDLAS technology is based on the Beer-Lambert absorption law. The theorem describes the process that the molecules in the gas medium absorb and weaken the incident light intensity at a specific frequency. Due to the spectral line broadening mechanism, the transmitted light intensity presents a curve with a certain absorption line intensity and a linear function. Querying the HITRAN database to obtain the spectral line intensity and the relevant parameters of the line fitting to determine the absorption curve. In the process of parameter calculation, the direct absorption technique or the wavelength modulation technique is selected to invert the temperature and component concentration of the gas medium.

For the two typical measurement methods of TDLAS, the main difference of the direct absorption method and the wavelength modulation method is that the wavelength modulation method of the incident light. The direct absorption method uses a low-frequency sawtooth wave to modulate the incident laser signal, which is susceptible to interference from low-frequency noise. The wavelength modulation technology superimposes a high-frequency sine wave on the low-frequency sawtooth wave to modulate the laser signal to

achieve "frequency shift", which can effectively suppress the interference of low-frequency noise. The direct absorption method and the wavelength modulation method are respectively suitable for strong gas absorption and weak absorption situations. The measurement system and the process of parameters calculation of the direct absorption method are relatively simple, but the measurement accuracy is limited by the low-frequency noise interference. The wavelength modulation method extracts and analyzes the normalized high of the transmitted light intensity. The calculation process of sub-harmonic signals is more complicated, but the accuracy and sensitivity of gas detection are higher, and it is less sensitive to noise caused by hardware system parameter settings.

Chapter 3

Multi-component Concentration Measurement Method Based on Neural Network

In this chapter, the McKenna combustion furnace is selected as the experimental object, the CFD simulation method of typical combustion field is introduced to predict the parameter distribution of the combustion field. In this chapter, the steps of geometric modeling of combustion field, setting of boundary conditions and parameter setting of chemical reaction model in the process of numerical simulation of combustion are mainly introduced. On the basis of simulation, the principle of selecting spectral lines in the process of measuring temperature and concentration by TDLAS method and the simulation analysis of absorption spectrum are introduced in detail. For the TDLAS temperature and concentration measurement system, this chapter introduces the geometric models of single-light path and multi-angle sensors. On this basis, the absorption of water vapor in the combustion field to the laser signals on multiple paths is obtained to prepare for subsequent neural network training Learning set.

Aiming at the neural network-based multi-component concentration prediction algorithm, this chapter introduces the theoretical model, signal transmission method and the unique advantages of the error back propagation neural network in detail. The multi-component prediction method based on the BP network was analyzed in detail, which mainly contains the implementation process of the concentration prediction algorithm, the simulation effect and the cause of the calculation error.

3.1 Forward simulation of the absorption spectrum of water vapor based on CFD numerical simulation

The process of combustion involves complex chemical and physical changes, including the disappearance, transformation and production of hundreds of components. Real-time measurement of various parameters of the combustion field is an important indicator for detecting combustion efficiency and controlling the combustion process. However, the

combustion parameter diagnosis of absorption spectroscopy is facing tremendous pressure in the measurement system and data processing. This chapter takes this challenge as a starting point and uses computational fluid dynamics simulation methods to simulate the McKenna combustion field parameters under multiple operating conditions. On the basis of the simulation results, combining with the relevant parameters of the spectral data from the HITRAN database, this chapter forwardly calculates the absorption spectra of H₂O on a single optical path and multiple angles to prepare a training set for subsequent neural network learning and training.

3.1.1 Combustion numerical simulation based on CFD

This work is based on the component transport finite rate chemical reaction model to numerically simulate the methane-air premixed combustion process of a flat flame burner under multiple different working conditions. The distributions of temperature, pressure, and concentrations of gas components of the combustion field can be obtained. These results also laid the foundation for further research on methane-air premixed combustion.

The flat flame produced by the premixed combustion of methane and air is a symmetrical disc-shaped thin-layer flame. Compared with flames obtained by the ordinary burners, the uniform distribution characteristics of the temperature and flow field of the flame can effectively improve the heating quality and heating speed, as well as shorten the heating time. Combustion in this situation not only saves fuel, but also reduce the loss of oxidation heat, thereby extending the life of the furnace body. Because the stability and symmetry of the premixed flame of the flat flame burner are very ideal, it is widely used in experimental measurement and numerical simulation comparison. At present, flat-flame burners have been widely used in heating furnaces abroad, and have achieved obvious economic results after being promoted in China. Methane has a unique tetrahedral molecular structure and large C-H bond energy and is a commonly used gas fuel in laboratory combustion testing. The combustion reaction of methane has the characteristics of high ignition temperature and low flame temperature. The main mechanism of methane high-temperature combustion is shown in Figure 3.1. It can be seen from the figure that methane absorbs energy and dissociates into free methyl groups, and then combines with oxygen atoms to form formaldehyde. Formaldehyde is further attacked by OH, H and O radicals to form formic acid groups. A series of molecules or groups react to convert to CO, and CO eventually generates carbon dioxide and water in the presence of OH and releases the heat of combustion [46]. The temporal and spatial changes of the H₂O concentration in the product can reflect the combustion process of methane and the state of the thermal motion of gas molecules. The concentration distribution of water vapor at a specific time represents a state of chemical thermodynamics and chemical kinetics. In this work, the absorption spectra of water vapor is used to predict the concentration distribution of the other remaining components in the combustion field produced during the combustion process.

cool down the burner nozzle, but also prevent unstable flame combustion caused by gas overheating [49].

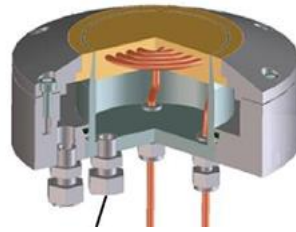


Figure 3.2-Sectional view of McKenna burner

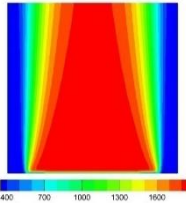
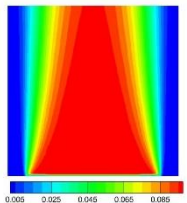
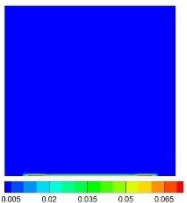
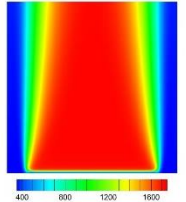
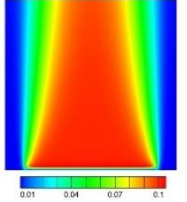
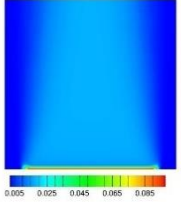
In the numerical calculation process, when the ideal combustion field to be measured is set to a rectangular area with length is 80mm and height is 100mm, regarding the setting of the boundary conditions of the calculation domain, we set the mixed fuel inlet and the protective gas nitrogen inlet as the velocity inlet, and the outlet boundary of the calculation domain is set as a pressure outlet and is perpendicular to the return flow direction of the boundary. In the FLUENT simulation calculation, we used a pressure-based steady-state solver and performed detailed calculations using the SIMPLE algorithm. As shown in the following table, in the simulation and experiment, the flow rate of methane is set from 1.78 L/min to 2.78 L/min, and the flow rate of air is always set to 10.6 L/min. With the sets of the flow rates of fuel and the air, the equivalent ratio is changed from 1.6 to 2.5 to ensure that methane is not completely combustion and there is a large amount of surplus. The nitrogen shielding gas flow is set to maintain 15.5 L / min to stabilize the flame. Taking into account the flow velocity of all gases set in the experiment, the viscous model is selected as the laminar flow model for numerical simulation in the FLUENT combustion simulation. A simplified mechanism of methane and air is used in the chemical reaction process, which includes 53 molecular and group reactions of 14 substances, as well as related parameters related to chemical reaction kinetics.

Table 3.1-Combustion simulation with different equivalent ratio flow settings

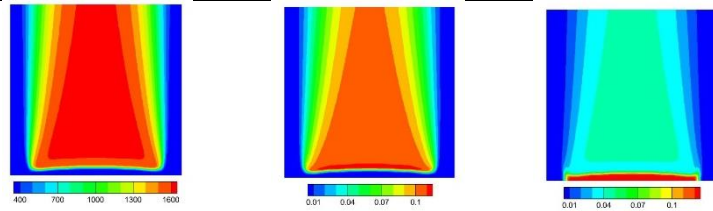
Methane flow (L/min)	1.78	1.89	2.00	2.12	2.23	2.34	2.45	2.56	2.67	2.78
Air flow (L/min)	10.6	10.6	10.6	10.6	10.6	10.6	10.6	10.6	10.6	10.6
Nitrogen flow (L/min)	15.5	15.5	15.5	15.5	15.5	15.5	15.5	15.5	15.5	15.5
Equivalence ratio (ϕ)	1.6	1.7	1.8	1.9	2.0	2.1	2.2	2.3	2.4	2.5

The distribution of temperature and pressure field and the concentration of water vapor and methane under working conditions when the flow rate of methane are 1.78 L/min (equivalent ratio equal to 1.6), 2.23 L/min (equivalent ratio equal to 2) and 2.78 L/min (equivalent ratio equal to 2.5) are shown in Figure 6. When the difference between the measuring height and the height of the combustion furnace plane is Height Above Burner equals to 5mm, the average flame temperature begins to drop at 20mm of the radial position of the area to be measured and reaches the ambient temperature at 37 mm. At HAB equals to 10 mm, the area with uniform temperature distribution becomes even narrower, and the temperature transition position appears at 17 mm near the center of the flame. When the HAB is increased to 15mm or higher, the uniform flame temperature area is narrower and the radical temperature gradient is larger. Similar to the temperature trend, the degree of incomplete combustion of methane is relatively small when the equivalence ratio is 1.6, a large amount of water vapor accumulates in the entire combustion area. The width of the area with uniformly water vapor distributed gradually decreases with the increase of the equivalent ratio. The volume fraction of water vapor also gradually decreases. Under the simulation conditions of oxygen-lean combustion, the unburned methane is mainly concentrated in the fuel inlet. As the equivalence ratio increases, more and more methane burns incompletely, and is gradually covered by the turbulence of the airflow of the computational domain. When the equivalence ratio reaches 2.5, it can be clearly seen that excessive unburned methane is dispersed in the entire calculation domain, and the volume fraction reaches 0.025.

Table 3.2-Distribution diagram of temperature, water vapor volume fraction, and methane volume fraction under different working conditions

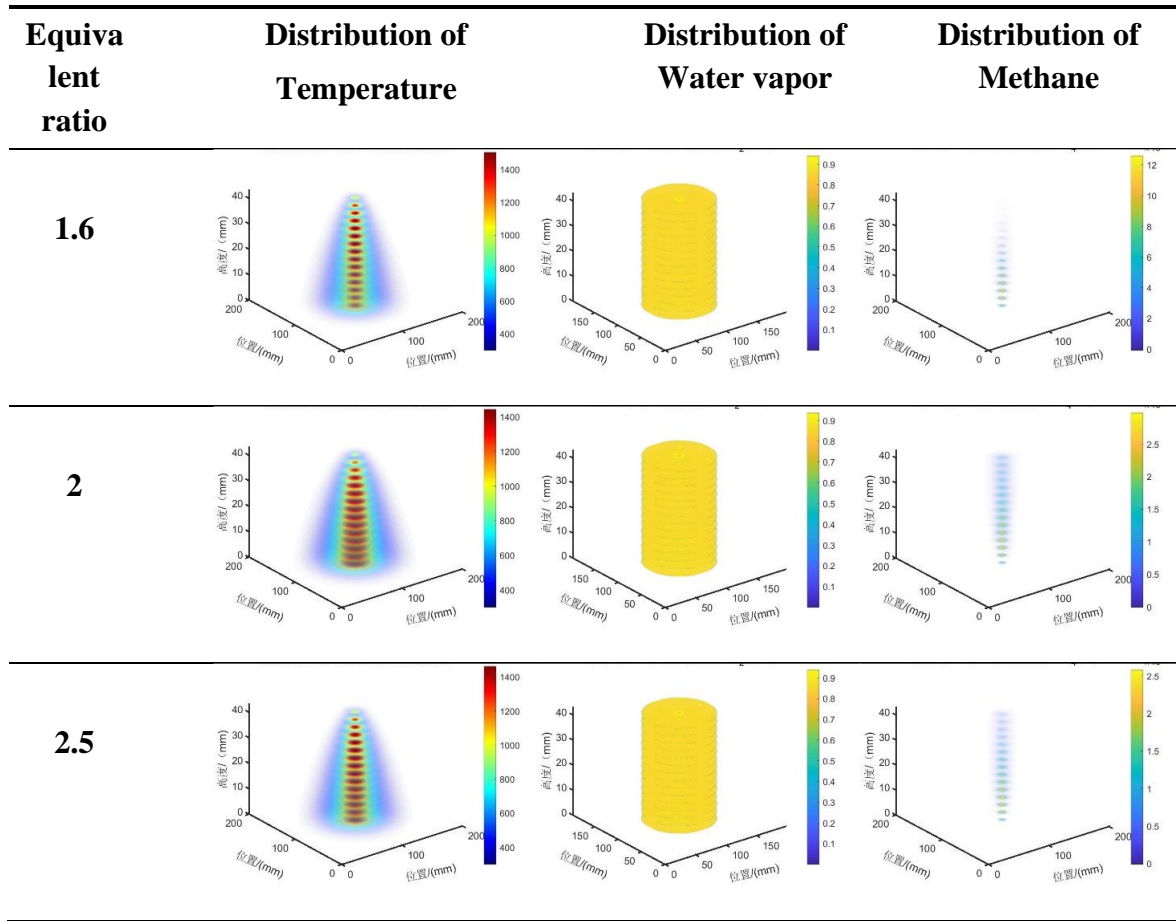
equivalent ratio	Parameters	Distribution of Temperature	Distribution of Water vapor	Distribution of Methane
1.6				
2				

2.5



In order to prepare the training set of the self-learning of neural network, in the process of combustion simulation calculation, the equivalence ratio is set from 1.6 to 2.5 at intervals of 0.1 to obtain the distributions of combustion parameters in the combustion zone of the flat flame burner under 10 oxygen-lean combustion conditions. Recording the combustion parameters of each node on the path with a height of 5mm to 45 mm with the interval of 3mm under each working condition, and taking them as the known environmental parameters to calculate the absorption spectrum of water vapor. Table 3.3 shows the distribution of methane, water vapor and temperature at each cross-section selected for training the neural network under the three working conditions of the equivalent ratio of methane to air of 1.6, 2 and 2.5. The trends of these three parameters are consistent with the above simulation results of CFD. As the degree of incomplete combustion of methane increases, excessive methane gradually remains and diffuses to the entire calculation domain with the turbulence of the airflow, while the volume fraction of water vapor produced by full combustion gradually decreases. The size of the high temperature area and the maximum temperature also have a gradually increasing trend.

Table 3.3-Distribution diagram of temperature, water vapor volume fraction, and methane volume fraction under different working conditions



3.1.2 The selection and analysis of the measurement spectrum line of methane and water vapor

There are abundant spectral signals with strong absorption in high-temperature environments of water vapor, it is possible to select the appropriate absorption line for temperature measurement. On the basis of obtaining temperature information from the absorption spectra of water vapor, a laser with a center wavenumber of 5938 cm^{-1} is selected to measure the concentration of methane. The HITRAN database covers the spectral data of dozens of molecules and their isotopes, mainly including spectral line intensity, broadening parameters, transition energy, etc., which are used to simulate the absorption and emission of light in the atmosphere. Checking the line intensity S of the absorption spectrum of methane in the range of wavenumbers from 5930 cm^{-1} to 5940 cm^{-1} from the database, as well as the air expansion coefficient γ_{air} , the self-expansion coefficient γ_{self} , and low energy state energy $E''(\text{cm}^{-1})$ to calculate the absorption spectral parameters of methane. As shown in 错误!未找到引用源。 , the suitable absorption spectrum for measuring the concentration of methane in the spectral band is chosen [50].

Table 3.4 --Spectral parameters of methane from 5937 cm^{-1} to 5940 cm^{-1}

Wave number (cm-1)	Line strength S(cm-1/(mol*cm-2))	Air spreading factor γ_{air}	Self-expanding factor γ_{self}	Low state ener (cm-1)
937.00915	3.97×10^{-25}	0.0653	0.079	157.1279
5937.06688	1.80×10^{-24}	0.06	0.077	815
5937.15126	1.41×10^{-24}	0.06	0.077	815
5937.22602	8.57×10^{-24}	0.054	0.07	575.1701
5937.34189	3.35×10^{-24}	0.054	0.07	575.0527
5937.3869	4.79×10^{-25}	0.0653	0.079	157.1389
5937.402	2.05×10^{-24}	0.0613	0.075	376.7304
5937.53023	2.83×10^{-24}	0.06	0.077	815
5937.545	6.19×10^{-25}	0.06	0.077	815
5937.64254	2.54×10^{-24}	0.058	0.074	376.8213
5937.72729	6.45×10^{-25}	0.058	0.074	376.7357
5937.79419	5.19×10^{-25}	0.06	0.077	815
5937.81841	3.86×10^{-24}	0.0591	0.073	470.8729
5937.83595	5.58×10^{-24}	0.0613	0.075	376.8048
5937.907	3.01×10^{-25}	0.06	0.077	815
5938.0571	2.18×10^{-22}	0.061	0.077	219.9135
5938.06475	3.74×10^{-22}	0.061	0.077	219.9151
5938.09404	6.17×10^{-22}	0.061	0.077	219.9198
5938.16703	3.65×10^{-22}	0.061	0.077	219.9368
5938.1897	3.57×10^{-22}	0.061	0.077	219.9413
5938.20875	5.59×10^{-22}	0.061	0.077	219.9452
5938.304	6.39×10^{-25}	0.06	0.077	815
5938.33915	2.47×10^{-24}	0.06	0.077	815
5938.37963	4.77×10^{-25}	0.06	0.077	815
5938.4218	9.47×10^{-25}	0.0631	0.076	293.1542
5938.54264	5.44×10^{-24}	0.06	0.077	815
5938.58391	2.92×10^{-24}	0.0631	0.076	293.1646
5938.62211	6.83×10^{-24}	0.0631	0.076	293.1266
5938.64901	2.00×10^{-25}	0.06	0.077	815
5938.65685	4.48×10^{-24}	0.0631	0.076	293.1542
5938.69326	3.42×10^{-24}	0.06	0.077	815
5938.7545	1.18×10^{-23}	0.0565	0.071	575.1701
5938.82524	1.52×10^{-23}	0.054	0.07	575.2229
5938.87182	1.02×10^{-24}	0.0565	0.071	575.0527
5938.965	2.11×10^{-25}	0.06	0.077	815
5939.02182	4.33×10^{-25}	0.06	0.077	815

5939.22116	4.12×10^{-25}	0.06	0.077	815
5939.35335	1.50×10^{-23}	0.05	0.067	814.6462
5939.44846	5.20×10^{-24}	0.05	0.067	814.6481
5939.45559	4.89×10^{-25}	0.0657	0.08	62.8782
5939.56296	2.45×10^{-25}	0.06	0.077	815

The absorption line intensity of methane in the wavelength range of 5937 cm^{-1} to 5940 cm^{-1} is obtained as shown in the figure below according to the parameters from the above table. It can be seen that in the entire wavelength range, the strong absorption line of methane is concentrated at 5938 cm^{-1} , the wavenumber point with the highest line intensity corresponds to 5938 cm^{-1} . Figure 3.3 is the line intensity of the absorption spectrum of methane on this spectral band. Methane molecules produce strong photons at the wave number of 5938 cm^{-1} . Which is the suitable absorption line for temperature measurement.

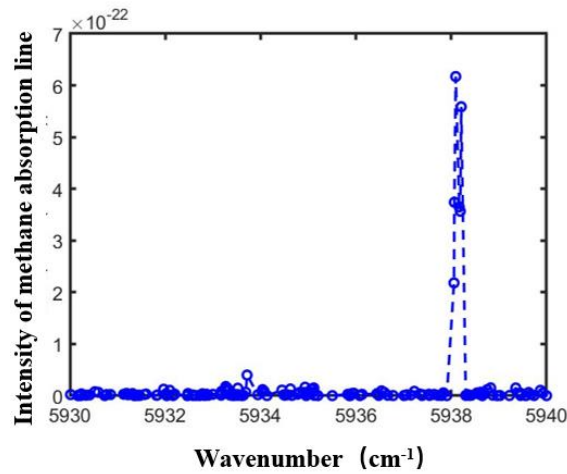


Figure 3.3-Intensity of methane absorption line in the wavenumber range of 5930 cm^{-1} to 5940 cm^{-1}

According to the HITRAN database, the simulated mixture of methane, carbon dioxide and water vapor are with volume fractions of 1%, 1%, and 1%, respectively. In the range of wave number from 5930 cm^{-1} to 5940 cm^{-1} , the pressure is set to 1atm, the length of the optical path equals to 10 cm, the temperature is set to 2000 K. The absorption spectra of these three components are shown in Figure 3.3. In this spectral range, the absorption of carbon dioxide and water vapor molecules has a relatively small effect on the absorption spectrum of methane, and can be ignored in numerical values, which is consistent with the above line intensity calculation results. It can be seen from the figure that methane molecules have a relatively independent and larger absorption peak near 5940 cm^{-1} , and shows the shape of double absorption peaks at 5938.3 cm^{-1} . In the process of experiment and simulation, the DFB laser with the center wavenumber of 5938 cm^{-1} is used to simulate and measure the concentration of methane. When using the measurement data for linear fitting, the absorption peak with the center wavenumber of 5938.3 cm^{-1} is selected for fitting.

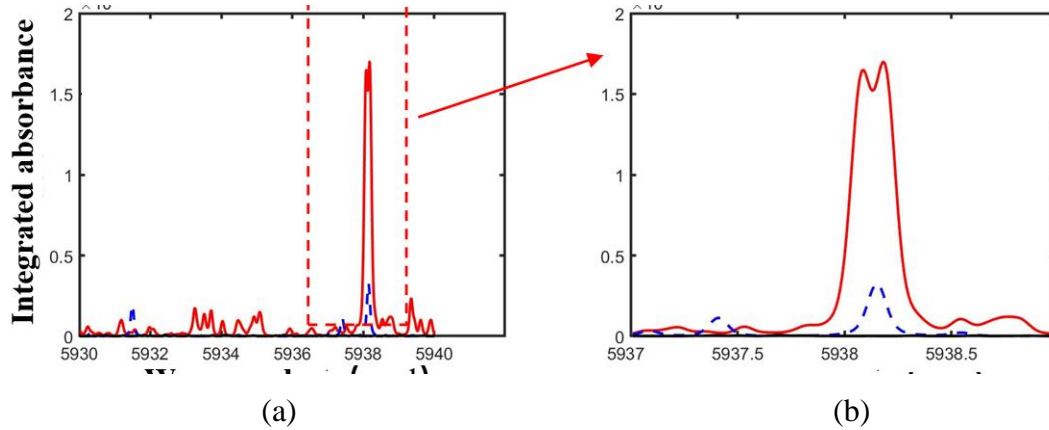


Figure 3.4 -The absorption spectrum of water vapor, carbon dioxide and methane in the range from 5930cm^{-1} to 5940cm^{-1} (a) The absorption spectrum in the range from 5930cm^{-1} to 5940cm^{-1} (b) The absorption spectrum of methane in the range from 5937cm^{-1} to 5939cm^{-1}

In this thesis, the two-line method is used for temperature measurement. It is necessary to select the absorption spectrum of water vapor on two wavebands, and calculate the average temperature on the optical path based on the ratio of the integrated absorption rates of the two. Two spectral lines with central wave numbers at 7185.6 cm^{-1} and 7444.4 cm^{-1} are selected to calculate the average temperature, under the environmental conditions of pressure equals to 1atm, the length of the optical path is set to 10cm, the temperature is 1500K, and the volume fraction of water vapor is 0.01. The spectral absorbance of water vapor in the two spectral bands ranging from 7180 cm^{-1} to 7190 cm^{-1} and from 7440 cm^{-1} to 7450 cm^{-1} are shown in Figure 3.5. There is an independent and obvious absorption peak on these two spectral bands. In the experimental measurement, the independent absorption peak is less affected by the surrounding absorption peaks, which can ensure the accuracy of the experimental measurement.

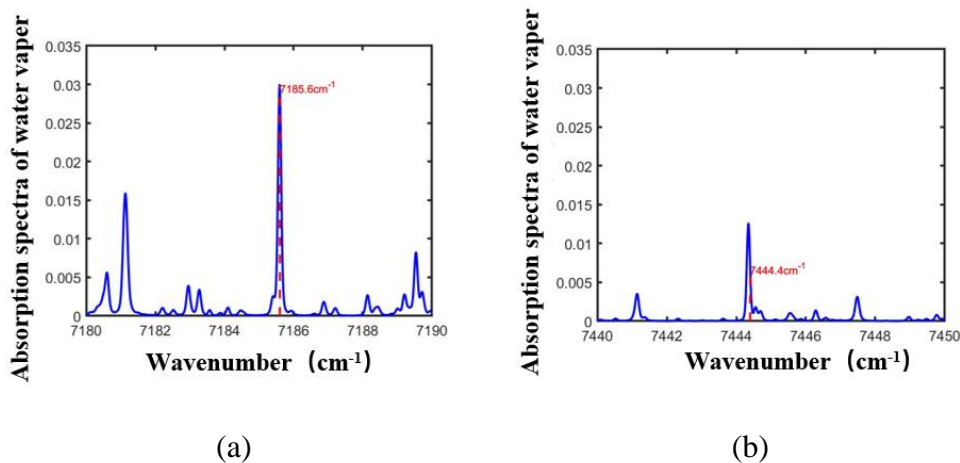


Figure 3.5-The absorption spectrum of water vapor in two spectral bands (a) Absorption spectra of water vapor from 7180cm^{-1} to 7190cm^{-1} (b) Absorption spectra of water vapor from 7440cm^{-1} to 7450cm^{-1}

It can be seen from the figure above that within the scanning wave number range of the DFB laser, both the selected spectral band have a relatively independent absorption peak. The value of the main absorption peak is greater than the value of the side peak, which is almost free from the interference of the surrounding absorption peak. It is suitable to be used as a spectral line pair for temperature measurement. The specific absorption information of water vapor on the two spectral bands is shown in the following table:

Table 3.5-Specific absorption information of water vapor absorption spectra on two spectral bands

Number	Center wave number /cm ⁻¹	Line strength /(cm ⁻¹ *mol*cm ⁻²)	Low state energy /cm ⁻¹	Energy difference /cm ⁻¹
1	7185.3537	1.005×10 ⁻²⁹	3750.4645	2534.2334
2	7444.1503	6.04 ×10 ⁻²⁸	1216.2311	

When using the dual-line method to measure temperature, it is not only important that the water vapor molecule has a separate and relatively strong absorption peak in the selected spectral band, but also the sensitivity of the two spectral lines for temperature measurement should be considered. The temperature sensitivity of the selected spectral line pair is defined as the sensitivity of the line intensity ratio to temperature, which is shown in the following formula:

$$\frac{dS/S}{dT/T} = \frac{hc}{k} \frac{|E_1'' - E_2''|}{T} \quad (1.1)$$

Among them, h is Planck's constant, k is Boltzmann's constant, c is the speed of light, and E_1'' and E_2'' are the corresponding lower state energies of the two spectral bands, respectively. According to the above formula, when the temperature T is a constant, the greater the energy difference of the lower state of the selected spectral line pair, the higher the temperature measurement sensitivity^[51]. In the high temperature range of 1100 K to 2000 K, the temperature measurement sensitivity of the two spectral lines of the range of 7185.3537 cm⁻¹ to 7444.1503 cm⁻¹ is shown in Figure 3.6 (a). It can be seen that in the temperature measurement range of 1100K to 2000K, the temperature measurement sensitivity of the two spectral lines decreases with the increase of temperature, but the whole temperature range has relatively high sensitivity, which makes it a suitable pair of spectral lines for temperature measurement. At the same time, in the temperature range of 1100 K to 2000 K, the line intensity ratio of the two spectral lines decreases monotonously and within a reasonable range, which conforms to the principle of the selection of two spectral lines in the temperature measurement, which can reduce the performance error.

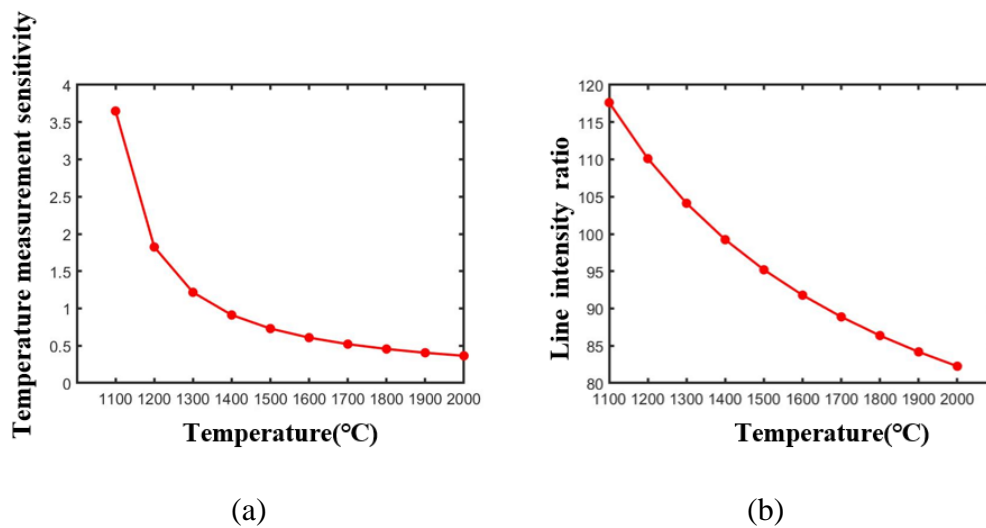


Figure 3.6-Temperature measurement sensitivity and line-strength ratio in the spectral range of 7185cm^{-1} and 7444cm^{-1} (a) Temperature measurement sensitivity in the spectral range of 7185cm^{-1} to 7444cm^{-1} (b) Line intensity ratio in the spectral range from 7185cm^{-1} to 7444cm^{-1}

3.1.3 Forward simulation of the absorption spectra of water vapor

(1) Simulation of the absorption spectra of water vapor on a single laser path

In order to calculate the absorption spectra of water vapor on a single laser path, supposing that a laser beam with center wavenumbers of 7185.6 cm^{-1} and 7444.4 cm^{-1} respectively pass through the combustion field are measured. Setting the total length of the absorption path (the distance between the collimator lens and the detector) is 10cm. Setting the temperature of the environmental area to room temperature, the pressure to 1atm, and the concentration of water vapor to 0.03% to calculate the absorption spectrum of water vapor. The combustion parameters in the flame zone are determined by CFD simulation results. According to the Beer-Lambert absorption law, the absorption spectra at different axial heights and radial positions of the flame is simulated. When the equivalent ratio of methane to air is 2, the measurement height is 2 cm on the laser path, the simulation results of the two spectral bands are shown in the Figure 3.7. There are two independent and relatively large absorption peak at the center wavenumbers of 7185.6 cm^{-1} and 7444.4 cm^{-1} .

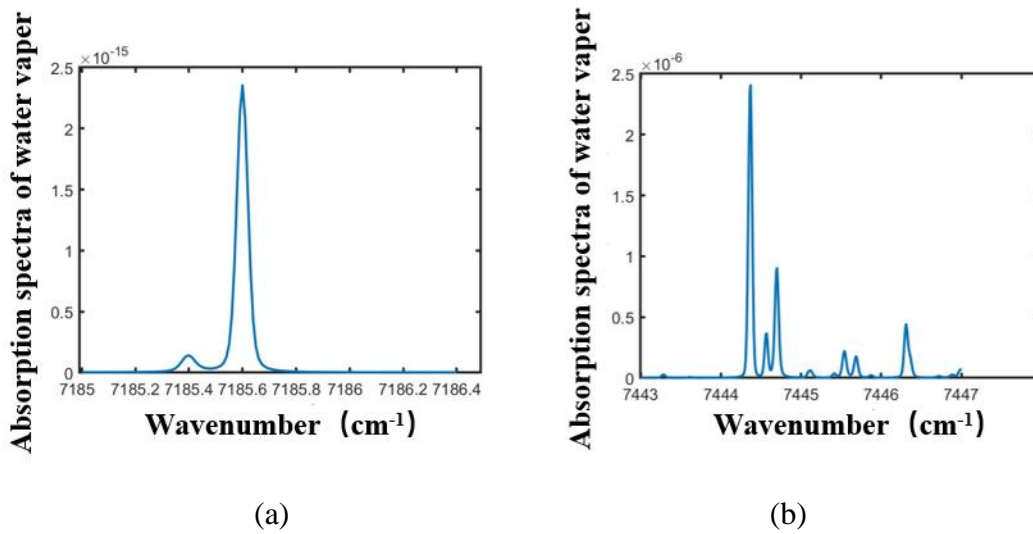


Figure 3.7-Simulation results of single optical path absorption spectrum (a) Absorption spectrum from 7180cm⁻¹ to 7190cm⁻¹ (b) Absorption spectrum from 7440cm⁻¹ to 7450cm⁻¹

According to the above simulation results, linear fitting is performed on the absorption spectra with central wavenumbers of 7185.6 cm⁻¹ and 7444.5 cm⁻¹, the integrated absorbance on each spectral band was calculated to prepare the training set for the subsequent self-learning of the neural network.

(2) Simulation calculation of absorption spectra of water vapor based on the five-angle spectral sensor

The regular pentagon sensor used in the laboratory is shown in Figure 3.8. The specific geometric parameters are as follows: the radius of the inscribed circle is 150 mm, the side length is 210 mm, twelve detectors are arranged at equal intervals on each side. The photosensitive surface of each detector is a circle with a diameter of 2mm, and the interval between adjacent detectors is 14.36 mm. The fan-shaped beam light source is placed at the five vertices of the five-view sensor, and the widening angle of this sensor is 50.62 degrees. The fan-shaped laser beam at each angle passes through the area to be measured and is received by the 24 detectors with the farthest distance to obtain absorption spectrum data on 120 different laser paths.

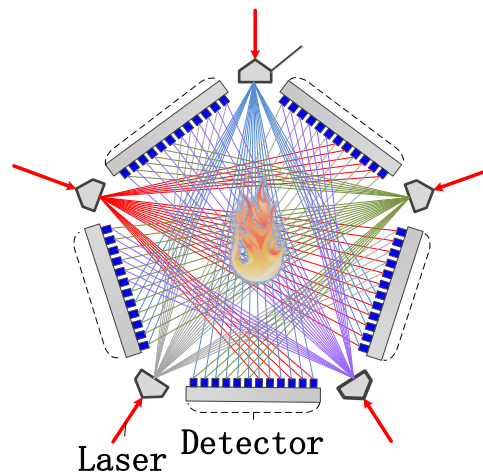


Figure 3.8-Optical path layout model for multi-angle absorption spectrum simulation

Combined with the geometric model of the pentagonal sensor shown in the figure above, the absorption information of water vapor detected by the detector array on each side is simulated, and then the integrated absorbance on each spectral band is calculated as the training set data of the neural network.

When the flame to be measured is strictly located in the center of the five-view sensor, using the spectral parameters provided by the HITRAN spectral database to simulate the absorption spectra generated by the lasers with the center wave numbers of 7185.6 cm^{-1} and 7444.5 cm^{-1} on the 120 laser paths, and further calculate the integrated absorption area. The integrated absorbance on the five-view detector array is shown in Figure 3.9. When the flame is strictly located at the center of the five-view sensor, due to the central symmetry of the combustion field, the integrated absorption area obtained by the detector arrays presents the similar value and trend, which is consistent with the actual situation.

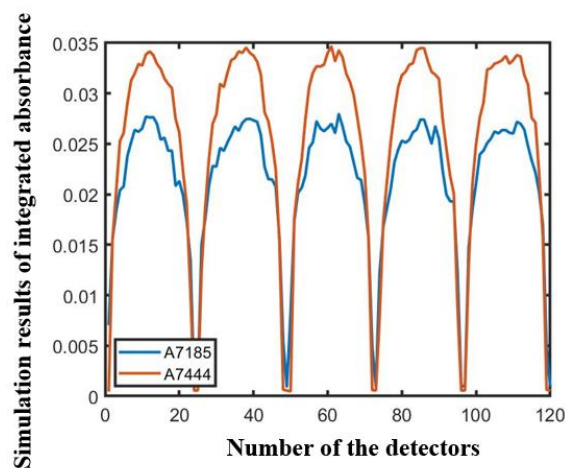


Figure 3.9-Simulation results of integrated absorbance on 120 paths when the burner is at the center of the sensor

In the actual two-dimensional combustion measurement, the flame to be measured is probably located at any position of the sensor. Combined with the sensor geometry model shown in the figure above, the fan-shaped laser beam emitted by the light source arranged at five angles passes through the area to be measured and illuminates to the 24 detectors farthest away. The absorption spectra of water vapor on the spectral band with center wavenumber of 7185.6 cm^{-1} and 7444.5 cm^{-1} on the 120 laser paths are simulated and shown in Figure3.10. When the measured flame is located at any position of the five-view sensor, the integrated absorbance obtained by the detector arrays no longer presents the same value and trend. In the spectral bands with central wave numbers of 7185.6 cm^{-1} and 7444.5 cm^{-1} , the integrated absorbance has the same changing trend at the same position.

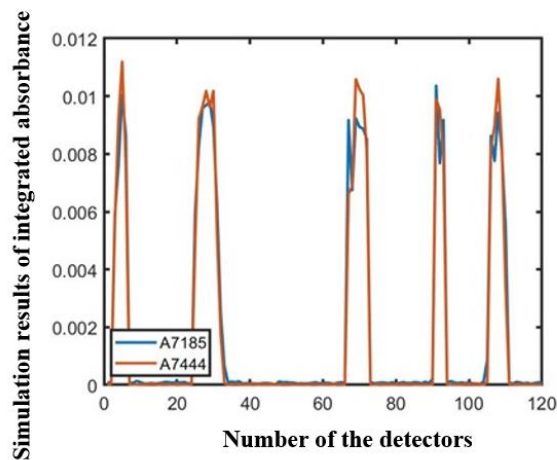


Figure3.10-Simulation results of the integrated absorption area on the 120 path when the burner is not strictly located at the center of the sensor

3.2 Multi-component concentration prediction method based on neural network

In the premixed combustion process of methane and air, the unburned methane and the combustion product water vapor can accurately reflect the fuel utilization rate under oxygen-lean combustion conditions. In order to use the absorption spectra information of the easily detectable component such as water vapor to measure the remaining components difficult to measure, such as the concentration information of methane, the neural network tool is introduced to measure the mapping relationship between the concentration information of methane by constructing the absorption spectra information of water vapor, so as to realize the use of limited measurement data to predict a variety of parameters. In this section, the introduction of the neural network algorithm into the multi-component concentration prediction process is mainly introduces, and simultaneously introducing how to use the CFD combustion numerical simulation and the calculation results of the absorption spectra to complete the training and self-learning of the neural network algorithm. At last, the feasibility verification of the algorithm for calculating the average temperature, average CH4

concentration and the two-dimensional distribution of CH₄ concentration in a single optical path based on neural network is verified.

3.2.1 Multi-component concentration prediction method based on neural network

Psychologist Warren McCulloch and mathematical logician Walter Pitts first proposed the concept of neural network model in 1943, and the algorithm model they proposed has continued to this day. Artificial Neural Networks are algorithmic mathematical models that simulate the behavioral characteristics of human brain neural networks and perform distributed parallel information processing [52]. Neural networks have powerful training and self-learning capabilities, and can obtain implicit connections between parameters through training and self-learning, without having to study its exact mathematical model. In the neural network algorithm, the typical three-layer neural network model is shown in the figure below. Because the three-layer neural network has a simple structure, stable working status, and easy hardware implementation, it is widely used in pattern recognition and classification, system simulation, fault intelligent diagnosis, image processing, function fitting, optimal prediction and many other aspects [53,54].

Multi-layer neuron structure can realize the approximation of any function. In this work, the few-spectra measurement and training method based on CFD numerical simulation and neural network model were introduced into the multi-component concentration measurement using laser absorption spectra. The concentration distribution of multiple gas components can be solved based on the absorption spectra of a small amount of easily detectable components.

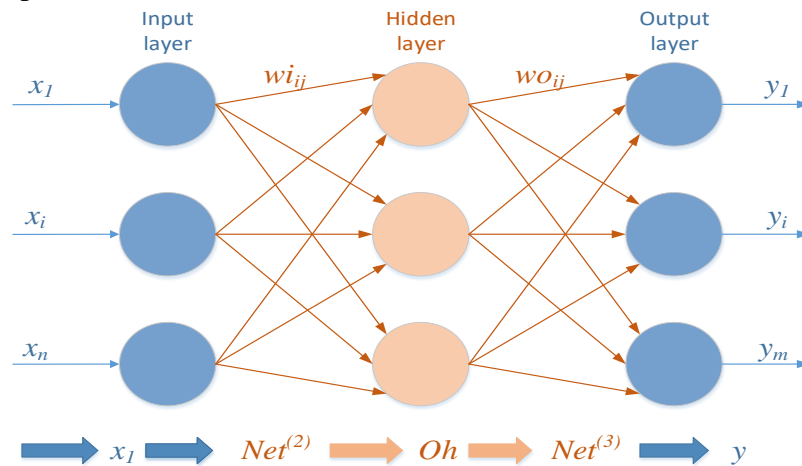


Figure3.11-Schematic diagram of three-layer neural network

Figure3.11 is a schematic diagram of a three-layer neural network. Each circle in the figure represents a node in the neural network model, that is, a neuron of the neural network. In the above figure, x represents the input signal of the neural network model, and y represents the output of the neural network model. $net^{(2)}$ 、 $net^{(3)}$ respectively represent the input of the hidden layer and the output layer, Oh represents the output of the hidden layer, and w_{ij}

represents the nodes between the input layer and the hidden layer. The corresponding weight, w_{ij} represents the weight of each node between the hidden layer and the output layer. The output value of the node of the previous layer is multiplied and summed by the corresponding weight of the node between the corresponding layer and the layer to obtain the output value of each neuron of the next layer. This value is used for the output of the node of the lower layer after the activation function corresponding to the node is used. Value calculation, the calculation process of the above-mentioned typical three-layer neural network algorithm can be expressed by the following formula.

$$net_i^{(2)} = \sum_{j=0}^m w_{ij} x_j \quad (1.2)$$

$$Oh = f(net_i^{(2)}) \quad (1.3)$$

$$net_i^{(3)} = \sum_{j=0}^q w_{ij} Oh_j \quad (1.4)$$

$$y_i = g(net_i^{(3)}) \quad (1.5)$$

Error backpropagation (BP) algorithm is a method for gradient calculation in artificial neural networks. Using the backward transmission of error signals, the weights of each layer in the neural network can be corrected [55]. The BP neural network repeats training and self-learning on the given input and output parameters of the training set, and constantly approaches the output target given by the user. The error propagates back to the input layer through the output layer, and the weights and thresholds of each layer of the neural network are continuously adjusted. When the training ends, the sum of the squared errors of the artificial neural network algorithm is minimized, and the square difference between the actual output and the expected output is used as the evaluation function of BP algorithm:

$$E = \frac{1}{2} (r_k - y_k)^2 \quad (1.6)$$

In the formula, r represents the expected output of the neural network algorithm, and y is the actual output. In practical applications, the gradient descent function is often selected to modify the weight coefficient. Under normal circumstances, an inertia correction link is generally added in the weight correction process to speed up the convergence of the algorithm. At this time, the correction value of the weight is:

$$\Delta w_k = -\eta \frac{\partial E_k}{\partial w} + \alpha \Delta w_k - 1 \quad (1.7)$$

Among them, η represents the learning rate, and α is the inertia coefficient [56], which can be set artificially during the neural network training process.

When using the BP neural network algorithm to simulate the spectral absorbance on the single light path, it is necessary to design the parameters of the neural network model rationally, the computational advantages of the neural network model should be used to realize the effect of using the limited water vapor absorption spectrum to calculate the concentration distribution of methane in the area to be measured. In this work, the input

signal x_i of the three-layer neural network model is the absorption spectra of water vapor in the spectral bands with the central wavenumber of 7185cm^{-1} and 7444cm^{-1} , and of 7185cm^{-1} to 7186.4cm^{-1} and 7443cm^{-1} to 7447cm^{-1} are selected in the calculation. The absorption spectra of each spectral bands are fitted to integrated absorbance, and the number of neurons in the input layer is adjusted with the change of the vector length. In the concentration prediction of methane on the single light path algorithm, the number of output neurons is only one, which is the average concentration of methane on the laser path. In order to realize reasonable self-learning of the network, the selection of the number of neurons in the hidden layer is very important. Too many neurons in the hidden layer will lead to over-fitting and increase the error surface depression, while too few neurons will lead to inability to learn accurately, causing the network training results to fall into the local optimum. The number of hidden layer neurons selected in this work is based on the following selection principles. In the average concentration prediction of methane on the single light path algorithm simulation, the number of hidden layer neurons is selected as 14 to achieve a reasonable neural network self-study.

Combining the geometric model of the multi-view sensor to predict the concentration distribution of methane in the combustion field, the input signal x_i of the three-layer neural network model is the absorption spectra of water vapor with the central wavenumber of 7185cm^{-1} and 7444cm^{-1} bands on the pentagonal 120 detector arrays. In the actual calculation, the absorption spectra of 7185cm^{-1} to 7186.4cm^{-1} and 7443cm^{-1} to 7447cm^{-1} are selected to fit the integrated absorbance. Then the information represented by the neurons in the input layer is the integrated absorbance with the central wavenumber of the 7185cm^{-1} and 7444cm^{-1} bands on the 120 laser paths. The neurons in the output layer represent the methane concentration value at 625 grid points in the area to be measured. In order to realize the reasonable self-learning of the neural network, a single hidden layer neural network is selected for algorithm simulation.

Introducing the three-layer BP neural network structure into the TDLAS multi-component concentration measurement process, each iteration can be regarded as a training of the neural network. The process of the multi-component concentration prediction method based on the neural network model can be represented in Figure3.12:

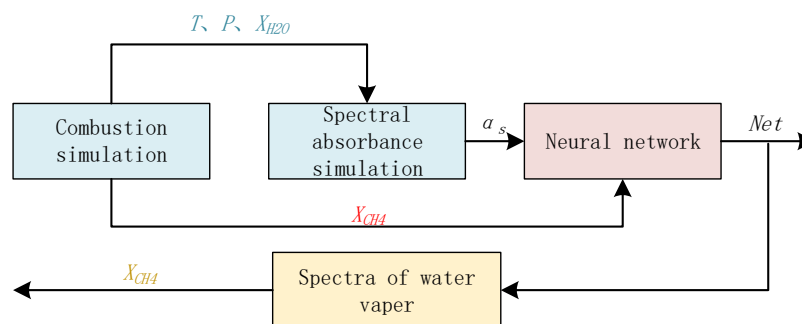


Figure3.12-Algorithm flowchart

The algorithm includes two processes. One is the learning and training process of the neural network. The CFD numerical simulation results are used to provide the input and output parameters of the neural network self-learning. According to the temperature, pressure, and component concentration distribution results of the combustion simulation, the absorption spectrum of water vapor is calculated as the input parameter for training the multi-component prediction neural network. The methane concentration distribution result obtained by the CFD simulation is used as the corresponding output parameter set. BP neural network uses the characteristics of automatically adjusting the weight of each layer during the self-learning process of the neural network to obtain the mapping relationship between the water vapor absorption spectrum and the methane concentration. The second part is to use the neural network completed by self-learning to perform the inversion of methane concentration. According to the water vapor absorption spectrum obtained by the experimental measurement, the neural network model completed by training is used to directly solve the concentration of methane on the same laser path or section.

In this work, the activation functions of the hidden layer and output layer are selected as follows:

$$f(x) = \tanh(x) = \frac{e^x - e^{-x}}{e^x + e^{-x}} \quad (1.8)$$

$$g(x) = \frac{1}{2}(1 + \tanh(x)) = \frac{e^x}{e^x + e^{-x}} \quad (1.9)$$

At the same time, in the self-learning process of the neural network, the weights of each layer of the neural network need to be initialized reasonably. Appropriate initial weights will help to improve the self-learning effect of the neural network. If the initial weight values are all set to be zero, the algorithm structure produces symmetry, and all the weight values in the neural network will be stable at the same value. At this time, the gradient descent algorithm of error back propagation loses its ability to optimize weights. Under normal circumstances, a smaller value should be randomly selected as the initial weight value of the neural network to break the symmetry of the algorithm, so as to ensure that the algorithm can update the weight during each iteration of the calculation.

3.2.2 Comparison and analysis of simulation results and original data of multi-component prediction methods

(1) The simulation calculation result of concentration of methane on a single laser path based on the prediction method of neural network

For the combustion parameters under ten operating conditions with the equivalent ratio obtained by CFD simulation between 1.6 and 2.5, Under each working condition, take the parameter information of 15 different height sections from 5 to 75cm to construct a parameter set for neural network training and learning. For 150 sets of data pairs of integrated absorbance and the average concentration of methane, 120 of them are randomly selected as

the training set of the neural network, and the remaining 30 sets are the test set. Taking the absorption spectrum information of the water vapor on the laser path at the center wave numbers of 7185 cm^{-1} and 7444 cm^{-1} respectively, that is, the integrated absorbance of the two spectral bands as the input parameters of the neural network, and the average concentration of methane on the corresponding path as the corresponding output parameters. The BP neural network is used to construct the mapping relationship between the absorption spectrum of water vapor and the average concentration of methane. Using the trained neural network to predict the average concentration of methane at different radial distances and different axial heights, the prediction results under noise-free and signal-to-noise ratios of 40 dB and 20 dB, respectively, are shown in Figure 3.13. Along the direction of the axial height of the flame center, the volume fraction of methane first increases briefly with the increase in height and then decreases continuously. At a height of 4.5 cm, the volume fraction of methane decreases to one third of the value at 0.5 cm. Under the simulation conditions of noise-free and signal-to-noise ratio of 40dB and 20dB respectively, the calculation results of the concentration prediction of methane method based on neural network show a trend consistent with the original data. The closer the position to the furnace surface, the greater the volume fraction of methane. On the contrary, the volume fraction of methane is smaller in the laser path near the top of the flame and passing through the central axis of the flame. Numerically, the relative error between the methane concentration calculated by the method proposed in this work and the original distribution does not exceed 0.5%, which has a good predictive effect.

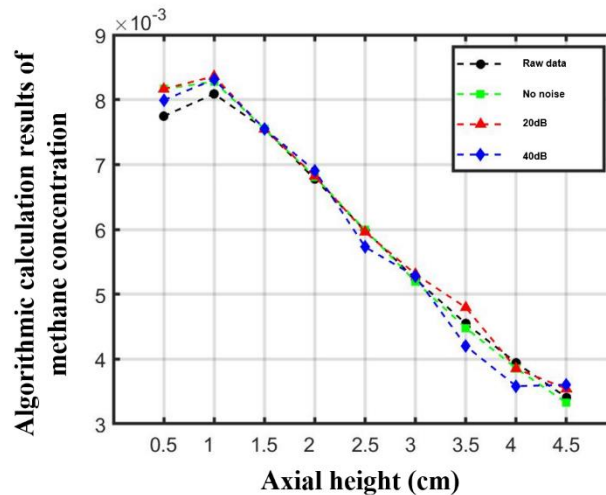


Figure 3.13-Algorithmic calculation results of methane concentration in a single optical path with different axial heights

According to the above figure, for the same laser path, the lower the signal-to-noise ratio simulation conditions, the larger the relative error between the methane volume fraction reconstructed by the neural network and the original value. In order to explore the trend of methane concentration in the radial direction of the flame, different positions are selected to perform the calculation algorithm proposed in this work. The network tool uses the

absorption spectrum of water vapor to calculate the average concentration of methane along the same path in the area to be measured. Under the simulation conditions of noise-free and signal-to-noise ratios of 40 and 20 dB, the closer the laser path to the combustion zone boundary, the lower the methane concentration, and the higher the methane concentration closer to the flame center. At different radial positions of the flame, the distribution of methane volume fraction is roughly a symmetrical structure with the flame centerline as the axis of symmetry. The lower the signal-to-noise ratio of the integrated absorption rate set in the simulation, the more unstable the prediction result of methane on the path based on the neural network algorithm, and the larger the relative error.

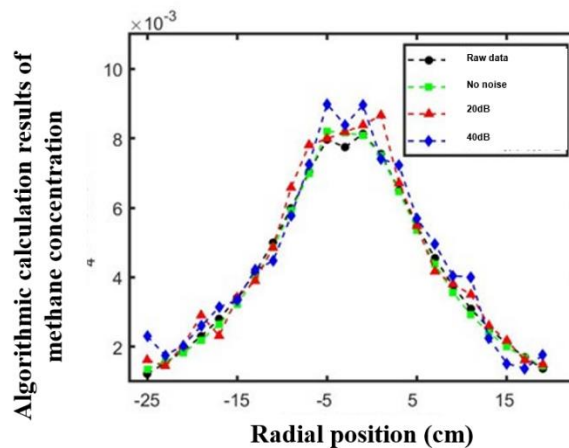


Figure3.14-Algorithmic simulation results of methane concentration in a single optical path with different radial distances

For the same laser path, although the reconstruction result of the algorithm can reflect that the average concentration of methane gradually decreases as the axial height increases, it gradually decreases with the radial position away from the flame center. But there is a relatively increasing error between the reconstructed result and the original result. In the case of a signal-to-noise ratio of 20 dB, the relative error can reach up to 0.5% at different axial heights of the flame and different axial positions at a height of 2 cm.

(2) The simulation calculation result of the average temperature on the single laser path based on the neural network prediction method

In order to explore the calculation effect of the neural network-based reconstruction method on the average temperature on the path, the absorption spectra information of water vapor on the laser path with the central wavenumber of 7185cm^{-1} and 7444cm^{-1} bands are used as the input parameters of the neural network, and the average temperatures on the corresponding path are used as the corresponding output parameters of BP neural network. The network is used to construct the mapping relationship between the absorption spectra of water vapor on the two spectral bands and the average temperature. After setting the training set and learning parameters, the self-learning of the neural network is carried out. The trained neural network is used to predict the average temperature of the laser path at different positions. The prediction results under noise-free and signal-to-noise ratios of 40dB and

20dB are shown in Figure3.15 and Figure3.16. The average temperature of the flame of a flat flame combustion furnace has a flat distribution range on the plane near the flame root and the plane of the flame top. The width of the flat area near the root of the flame is about 25 cm, and the flame temperature is high. On the plane near the top of the flame, the range of the flat temperature distribution is reduced, the width is about 18 cm, and the highest temperature is about 800K. Under the simulation conditions of noise-free and signal-to-noise ratio of 40 and 20 dB, respectively, the temperature calculation results on the laser path near the bottom of the flame and the top of the flame that passing through the center of the flame can derive that the lower the signal-to-noise ratio, the greater the relative error between the reconstructed result and the original result for the same laser path. The flame temperature is approximately an axisymmetric distribution. There is an obvious high temperature area at the flame position, and the temperature gradually decreases to room temperature near the edge of the flame. Under the simulation condition that the signal-to-noise ratio is 20dB, compared with the original distribution result given by the CFD method, the average temperature on the path is calculated by the neural network method, and the maximum relative error is within 0.5%.

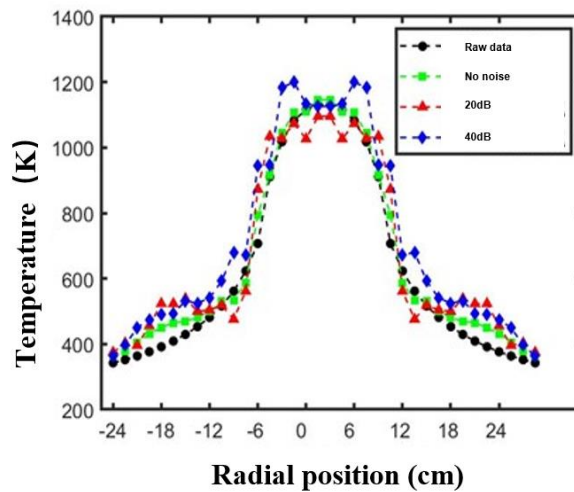


Figure3.15-Temperature simulation results of a single optical path at different radial positions of the flame when the measuring height is 2cm

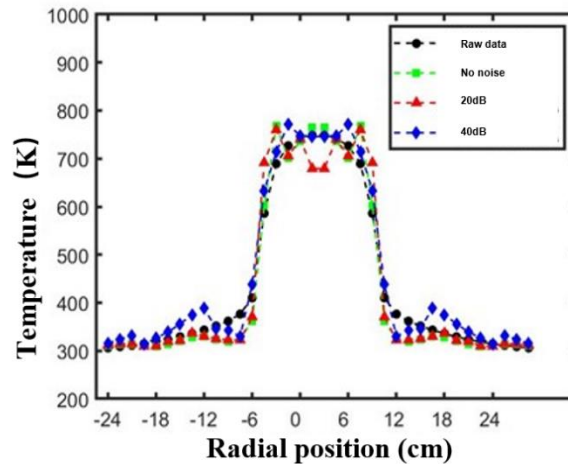


Figure3.16-Temperature simulation results of a single optical path at different radial positions of the flame when the measuring height is 5cm

(3) The simulation results of the two-dimensional distribution of methane concentration based on the prediction method of neural network

In order to improve the spatial resolution of the neural network-based concentration and temperature reconstruction method, the geometric model of the five-view sensor is used as the simulation object. The absorption spectrum information of the water vapor on the 120 laser paths at five angles at the center wavenumbers of 7185 cm^{-1} and 7444 cm^{-1} respectively in the two spectral bands, that is, the integrated absorption area of the two bands is used as the input parameter of the neural network. The two-dimensional distribution of methane concentration on the corresponding section is used as the corresponding output parameter. The BP neural network is used to construct the mapping relationship between the absorption spectra of water vapor and the average concentration of methane. The trained neural network is used to predict the average concentration of methane at different radial distances and different axial heights. The prediction results under noise-free and signal-to-noise ratios of 40 dB and 20 dB are shown in Figure3.17. When the equivalence ratio of methane and air is 2, at the cross section near the flame root, the excess methane is not fully burned and accumulates above the furnace surface. In the area to be measured where the length and height of the calculation domain are 8 cm, respectively, methane is evenly distributed on the furnace surface.

A neural network-based calculation method is used to reconstruct the concentration distribution of methane. Under the simulation condition of an equivalence ratio of 2, the reconstruction method proposed in this work is compared with the distribution results given by the original CFD. It can be seen that the proposed algorithm has an effect on the corresponding cross-section. The prediction result of the concentration distribution of methane is slightly smaller than the original distribution. But under the simulation conditions of no noise and a signal-to-noise ratio of 40 dB and 20 dB, the area of high concentration distribution and the edges of high and low concentration changes can be accurately predicted.

However, it is worth pointing out that under the simulation condition with a new construction ratio of 20 dB, the error between the distribution of methane calculated by the neural network-based concentration reconstruction method and the original distribution reaches 10%, and the overall value is too small. This may be caused by improper selection of parameters during neural network training.

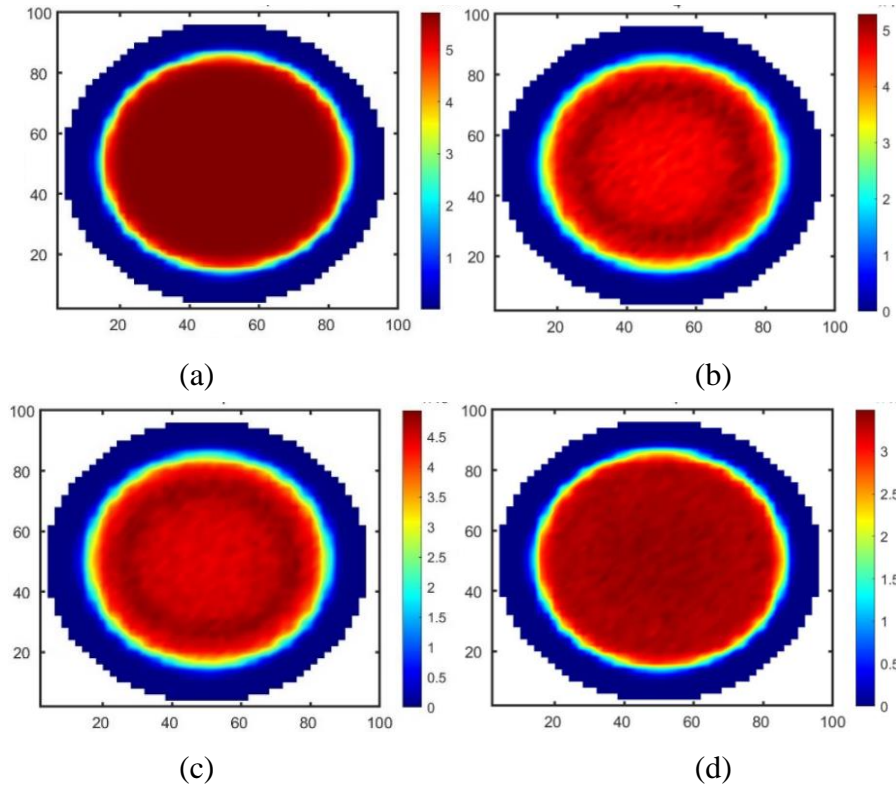


Figure3.17-Algorithmic calculation results of methane concentration distribution at the root of the flame (a) Methane concentration distribution given by CFD (b) Algorithm reconstruction result when no noise is added (c) Algorithm reconstruction results when the signal-to-noise ratio is 40dB (d) Algorithm reconstruction results when the signal-to-noise ratio is 20dB

When the equivalence ratio of methane and air is 2, incompletely burned methane gathers above the flame due to the influence of airflow turbulence and molecular motion in the cross section near the top of the flame. The absorption spectrum information of the water vapor on the 120 laser paths corresponding to the five angles through the flame surface at the central wavenumbers of 7185 cm^{-1} and 7444 cm^{-1} respectively is used as the input of the neural network to predict the methane concentration on the corresponding cross-section two-dimensional distribution. The results are shown in the Figure3.18. It can be seen that at the top of the flame where the methane concentration is small and the high concentration range is small, the prediction results of the proposed algorithm for the concentration distribution of methane on the corresponding cross section are numerically better than the original distribution, and the range of high concentration distribution area can be accurately predicted.

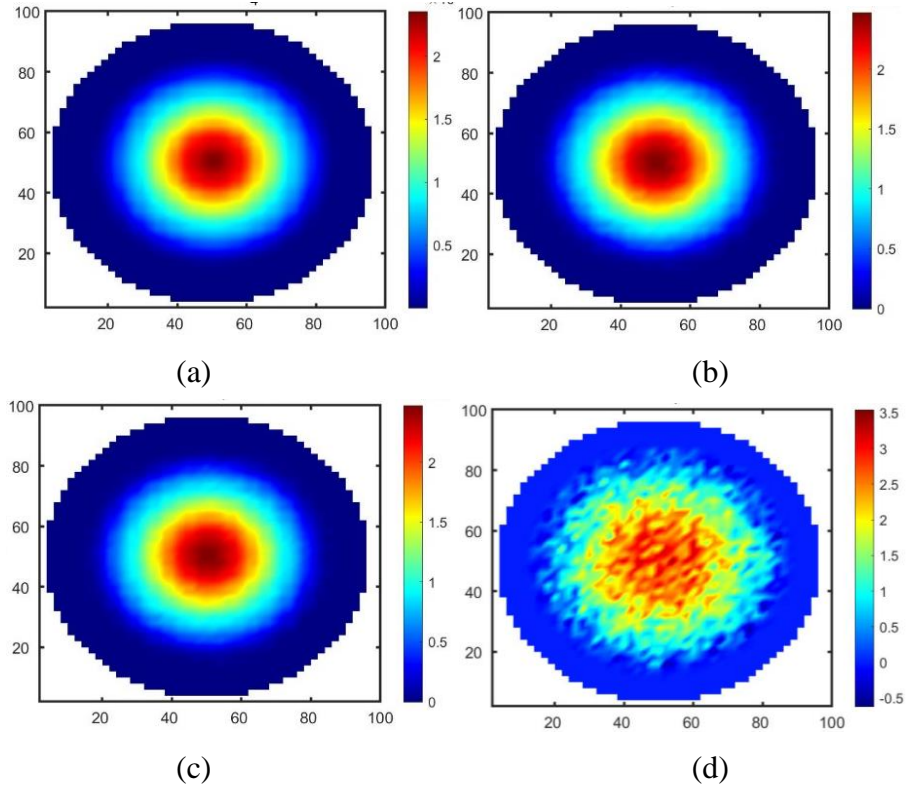


Figure3.18 -Algorithmic calculation results of methane concentration distribution at the top of the flame (a) Methane concentration distribution given by CFD (b) Algorithm reconstruction result when no noise is added (c) Algorithm reconstruction results when the signal-to-noise ratio is 40dB (d) Algorithm reconstruction results when the signal-to-noise ratio is 20dB

For different positions at the bottom and top of the flame, a neural network is used to directly reconstruct the concentration distribution of methane using the absorption spectra of water vapor. Under different noise levels, it can reflect the approximate area of the high and low concentration distribution. However, compared with the original distribution of the prediction results under different signal-to-noise ratios, the mean square error is shown in the figure. Under the condition of the signal-to-noise ratio of 60dB, the reconstruction error based on the neural network method is very small, almost close to zero, but under the condition of the signal-to-noise ratio of 20 dB, the relative error between the reconstructed distribution and the original distribution reaches 0.3.

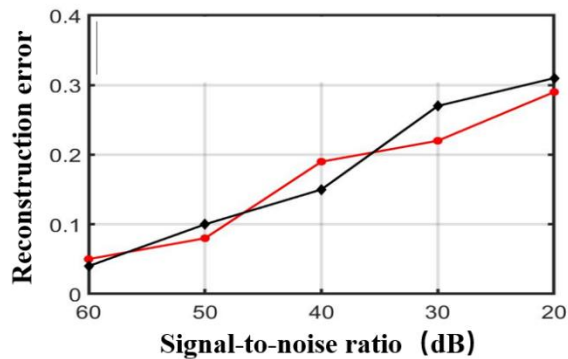


Figure3.19-Reconstruction error under different signal-to-noise ratio conditions

Considering that in actual measurement, the Mckenna combustion furnace is located at any position of the five-view sensor, and the spectral information detected by the detector array is simulated and calculated. The integrated absorbance at each angle is calculated after linear fitting. Neural network is used to predict the two-dimensional distribution of the temperature in the combustion area to be measured. When the equivalence ratio of fuel and air is set to 2, the distribution of temperature is shown in Figure3.20. When the equivalence of methane and air ratio is 2, the flat flame combustion furnace is located at any position in the area to be measured by the five-view sensor. The absorption spectra information of water vapor in the spectral bands with the central wavenumber of 7185 cm^{-1} and 7444 cm^{-1} on the 120 laser paths corresponding to the five angles through the flame surface are taken as the input parameters of the neural network to predict the distribution of methane on this section. It can be seen that when the flat-flame burner is located at any position in the measurement area of the five-angle sensor, the neural network-based prediction method proposed in this work has good calculation results for the two-dimensional distribution of methane. This method can not only accurately calculate the area and position of the high and low concentration distribution, but also the calculation results are numerically consistent with the original data given by the CFD simulation.

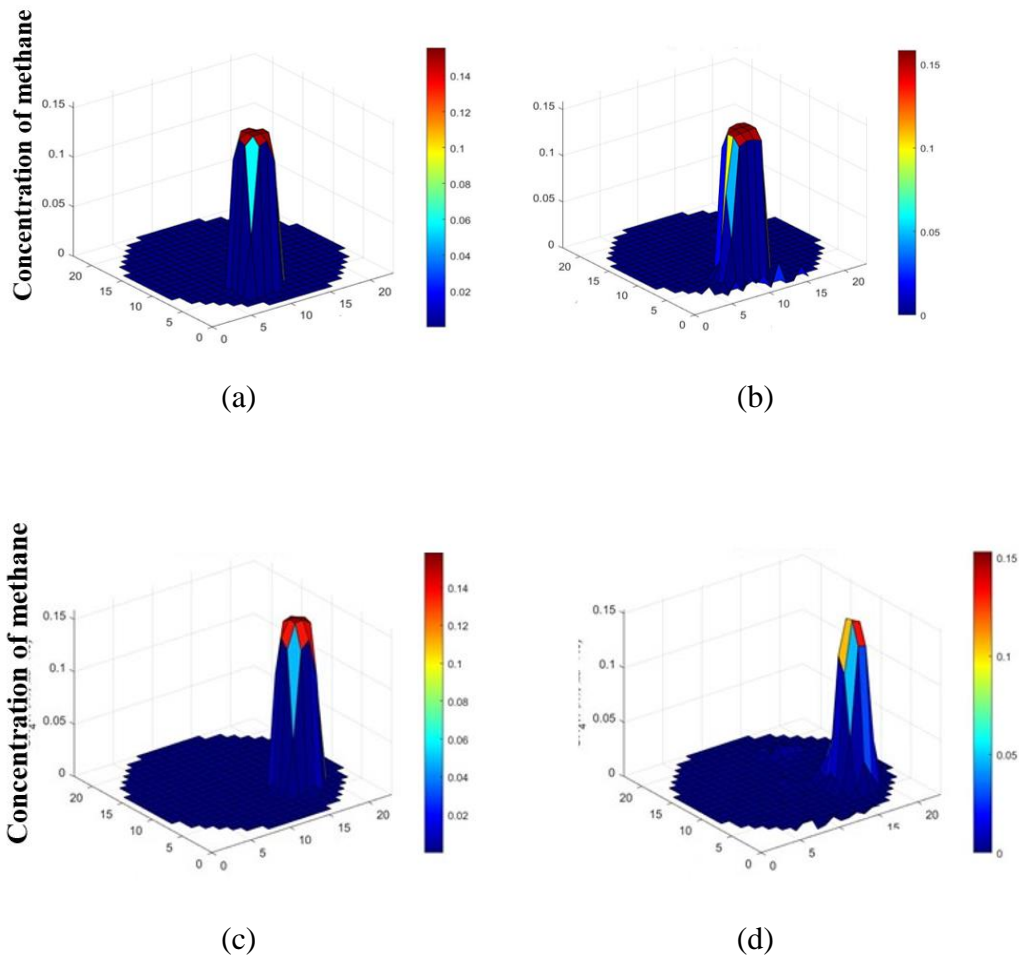


Figure3.20-Simulation results of methane concentration when the burner is at any position of the sensor(a) Distribution of methane concentration given by CFD (b) Algorithm reconstruction results when there is no noise(c) Distribution of methane concentration given by CFD (d) Algorithm reconstruction results when there is no noise

(4) Simulation results of two-dimensional temperature distribution using neural network-based algorithms

Taking the geometric model of the five-angle sensor as the simulation object, the absorption spectra information of the water vapor at the center wavenumbers of 7185cm^{-1} and 7444cm^{-1} on the 120 laser paths at five angles is simulated. The integrated absorption area of the two bands is used as the input parameter of the neural network, and the corresponding cross-sectional temperature distribution is used as the output parameter. The BP neural network is introduced to construct the mapping relationship between the absorption spectrum of water vapor and the temperature distribution. The trained neural network is used to predict the distribution of temperature at different radial distances and axial heights of the flame. The prediction results under noise-free and signal-to-noise ratios of 40dB and 20dB are shown in Figure3.21:

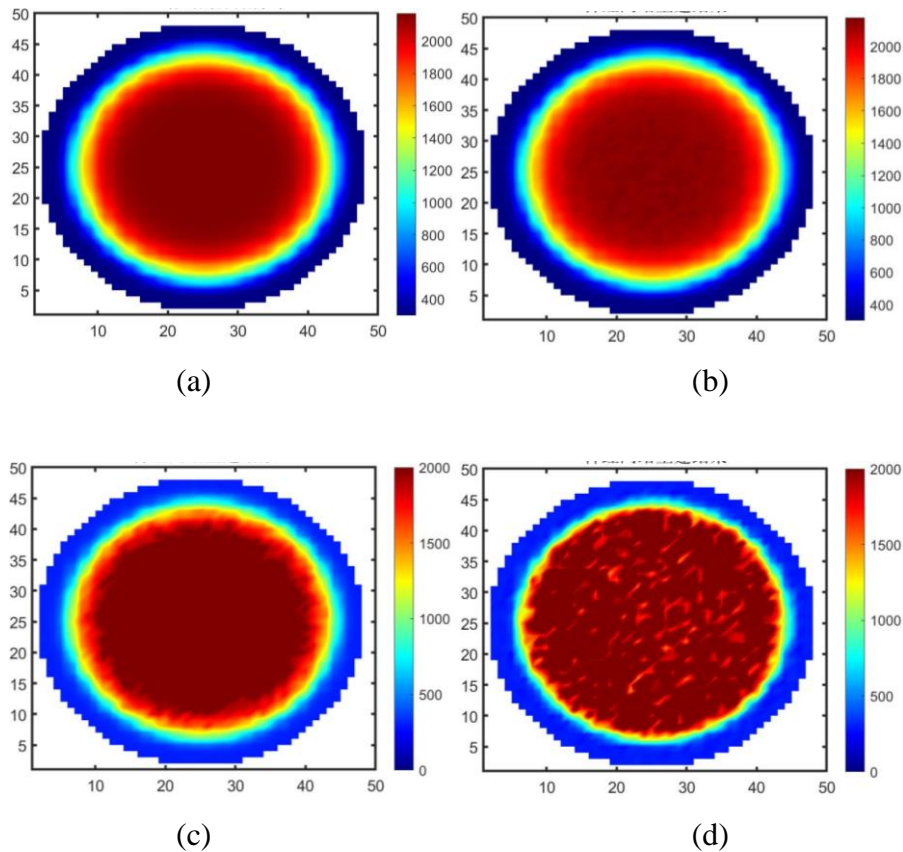


Figure3.21-The simulation results of the flame root temperature distribution algorithm(a) Temperature distribution given by CFD (b) Algorithm reconstruction result when no noise is added(c) Algorithm reconstruction results when the signal-to-noise ratio is 20dB (d) Algorithm reconstruction results when the signal-to-noise ratio is 40dB

Under the working condition of equivalence ratio of 2, the original distribution of the temperature field near the top of the flame is shown in the figure below. Without adding

noise and the signal-to-noise ratio is 40dB and 20dB respectively, the neural network method is used to carry out the temperature distribution. In noise-free condition, the reconstruction results given by the neural network method are relatively large in the high temperature zone and the temperature is higher than the original distribution, but it can accurately reflect the trend of high and low temperature changes and has a good reconstruction effect on the edge of the temperature boundary. When the signal-to-noise ratio is 40 dB and 20 dB respectively, the neural network-based algorithm has a poor reconstruction effect on the edge of the temperature boundary. The edge of the reconstructed temperature appears blurred, which cannot reflect the trend of temperature changes perfectly. However, it can reflect the range of high and low temperature zones in the combustion field.

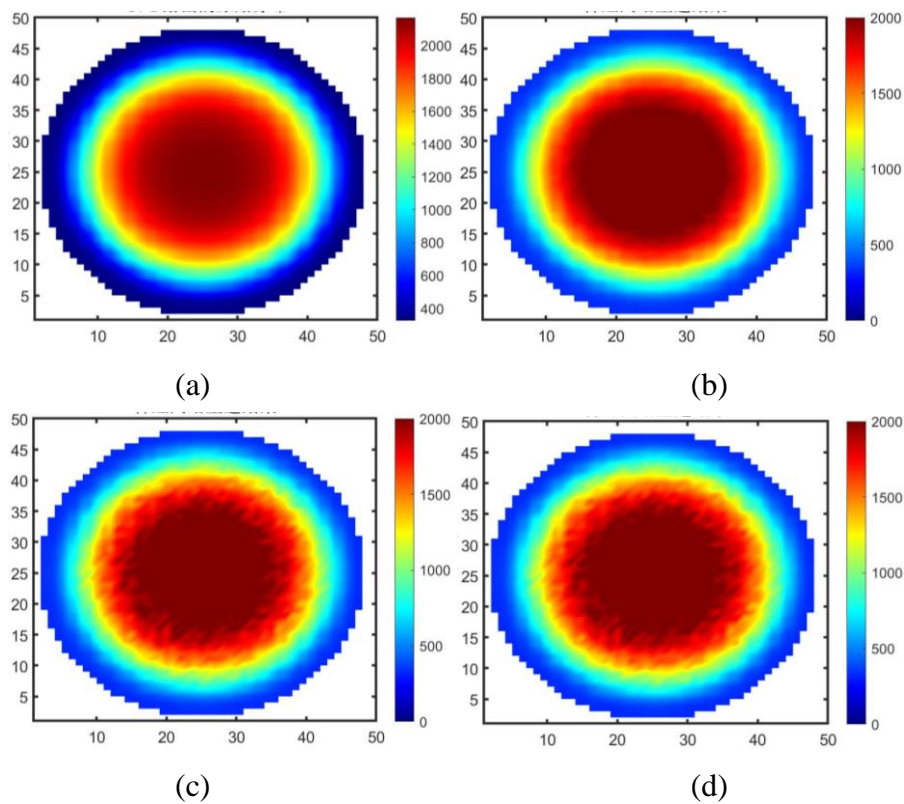


Figure3.22-Simulation results of the temperature distribution algorithm at the top of the flame(a) Temperature distribution given by CFD (b) Algorithm reconstruction result when no noise is added(c) Algorithm reconstruction results when the signal-to-noise ratio is 20dB (d) Algorithm reconstruction results when the signal-to-noise ratio is 40dB

For different positions at the bottom and top of the flame, the temperature distribution is directly reconstructed using the absorption spectra on two spectral bands of water vapor by means of the neural network. Under different noise levels, the general area of the high and low temperature distribution can be reflected. In the case of different signal-to-noise ratios, the mean square error of the prediction result compared with the original distribution is shown in the figure. When the signal-to-noise ratio is 60 dB, the reconstruction error based on the neural network method is very small, and when the signal-to-noise ratio is 20 dB, the

reconstruction error reaches 0.25. As the signal-to-noise ratio gradually decreases, the mean square error of reconstruction tends to gradually increase.

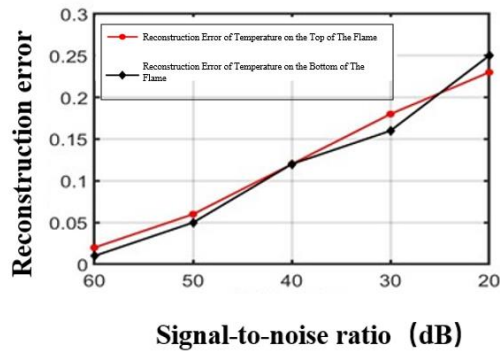
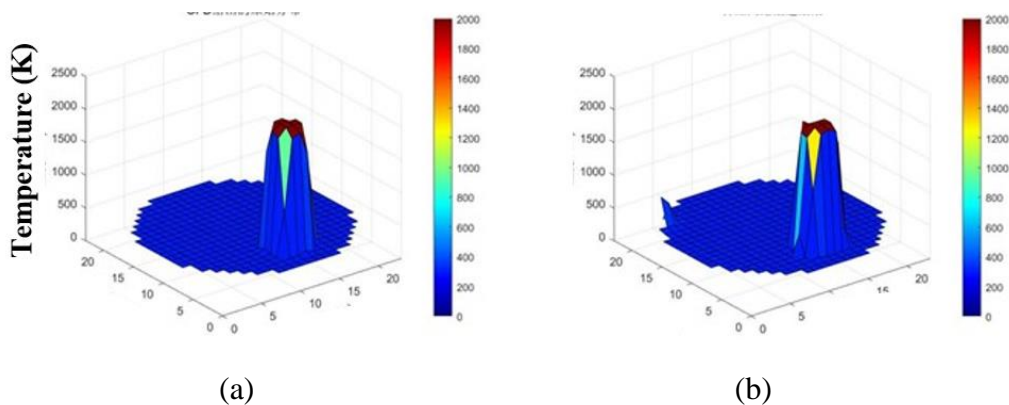


Figure3.23-Relative error of temperature reconstruction under different signal-to-noise ratio conditions

Considering that in the actual measurement, the Mckenna combustion furnace is located at any position of the five-view sensor. under these circumstances the spectral information detected by the detector array is simulated and calculated. The integrated absorbance at each angle is calculated after the linear fitting is performed for each transmitted light intensity signa. The two-dimensional distribution of the temperature is predicted using the neural network tool. The flat flame burner is located at any position within the measuring area of the five-view sensor. When the equivalent ratio of methane to air is 2, the absorption spectra of the water vapor on the 120 laser paths corresponding to the five angles through the flame surface at the central wavenumber of 7185 cm^{-1} and 7444 cm^{-1} are used as the input parameters of the network self-learning, The corresponding cross-sectional temperature distribution are the output parameters to perform the self-learning of the neural network. Using the trained neural network to estimate the two-dimensional temperature distribution, it can be seen that when the flat-flame burner is located at any position in the area by the five-view sensor, the neural network-based prediction method proposed in this work has good calculation results for the distribution of the two-dimensional temperature field. This method can not only accurately calculate the size and location of the high temperature area, but also the temperature calculation results are numerically consistent with the original data given by the CFD simulation.



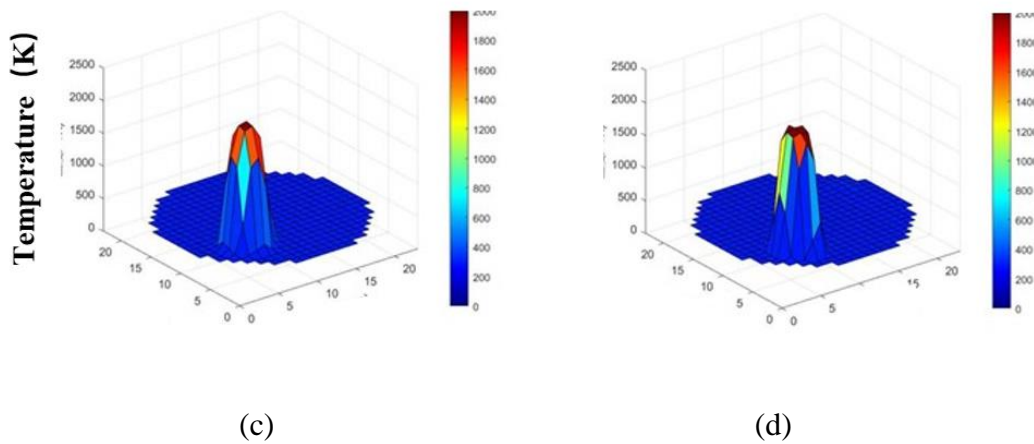


Figure3.24-Temperature simulation results when the burner is at any position of the sensor(a) Temperature distribution given by CFD (b) Algorithm reconstruction result when no noise is added(c) Temperature distribution given by CFD (d) Algorithm reconstruction result when no noise is added

Using the integrated absorbance of water vapor on 120 laser paths at five angles to predict the concentration distribution of methane and the distribution of temperature when the burner is located at any position of the sensor. the mean square error of the superimposed distribution under different signal-to-noise ratio conditions are as shown in Figure3.25. As the signal-to-noise ratio gradually decreases, the mean square error between the temperature and concentration distribution predicted by the reconstruction method based on neural network and the original distribution gradually increases.

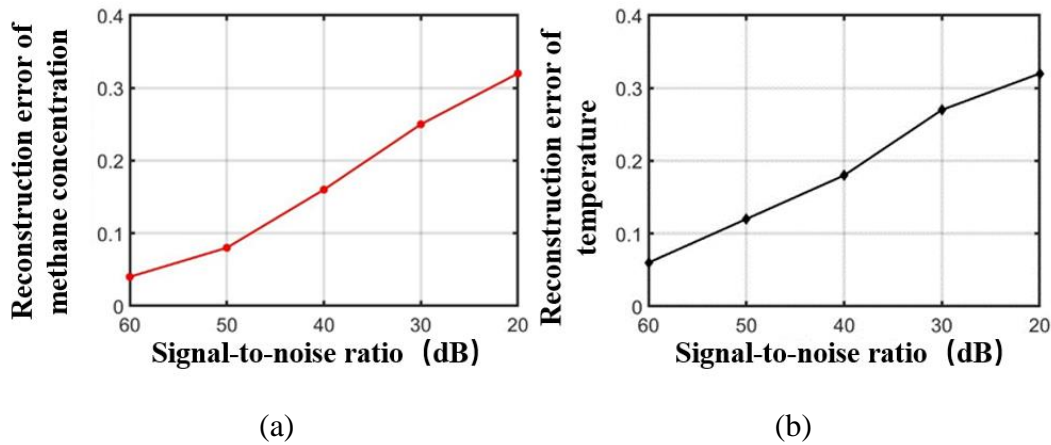


Figure3.25-Reconstruction error of different signal-to-noise ratio

(a) Reconstruction error of temperature distribution under different signal-to-noise ratio (b) Reconstruction error of concentration distribution under different signal-to-noise ratio

3.3 Summary of this chapter

This chapter firstly uses CFD simulation software to give the spatial distribution of the combustion field parameters of the premixed flame of methane and air based on the Mckenna burner under different working conditions. In the simulation process, the combustion area reached by the ideal axis symmetry is simplified into a simple two-dimensional computational domain object, combined with the GRI Mesh3. Chemical reaction kinetic mechanism model and FLUENT's powerful ability to simulate combustion reactions to simply and intuitively Two-dimensional distribution of various combustion parameters.

On the basis of CFD combustion simulation, combined with the geometric model of the average temperature and gas component concentration measurement single optical path, the absorption spectra of water vapor in the combustion environment based on the Mckenna burner is simulated forward. When solving the distribution information of the combustion parameters, combined with the geometric model of the two-dimensional five-view sensor, the absorption spectra of the water vapor molecules in the combustion field at multiple angles in the regular pentagonal coverage area is solved. With the help of neural network tools, mining the numerical relationship between the water vapor generated by combustion under different working conditions and the temperature and the distribution of the temperature under the working conditions, so as to realize the distribution of temperature, water vapor concentration and methane concentration can be solved by using water vapor absorption spectrum information. After completing the simulation of the TDLAS multi-component concentration measurement algorithm based on the neural network with a few spectral lines, the accuracy of the algorithm was verified by the training set. In the verification experiment of single optical path average concentration inversion, the signal-to-noise ratio was 40dB, In the case of 20dB, the calculation result of the algorithm can accurately reflect the trend that the average concentration of methane on the laser path gradually decreases as the axial height of the flame increases and the radial distance increases. In the process of reconstructing the two-dimensional distribution of methane and temperature using the neural network-based algorithm, the absorption spectra of water vapor obtained by the multi-angle sensor detector array are used to directly reconstruct the distribution of methane and temperature in the combustion field to be measured. It can be seen from the simulation results that the simulation results of the neural network-based multi-component concentration prediction method are compared with the original CFD simulation results. The proposed algorithm can accurately reflect the high and low temperature distribution area and the trend of change in the combustion zone. Under the condition that the signal-to-noise ratio is 40dB and 20dB respectively, although the reconstruction results are fuzzy in the boundary of temperature change, the prediction of high temperature and high concentration distribution area is more accurate. The relative error of the prediction of two-dimensional distribution of temperature and concentration of methane is in within 10%.

Chapter 4

Multi-component Concentration Measurement Experiment and Algorithm Feasibility Verification

In order to verify the accuracy of the multi-component concentration prediction algorithm of TDLAS with absorption spectra of a few components based on neural network proposed in this thesis, the single-path laser absorption spectrum measurement system is used to carry out multi-component concentration measurement experiments. The experiment uses time-division multiplexing to control three excitations with center wavelengths of 7185 cm^{-1} , 5938 cm^{-1} , and 7444 cm^{-1} emitters laser at different times. In the experiment, the absorption spectrum of the water vapor produced by the premixed combustion of the flat flame combustion furnace, as well as the concentration of water vapor and the concentration of methane were measured. The algorithm proposed by the subject is used to calculate the concentration of methane, and the calculation result is compared with the experimental measurement result, which proves the feasibility of the algorithm proposed in this thesis.

In this chapter, firstly, the system equipment of single optical path multi-component measurement experiment is introduced. Specifically including the core modules of laser controlling, data acquisition and gas flow rate controlling. Then, the process of experimentally measuring the water vapor absorption spectra is introduced. The average temperature on the laser path is calculated and compared with the temperature measured by the thermocouple. The accuracy of the method for measuring the temperature of the laser absorption spectrum is analyzed.

4.1 Measurement experiment of the average temperature and the average concentration of multiple components on a single laser path in the combustion field

4.1.1 Temperature and multiple component concentration measurement experimental system

The experimental device is shown in Figure4.1. The experiment adopts time-division multiplexing method to control three lasers to emit light in a time-sharing manner using a

laser controller. The three-band lasers are divided into two beams after passing through two two-to-two fiber couplers. One laser beam passes through the collimator lens and is received by the detector through the area to be measured, and the transmitted light intensity signal of the component to be measured is obtained. Another laser beam passes through the etalon to obtain the relationship between the laser wavelength and time. In the experiment, a B-type thermocouple is used to measure the flame temperature, which is used as a control for the experimental temperature measurement results. The following is a brief introduction of each part of the experimental device:

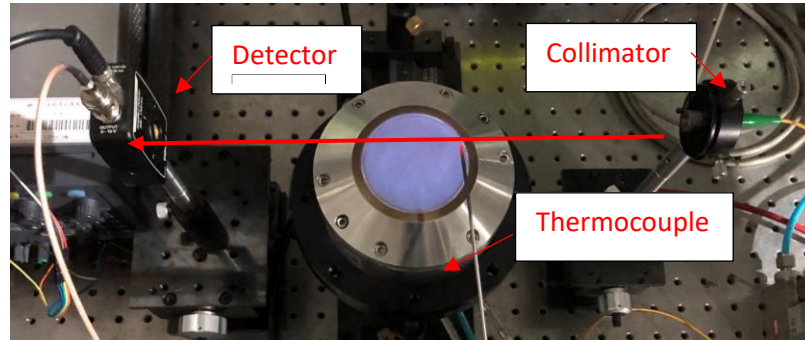


Figure4.1-Single optical path experimental system diagram

(1) Laser control module

The laser control components mainly include the laser core board and the laser. The host computer issues instructions to control the laser core board to turn on or off the laser through the USB interface. Through the CPCI bus on the back panel of the chassis, all laser core boards receive the instructions and complete the corresponding actions. Distributed feedback semiconductor lasers have a built-in Bragg grating. The single-mode output of the laser is realized through the frequency-selective characteristics of the grating. It has the advantages of large output optical power, small divergence angle, extremely narrow spectrum, high modulation rate, and suitable for long-distance communication. It is also widely used in TDLAS combustion parameter measurement. In this experiment, two distributed feedback laser with a center frequency of 1391.8 nm and 1343.4 nm are used as the light source to measure the absorption spectra of water vapor. The wavelength scanning ranges of the two lasers were 7185.3 cm^{-1} to 7186.2 cm^{-1} and 7444.1 cm^{-1} to 7445.1 cm^{-1} , respectively. A distributed feedback laser with a center wavelength of 1684nm was selected as the laser light source to detect the concentration of methane in the combustion field, and the wavelength scanning range is from 5937.2 cm^{-1} to 5939 cm^{-1} . The laser control module used in the experiment is shown in Figure 4.2 below. The laser controllers from left to right control the scanning time and waveband of the lasers with center wavelengths of 1391.8 nm, 1684 nm and 1343.4 nm respectively.

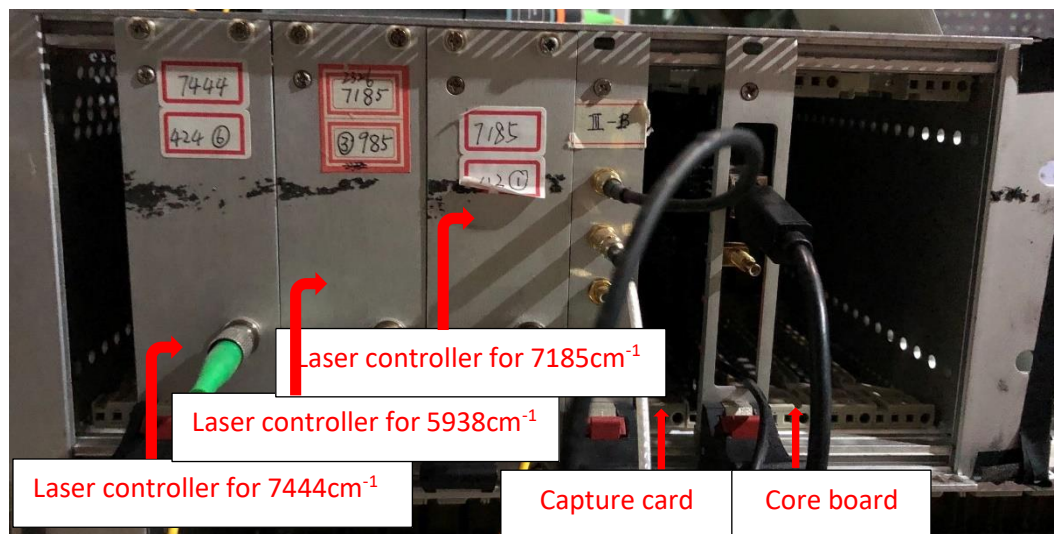


Figure 4.2- Laser control module and data acquisition module

The output wavelength of DFB laser is mainly adjusted by temperature control and current control for coarse and fine adjustment respectively. Through FPGA programming, different voltage values are applied to the different pins of the DFB laser to control the laser to output a stable and variable voltage, so as to realize the laser scanning the laser of the specified band. For the direct absorption method, the output wavelength and performance are modulated to make the output laser wavelength appear in the form of a sawtooth wave, sweeping across the absorption spectrum of the component to be measured. The three lasers used in the experiment use time division multiplexing to output scanning lasers. The light intensity spectrum with the center frequency of 1391.8 nm and 1684nm are scanned firstly, and then the spectra with the center frequency of 1343.4nm is scanned. The three laser beams are coupled by a fiber coupler and transmitted through the fiber and collimated. After passing through the gas to be measured, the transmitted light intensity signal is received by the photodetector.

(2) Signal acquisition and data processing module

A photodetector is used to convert the optical signal into an electrical signal. In the experiment, the PDA10DT-EC photodetector produced by THORLABS is used to detect the laser light intensity signal of the three bands. After the detector detects the light intensity signal, it is converted into an electrical signal, which is transmitted to the upper computer through the acquisition card. The data acquisition module used in the experiment includes the acquisition card and the core board of the acquisition card. The acquisition card has four acquisition channels, the storage capacity is 1GB, and the acquisition rate of each acquisition channel is 20 MS/s. The core board of the capture card receives instructions from the host computer through USB, and controls the capture card to switch between different working states through the CPCI bus on the back panel of the chassis. The capture card core board controls the capture card to perform data collection and upload operations. The capture card uploads the collected data to the core board through the CPCI bus on the back panel of the chassis, and then uploads the core board to the host computer through the USB interface. As

shown in Figure 29, the data acquisition board used in the experiment has four channels, of which channel 1 is the trigger signal from the core board, and channel 2 is used to collect the transmitted light intensity signal obtained by the photodetector.

(3) Gas flow controller

In the experiment, a three-channel mass flow controller is used to control the combustion conditions of the McKenna burner, as shown in Figure 4.3. The gas mass flow meter directly measures the mass flow of the gas medium passing through the flow meter, and directly displays the current flow rate of the gas medium on the display screen, which is convenient for users to adjust and control. In the experiment, we keep the air flow rate of the first channel on the left at 10.6 L/min, adjust the flow rate of methane to 2.23 L/min, 2.4 L/min, and 2.56 L/min to achieve the change of the equivalent ratio of methane to air, and ensure that the nitrogen flow rate is 10.0 L/min, protect the combustion from the turbulence of the surrounding airflow, thus forming a stable burning flame.



Figure 4.3-Mass flow controller

4.1.2 Measurement of water vapor absorption spectrum and calculation of average temperature and analysis of measurement results

(1) Measurement of Water Vapor Absorption Spectrum on a Single Laser Path in Combustion Field

The experimental system is shown in Figure 4.4. In the experiment, three DFB lasers with center wavenumbers of 7185 cm^{-1} , 7444 cm^{-1} and 5938 cm^{-1} were used as the light source. The three lasers were divided into two paths by two two-to-two fiber splitters and driven to generate characteristic absorption covering water vapor and methane. One laser beam passes through the etalon after passing through the collimator lens to obtain the relationship between the laser output wavelength and time. Another laser beam exits a parallel beam after passing through the collimator, the transmitted light after passing through the beam splitter passes through the flame area to be measured, and the transmitted light intensity signal is received by the photodetector. The collimating mirror and the detector are arranged as close as possible on both sides of the flat flame combustion furnace to reduce the influence of the absorption of components outside the flame area on the measurement results. The three

lasers of different wavelength bands adopt time-division multiplexing, scanning in time-sharing, and the absorption signals of water vapor at the central wavenumbers of 7185 cm^{-1} and 7444 cm^{-1} spectral bands and the absorption signal of methane at 5938 cm^{-1} are obtained.

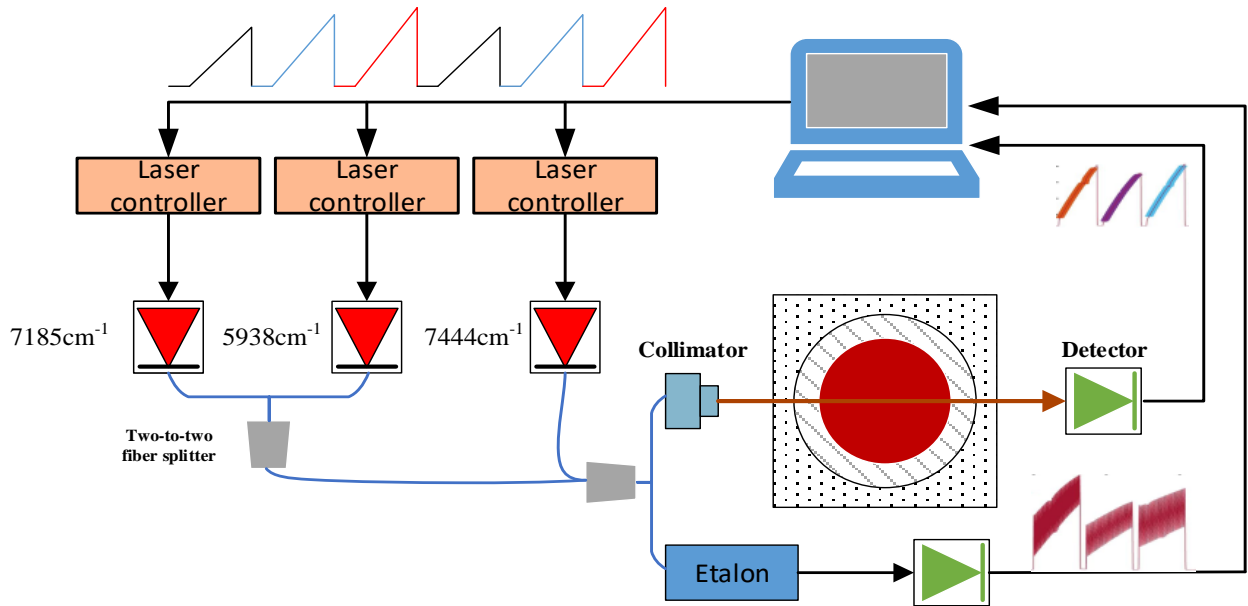


Figure 4.4- Experimental system diagram of single optical path

In the actual measurement process, the flame is produced by a McKenna burner, which is fixed on a horizontal stage with a displacement control accuracy of 1mm. The absorption spectra of water vapor on the laser path at different positions in the radial direction of the flame can be measured by controlling the horizontal displacement of the stage. The collimator and detector used in the experiment are placed on two vertical height displacement stages, and the height of the collimator and detector is adjusted jointly to realize the measurement of the water vapor absorption spectra on the laser path at different heights of the flame axis.

The mass flow meters are used in the experiment to control the flow of methane and air respectively and realize the measurement of the absorption spectra of water vapor under the combustion conditions with the equivalent ratio of 2.15, 2.3, and 2.5. In the experiment, a three-channel mass flow controller is used to control the methane flow to 2.23 L/min, 2.4 L/min and 2.56 L/min, the air flow to 10.6 L/min. The flow of nitrogen protector is set to 15.5 L/min to protect the flame from affecting by the surrounding air. The absorption spectra of water vapor at the radial positions of 0.5 cm, 1 cm, 1.5 cm, 2 cm, 2.5 cm and 3 cm, the axial height from the burner plane is 2 cm, 2.5 cm, 3 cm, 3.5 cm, 4 cm and 4.5 cm under different oxygen-lean combustion conditions were measured. And then the direct absorption method was used to calculate the average temperature on the corresponding laser path.

When measuring the absorption spectra of water vapor and methane on the same optical path simultaneously, three lasers were controlled to emit light in a certain time sequence by time division multiplexing method to obtain the scan signals of the absorption spectra on the three spectral bands of 50 sampling periods. As is shown in Figure 4.5, the yellow line represents

the transmitted light intensity signal on the three wavebands, and the blue line is the etalon signal on the corresponding waveband. In a sampling period, the signal from left to right is the direct absorption signal modulated by sawtooth wave with a frequency of 20k Hz. Following by the absorption signal of water vapor at the center wave number of 7185 cm^{-1} , the absorption spectra of methane at the center wave number of 5938 cm^{-1} and the absorption water vapor on the wavelength band with the center wavenumber of 7444 cm^{-1} are as shown. The signal in the second half represents the wavelength modulated absorption signal on the spectral bands with center wavenumber of 7185 cm^{-1} , 5938 cm^{-1} , and 7444 cm^{-1} under high-frequency sine wave modulation. In the experiment, the spectra signal of water vapor and methane obtained by direct absorption was used to invert and calculate the combustion parameters.

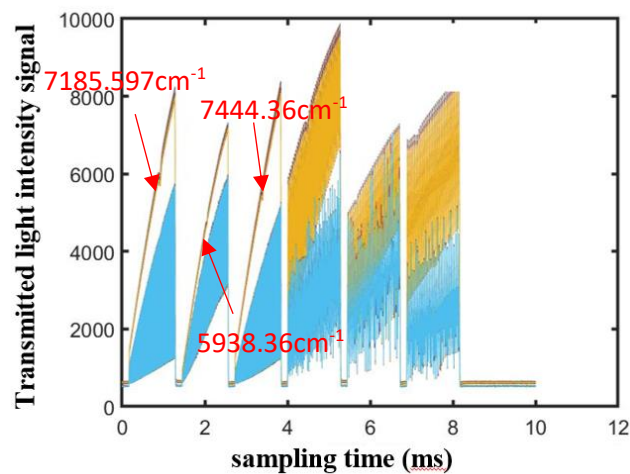


Figure4.5-Transmitted light intensity signal

In one scanning period, the wavelength scanning frequency of the DFB laser is 5k Hz. Each harmonic signal lasts 0.15 ms and the phase difference of the scanning signal is π . The ADC with the sampling frequency of 20K Hz is used to obtain the transmission signal within 0.4 ms. As is shown in the figure above, the light intensity signal and the etalon data are collected and then transmitted to the host computer through the chassis backplane. According to the etalon signals on the two spectral bands, the relationship between the wavelength and the time can be obtained. The direct absorption method is used to calculate the average temperature, and the transmitted light intensity and etalon signal in a period are intercepted. The result is shown in Figure4.6, figure (a) is the transmitted light intensity signal corresponding to the three wavebands, and figure (b) is the etalon signal corresponding to the three wavebands. The absorption spectra of the corresponding components in the frequency band were measured respectively to calculate the integrated absorbance at the corresponding center frequency, and further calculate the temperature and concentration.

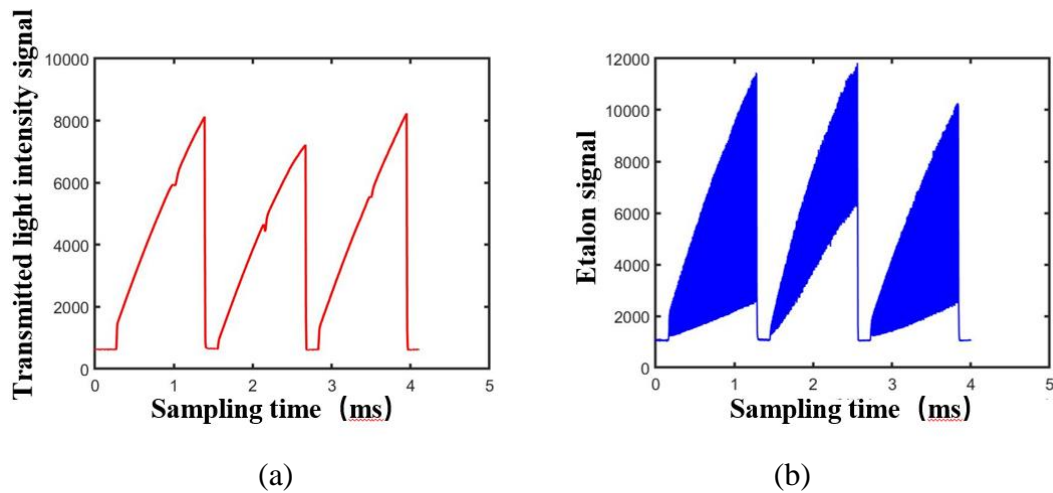


Figure 4.6-Light intensity signal and etalon signal in one scanning period (a) Transmitted light intensity signal (b) Etalon signal

As is shown in Figure 4.7, in the process of data processing, the three-segment transmitted light intensity signal of sawtooth scanning is truncated. Subtracting the DC bias signal corresponding to zero light intensity to obtain the transmitted light intensity signal of each spectral band.

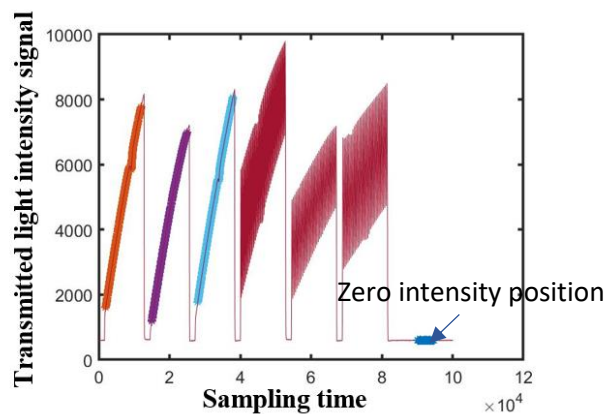


Figure 4.7-Sectional truncation of the light intensity signal

The transmitted light intensity signals at the two spectral bands with the central wavenumber of 7185cm^{-1} and 7444cm^{-1} , which have been processed by subtracting the zero offset, are truncated and baseline fitted respectively. The results are shown in Figure 4.8. At the frequencies corresponding to the center wavenumbers of 7185 cm^{-1} and 7444 cm^{-1} , corresponding to the two larger absorption peaks of water vapor. The data in the two intervals before and after the absorption peak are selected respectively to perform baseline fitting to calculate the spectral absorbance on the two spectral bands.

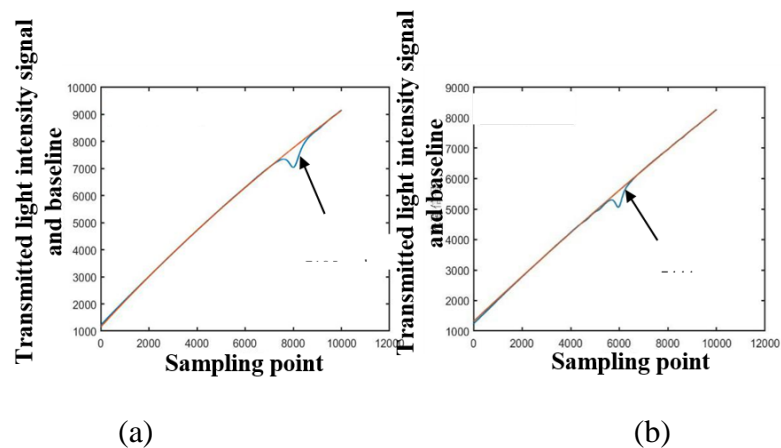


Figure 4.8 - The transmitted light intensity and baseline of the spectral band with the central wavenumber of 7185 cm⁻¹ and 7444 cm⁻¹ (a) The transmitted light intensity and baseline of the spectral band with the central wavenumber of 7185 cm⁻¹ (b) The transmitted light intensity and baseline of the spectral band with the central wavenumber of 7444 cm⁻¹

After obtaining the transmitted light intensity and the baseline signal, the Gauss-Newton nonlinear fitting method is used to obtain the fitting parameters of the Voigt line type. After obtaining the fitting parameters, the integral absorbance, Gaussian half-width and Lorentz half-width will be further got. The linear fitting results of the transmitted light intensity on the two bands are shown in Figure 4.9. According to the spectral simulation results performed in the previous chapter, there is a small side peak near the main absorption peak of the center wavenumber 7444 cm⁻¹. In the process of linear fitting, we choose to avoid the light intensity data of the side peak position for linear fitting to reduce the calculation error.

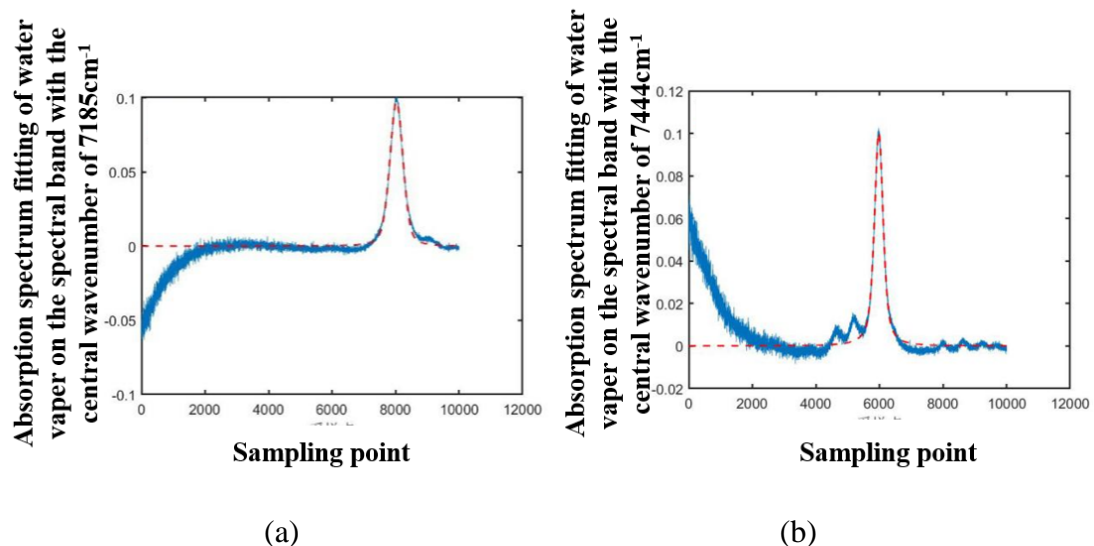
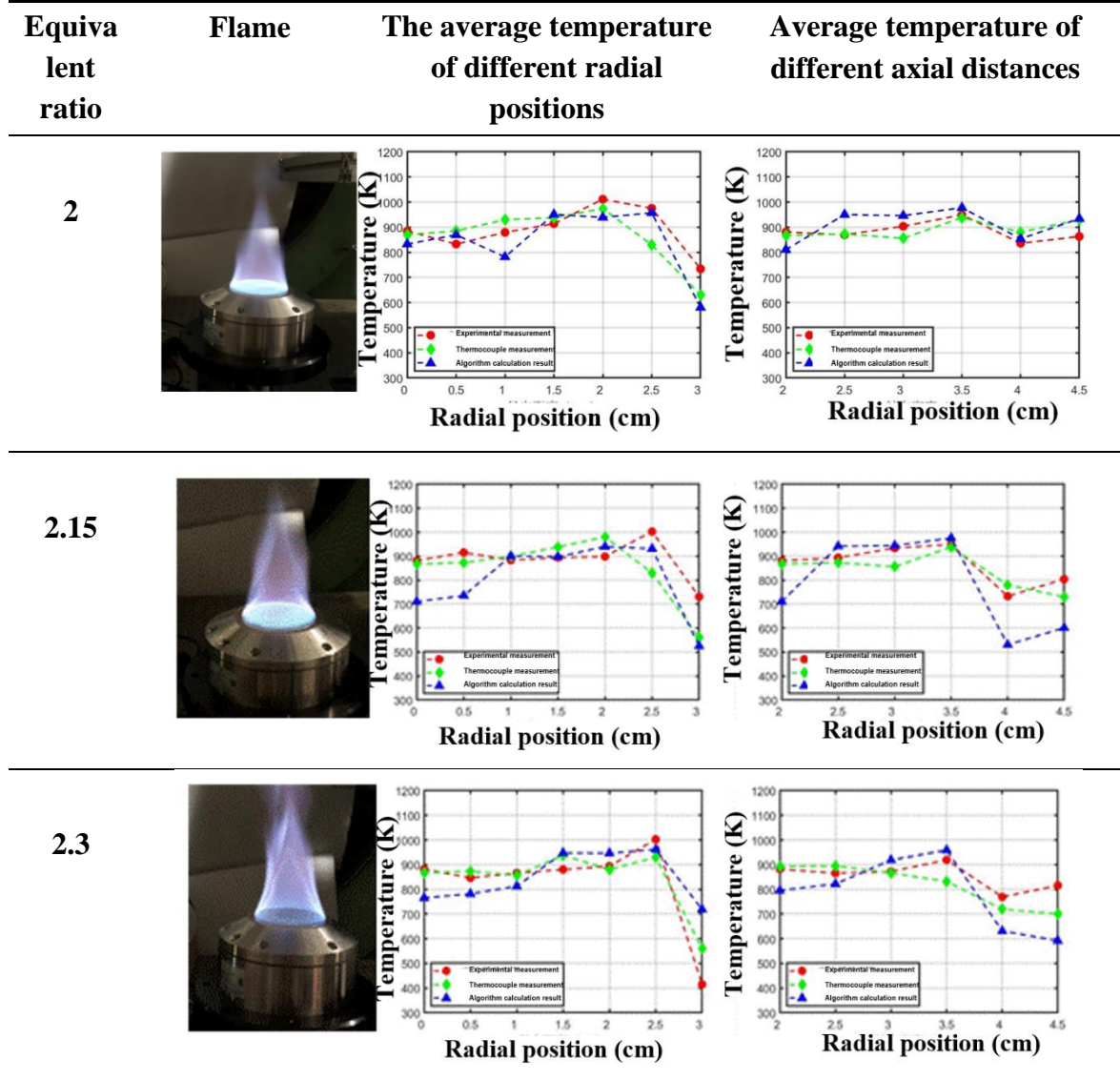


Figure 4.9 - Absorption spectrum fitting of water vapor on the spectral band with the central wavenumber of 7185 cm⁻¹ and 7444 cm⁻¹ (a) Absorption spectrum fitting of water vapor on the spectral band with the central wavenumber of 7185 cm⁻¹ (b) Absorption spectrum fitting of water vapor on the spectral band with the central wavenumber of 7444 cm⁻¹

(2) Calculation results of average temperature and concentration of water vapor on a single laser path in the combustion field

In order to verify the accuracy of the two-line ratio method, the temperature in different working conditions was measured by thermocouples in the experiment. When the equivalence ratio is 2, 2.15 and 2.3, and the axial height is 2cm, the average temperature change on the laser path is shown in Figure 40. It can be seen that when the equivalence ratio is 2, in the range of the radial distance from 0 to 1.5 cm, the flame temperature has a small change and basically shows a flat trend. In the range of radial distance from 1.5cm to 2cm, the temperature has a slow rising trend, and the flame temperature has a sharp and large drop in the range of radial distance from 2.5 cm to 3 cm. The measurement result of thermocouple is smaller than that of TDLAS, which may be related to the upper limit of the hot spot measurement used in the experiment. When the equivalent ratios are set to 2.15 and 2.3, the average flame temperature basically shows a constant first and then slowly increases in the range of radical distance from 0 to 2.5 cm. In the range of radial distance from 2.5 cm to 2 cm, the flame temperature decreases sharply. And as the equivalence ratio gradually increases, the stability of flame combustion gradually becomes worse. The outside of the flame is affected by airflow and incomplete combustion. And as the axial height and radial distance of the flame increase, the range of flame temperature changes gradually becomes larger. In the range of axial height of 2 cm to 4.5 cm, the average temperature along the flame centerline is relatively flat when the equivalence ratio is 2, and there is a tendency to decrease in the range of 3.5 cm to 4.5 cm. When the equivalence ratio gradually increases to 2.15 and 2.3, the flame temperature line rises steadily to 3.5 cm, and then a downward trend appears along the axial distance of the flame center. This may be due to the gradual decrease in the ratio of methane and air premixed combustion under oxygen-lean combustion conditions. At the same time the diffuse combustion of methane resulting in the increased instability of methane combustion, fluctuations in the average temperature and a decrease in the temperature at the top of the flame. During the experiment, the equivalence ratios were set to 2, 2.15, and 2.3 respectively, and the average temperature of the laser path at different axial heights and different axial distances of the flame was measured. Combining the neural network algorithm and using the absorption spectra of water vapor to directly calculate the average temperature on the laser path. Combining the neural network algorithm, the average temperature on the laser path is directly calculated by the absorbance of water vapor. The calculated results is compared with the temperature results obtained by the direct absorption method. Although there is a certain deviation between the two at some positions, the temperature change trends at different axial heights and radial distances calculated by the algorithm proposed in this work have good consistency within the error tolerance with the temperature results obtained by direct absorption calculations and thermocouple measurement results.

Table 4.1-Average temperature measurement result of single optical path



From the above results, the calculation result of the average temperature on the laser path by the neural network has a relatively large error compared with the experimental measurement result. The error at some positions can even reach 100°C. But for the experimental conditions with equivalence ratios of 2, 2.15, and 2.3, the temperature results predicted by the neural network algorithm and the experimental measurement results have a good consistent trend in the different axial heights of the flame. Under the working condition of the equivalent ratio of 2, the temperature basically increases gradually with the increase of the measuring height. When the equivalent ratio increases to 2.15 and 2.3, the temperature first slowly increases with the height and then has a downward trend. At the measuring heights of 2cm above the burner, the prediction results obtained by the neural network-based algorithm and experiment can show that the flame temperature first slowly rises to a radial position near 2.5cm and then drops rapidly to the edge of the flame. This can also reflect that in the case

of oxygen-lean combustion, the part of the flame produced by the combustion of the mixed fuel of methane and air is a diffusion flame. The temperature of the Mckenna burner is characterized by a stable distribution and then a rapid decrease after increasing at the boundary of the inner and outer flames.

On the basis of obtaining the average temperature, the absorption spectra in the spectral band with the center wavenumber of 7185 cm^{-1} can be selected to calculate the average concentration of water vapor on the measuring laser path. The result is shown in Figure4.10. The instability of flame combustion increases and the change in the distribution of water vapor increases as the equivalence ratio gradually increases. In order to use the absorption spectra of water vapor to calculate the concentration of water vapor while calculating the concentration of methane on the same path, for the absorption spectra of water vapor obtained by experimental measurement, on the one hand, the trained neural network object is used to directly solve the average concentration of methane on the laser path. On the other hand, the average temperature on the path is calculated according to the two-line method. Taking the calculated temperature as a known parameter, and further solving the average concentration of methane based on the methane absorption spectrum measured by the experiment, it is used as a control for the calculation result of the algorithm. The specific calculation results will be introduced in detail in section 4.2.

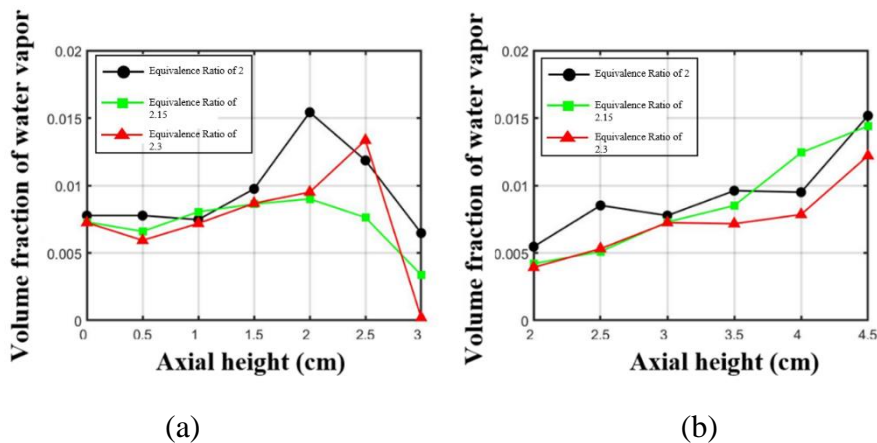


Figure4.10 -Average concentration of water vapor under different working conditions

(a) Average concentration of water vapor at different radial distances (b) Average concentration of water vapor at different axial heights

4.2 Measurement experiment and result analysis of the average concentration of methane on a single laser path in the combustion field

4.2.1 Measurement experiment of average methane concentration

In order to verify the accuracy of the algorithm's prediction results, the average concentration of methane on the same path is calculated based on the methane absorption signal on the spectral band with a central wavenumber of 5938 cm^{-1} after obtaining the average temperature on the path. In the experimental measurement process, perform baseline fitting and Voigt line fitting on the absorption signal of methane is performed firstly. The fitting processes are shown in Figure 4.11. Then the integrated absorbance of methane at the center wave number and the average concentration of methane are calculated. The variation trend of the average methane concentration in the radial distance is consistent with the concentration results obtained by direct absorption calculations.

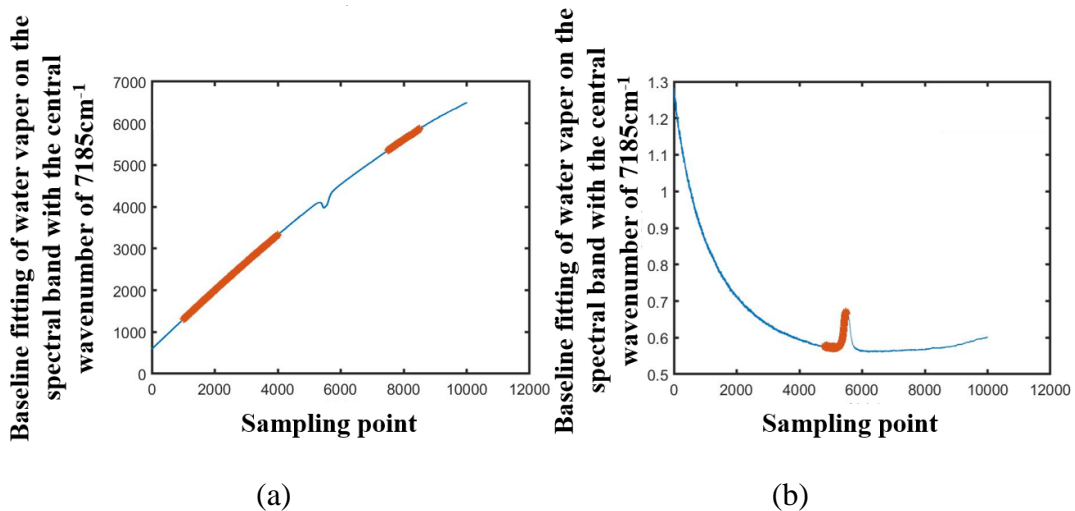


Figure 4.11-Methane transmitted light intensity signal and linear fitting Baseline fitting on the spectral band with a central wavenumber of 5938 cm^{-1} (b) Fitting the absorption spectrum on the spectral band with a central wavenumber of 5938 cm^{-1}

Based on the experimental measurement of the absorption spectrum of water vapor, the neural network-based multi-component concentration prediction algorithm proposed in this work is used to predict the average concentration of methane on the path of different heights in the axial direction of the flame and different distances in the radial direction. Under the working conditions where the flow rates of methane and air are 2.23 L/min and 10.6 L/min , and the height range along the flame axis from 2 cm to 4.5 cm , the path through the center of the flame is calculated according to the direct absorption method. The result of the average concentration is shown in the figure below. In the range of the flame radial distance from 0 cm to 3 cm and the axial measurement height is 2 cm , the experimental measurement results of the average concentration of methane are shown in the figure below. It can be seen that as the axial height increases, the average concentration of methane increases. This may be

because the excess unburned complete methane has a small mole fraction and is gradually concentrated on the flame under the influence of the mixed premixed gas flow, which completely burns at the bottom of the flame to produce a large amount of carbon dioxide and water vapor. On the radial path with a height of 2 cm, as the laser path is farther and farther from the flame center area, the average concentration of methane gradually decreases. During the combustion process, the presence of protective gas makes the flame concentrate on the furnace surface without being affected by the influences of the surrounding airflow.

4.2.2 Comparative analysis of the prediction results of the average methane concentration algorithm and the experimental measurement results

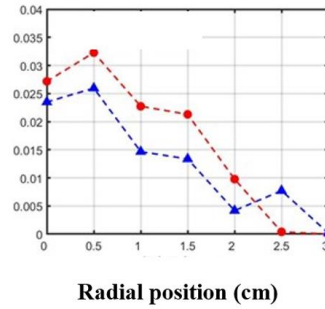
The average concentration of methane calculated by the direct coefficient method and the calculation results based on the prediction results of the neural network proposed in this thesis at different positions are shown in Figure 43. The flow rates of methane and air are set to 2.23 L/min and 10.6 L/min to achieve the condition setting of equivalence ratio of 2. The flow rates of methane and air are set to 2.4 L/min and 10.6 L/min and 2.56 L/min and 10.6 L/min to achieve the condition setting of equivalence ratio of 2.15 and 2.3. The methane concentration at different positions along the axial height and radial distance of the flame is shown in Table 4.2.

Table 4.2-Measurement results of the average concentration of methane on a single optical path

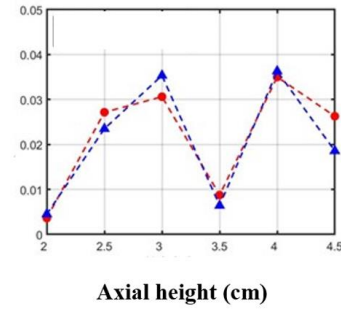
Equivalent ratio	The average concentration of methane of different radial positions	Average concentration of methane of different axial distances
2		

2.15

The average concentration of methane at different radial positions when the equivalence ratio is 2.15

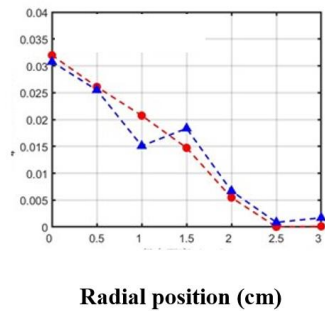


The average concentration of methane at different axial heights when the equivalence ratio is 2.15

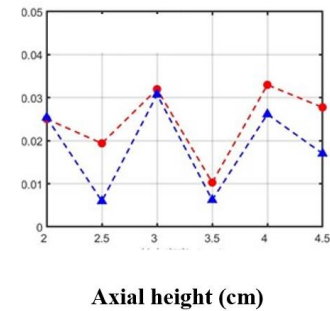


2.3

The average concentration of methane at different radial positions when the equivalence ratio is 2.3



The average concentration of methane at different axial heights when the equivalence ratio is 2.3



From the above results, the calculation result of the average concentration of methane on the laser path based on the neural network algorithm has a relatively large relative error compared with the experimental measurement result, and it can even reach 10% in some locations. But for the experimental conditions with equivalence ratios of 2, 2.15, and 2.3, the results of the average concentration of methane predicted by the neural network algorithm and the experimental measurement results have an obvious and consistent trend at different axial heights from the bottom to the top of the flame. Under the condition of equivalence ratio of 2, the average concentration of methane basically decreases with the increase in height. At the measuring height of 2 cm, the prediction results of the neural network-based algorithm and experimental data show that the temperature firstly slowly rises to a radial position near 2.5 cm and then drops rapidly to the edge of the flame. It shows that in the case of oxygen-lean combustion, the excess methane mainly accumulates around the furnace surface near the gas outlet. With the progress of combustion and the turbulent influence of the airflow, the completely combusted methane gradually diffuses to the top of the flame. The average concentration gradually decreases with the increase of the flame axial height, and gradually decreases to zero with the increase of the measured radial distance.

4.3 Measurement experiment and result analysis of two-dimensional temperature distribution in combustion field

The two-dimensional temperature distribution of the stable flame produced by the Mckenna burner is measured by the multi-view sensor system. The time-division multiplexing method

is used to cover the central wave numbers of water vapor at 7444.36 cm^{-1} and 7185.6 cm^{-1} in one scanning period. Absorption spectra on two bands. In the experiment, the scanning frequency of each DFB laser is 20K Hz, and it takes 0.2 s to complete the scanning of the two spectral bands. The TDLAS five-angle tomography sensor system has 12 photodiodes evenly distributed on each side. The fan-shaped laser beam emitted by the light source at each vertex of the pentagon covers the 24 detectors with the farthest distance, and can obtain all the projection data of 120 different paths. In the process of reconstructing the two-dimensional distribution of temperature based on the neural network algorithm, the integrated absorbance of water vapor on the two wavebands with the central wavenumber of 7444.36 cm^{-1} and 7185.6 cm^{-1} on 120 laser paths arranged in sequence to directly calculate the temperature values on the grids of the area to be measured. Thereby, the temperature distribution result in the two-dimensional area to be measured is obtained.

In the experiment, the air flow rate is set to 16.5 L/min and 22.5 L/min and the methane flow rate is set to 1.7 L/min to ensure the equivalent ratio of methane to air is 0.98 and 0.8. The nitrogen shielding gas flow is set to 22.5 L/min to reduce the influence of the surrounding airflow on the flame. Adjusting the height of the sensor to of 3 cm above the furnace surface of the burner, and measuring the absorption spectra of water vapor in the combustion field on the laser path passing through the section. After sequentially obtaining the transmitted light intensity signals on 120 channels, the integrated absorbance is obtained through the fitting of the Voigt linear function. The two-dimensional distribution of temperature on the cross section is reconstructed using the neural network-based algorithm, and the results are as follows. In the area where the burner is located, the highest temperature reaches $2000\text{ }^{\circ}\text{C}$, and the high temperature area is approximately circular. At the same time, the traditional Landweber algorithm is used to reconstruct the temperature of the temperature section with a height of 3 cm on the flame surface. In the same ROI of the entire sensor, the reconstructed temperature field is shown in the figure below. In the area to be tested, the highest temperature of the high temperature area reconstructed by the Landweber algorithm is up to $2500\text{ }^{\circ}\text{C}$, and there is slightly different from the calculation result of the neural network algorithm. This may be due to the errors in the simulation of turbulent combustion and the deviation of the chemical reaction mechanism that characterizes the chemical reaction kinetics in the simulation of Mckenna methane and air premixed flame in the process of numerical simulation of combustion. At the same time, in the process of experimental measurement, some random and systematic errors in the measurement were also introduced by the equipment and hardware facilities.

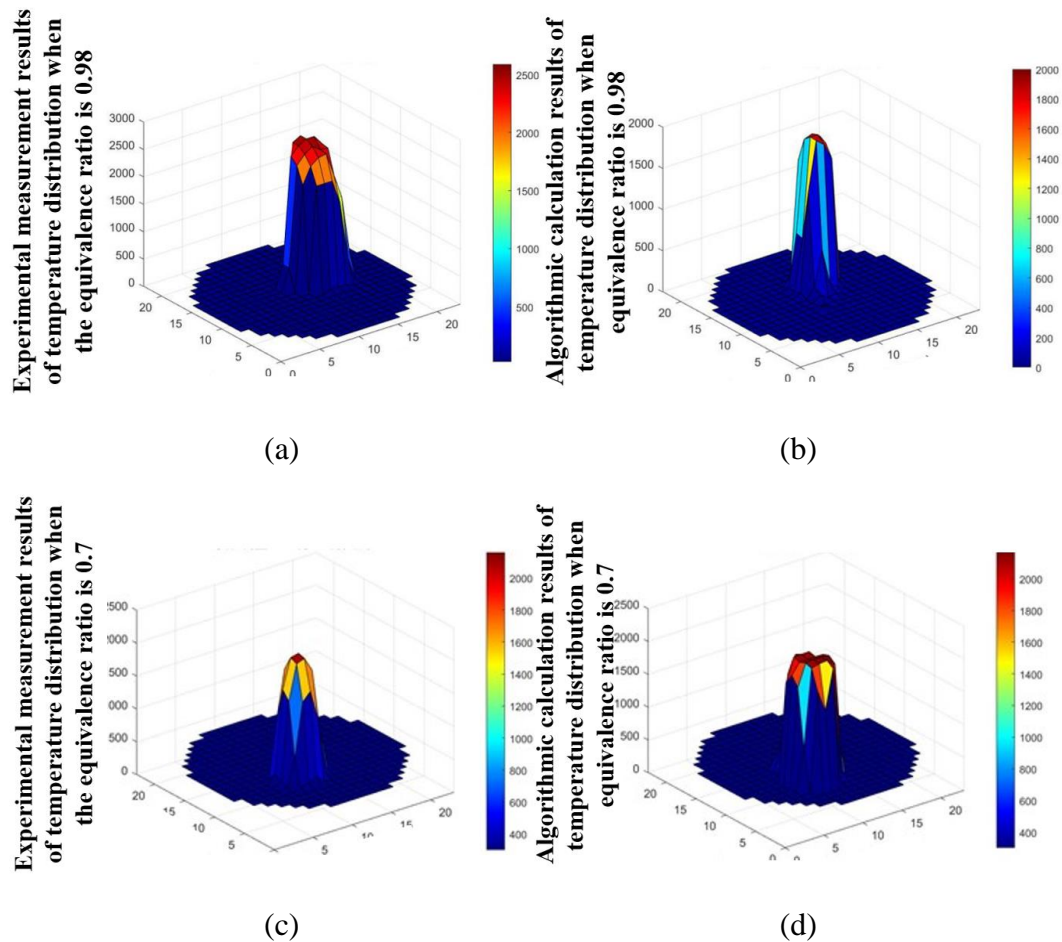


Figure 4.12-Algorithm reconstruction and experimental measurement results of two-dimensional distribution of temperature (a) Experimental measurement results of temperature distribution when the equivalence ratio is 0.98 (b) Algorithmic calculation results of temperature distribution when equivalence ratio is 0.98 (c) Experimental measurement results of temperature distribution when the equivalence ratio is 0.7 (d) Algorithmic calculation results of temperature distribution when equivalence ratio is 0.7

4.4 Summary of this chapter

In this chapter, we mainly introduce the experimental system and result analysis for the water vapor absorption spectrum in the flame gas and the average concentration measurement of methane on a single optical path. The experimental system mainly includes three parts: the laser control part, the photoelectric detection and signal acquisition system, and the subsequent data processing algorithm. When measuring the concentration of methane in the combustion field of McKenna burner, a DFB laser with a center wavenumber of 5939.3cm^{-1} is selected to measure the absorption spectra of methane, and two DFB lasers with center wavenumber of 7185cm^{-1} and 7444cm^{-1} are selected to measure the absorption spectra of water vapor and calculate the average temperature on the laser path. In the experiment, three lasers were controlled sequentially emit lasers at different times to obtain the absorption spectra data of water vapor and methane at different wavelength bands simultaneously. In

order to verify the accuracy of the temperature measurement results of the laser absorption spectroscopy technology, the B-type thermocouple was used in the experiment to measure the temperature at different positions of the flame under different working conditions at a single point. The results show that the calculated results of TDLAS are consistent with the measured values of the thermocouple in trend.

In the process of algorithm verification, the absorption spectra of water vapor in the two spectral bands obtained by measurement are used as the input parameters of the algorithm. The average concentration of methane on the laser path is directly calculated by the direct absorption method in the experiment, and compared with the results calculated by direct absorption method in the experiment. In the experiment, the equivalence ratio is set to 2, 2.15 and 2.3. The average temperature on the path of the flame axial height in the range of 2cm to 4.5cm under different working conditions, as well as the average temperature of the the axial height of 2cm and the radial distance of 0 to 3cm are measured. The average concentration of methane calculated by the neural network-based prediction algorithm proposed in this work and the experimental measurement results have consistent changes in different flame axial and radial positions. The relative error between the calculation of the average methane concentration and the solution of the traditional direct absorption method is within 5%. Under different working conditions, the temperature and concentration tend to decrease gradually as the height rises. At the measuring height of 2 cm, the average temperature and the concentration of methane in the combustion field almost maintain constants in the range of 0 to 1.5 cm and exhibit a flat distribution. In the radial distance of 1.5 to 2.5 cm, the average temperature and concentration of methane increase slowly. In the range of 2.5 cm to 3 cm, the temperature and concentration of methane of the flame drop sharply to room temperature and zero, respectively near the edge of the flame. Using the integral absorbance of water vapor at multiple angles, the relative error of the temperature reconstruction to be measured is within 10%. In the region of interest of the sensor, the algorithm reconstruction result is consistent with the temperature distribution calculated by the traditional method in position, size and trend.

Chapter 5

Summary And Outlook

Combustion reaction is the most direct and effective way of fuel energy conversion. The combustion of coal, oil, natural gas and other fuels affects all aspects of industrial production and life. The combustion reaction of fuel involves thousands of complex physical and chemical changes. The measurement of gas component concentration and gas temperature during the combustion process is not only conducive to real-time monitoring and control of the combustion process, ensuring safe production, but also for optimization Combustion chamber design, improving combustion efficiency, and reducing pollutant emissions also have important research significance. TDLAS is widely used in the measurement of combustion parameters, and its development trend has gradually transitioned from single-point measurement of a single component and a small number of parameters to the detection of trace gases and simultaneous measurement of multiple components and multi-parameters and multi-dimensional distribution reconstruction. However, multi-parameter measurement still faces problems such as complex measurement system, low content of some components, weak absorption, difficulty in obtaining absorption spectrum signals, and overlapping absorption spectra of multiple components. Based on this research status, this work combines the two tools of CFD combustion simulation and neural network algorithm to study the multi-component concentration measurement method based on TDLAS with few absorption lines. The specific research content and conclusions include the following aspects.

(1) First, the basic theory involved in the combustion reaction is briefly described, with emphasis on the theoretical basis for using the absorption spectra information of water vapor to solve the remaining components to be measured during the combustion process. Secondly, the basic principle of temperature measurement by laser absorption spectroscopy is introduced in detail, with emphasis on two important parameters of linear function and line intensity, and the influencing factors of different linear functions are introduced in detail. Then the direct absorption method and wavelength modulation method of laser absorption spectroscopy are introduced. The characteristics of these two measurement methods and their applicable occasions are compared and discussed.

(2) In the experiment, the Mckenna combustion furnace was selected as the simulation and measurement object. The CFD method was used to simulate the premixed combustion flame with the equivalent ratio of methane and air of 1.6 to 2.5 in the case of oxygen-lean combustion. According to the principle of selection of spectral lines for temperature measurement by the two-line ratio method, selecting spectral bands suitable for water vapor and methane absorption spectrometry by querying the HITRAN database. Combining the existing single-channel and multi-angle detector models in the laboratory to simulate the combustion field Forward simulation of water vapor absorption spectrum. Secondly, the neural network-based TDLAS multi-component concentration prediction algorithm with few lines is proposed, and the feasibility and accuracy of the algorithm are verified by CFD simulation data. In the single optical path measurement system, the proposed algorithm predicts the relative error of the average concentration of methane on different working conditions and different paths within 0.5%. For the prediction results of the two-dimensional distribution of methane, the flat flame burner is located at five angles. The relative error of the reconstruction of methane concentration distribution in the area to be measured at any position of the sensor is also within 10%.

(3) In the experiment of measuring the absorption spectra of water vapor and methane in the flame, the spectral bands with the center wave numbers of 7185cm^{-1} and 7444cm^{-1} were selected to measure the absorption spectra of water vapor and then calculate the average temperature on the laser path. The spectral band with the center wavenumber of 5938cm^{-1} was selected to measure the average concentration of methane. In the experiment, the combustion conditions were set to 2, 2.15, and 2.3, and the change of the flame temperature and concentration of methane within the range of 0.5 cm to 5 cm in the axial height of the flame, and the axial height of 2 cm and the radial distance in the range of 0 to 3 cm were measured. In order to explore the accuracy of TDLAS temperature measurement, a B-type thermocouple was used in the experiment to perform a single-point measurement in the flame field. The trend of the flame zone of the flat flame combustion furnace under different working conditions was analyzed and discussed, the feasibility and accuracy of the algorithm proposed in this work were verified.

In order to verify the feasibility of the algorithm, this work uses a one-dimensional concentration and temperature measurement system to obtain the average information of temperature and concentration on the laser path for the experimentally measured Mckenna symmetric flame, which verifies the feasibility of the algorithm proposed in this work.

On this basis, the following prospects are made for the next work:

(1) The next step is to use the existing five-angle two-dimensional sensor in the laboratory to complete the measurement of the flame zone temperature and the two-dimensional distribution of methane concentration combined with the tomography algorithm. Then verifying the feasibility of the neural network-based two-dimensional temperature and methane concentration prediction algorithm. Next, the numerical simulation of the three-dimensional flame field is carried out. Based on the construction of the three-dimensional

sensor in the laboratory, the simulation and experimental verification of the three-dimensional multi-component concentration prediction algorithm are completed.

(2) Then the in-depth research on the detailed mechanism of methane combustion will be conducted. The basic theoretical support of combustion reaction and the relationship between the concentration of combustion product water vapor and reactant methane in the process of methane combustion under different equivalent ratios will be further study. The relationship between methane and water vapor will be constructed numerically, and the feasibility of the algorithm proposed in this work can be verified theoretically.

(3) When measuring the absorption signal of methane with a DFB laser near the center frequency of 1684nm, two absorption peaks connected together can be obtained. During the experiment, the absorption intensity signal is used to linearly fit the absorption spectrum. One of the absorption peaks is selected for fitting, and then we should further study the influence of simultaneous multi-peak fitting on the concentration measurement results.

(4) Based on the measurement of the Mckenna combustion furnace as the object, the measurement and analysis of a variety of combustion objects are carried out, and the universality of the neural network-based multi-parameter prediction algorithm proposed in this work under different combustion conditions is analyzed.

Acronyms

TDLAS Tunable Diode Laser Absorption Spectroscopy

DFB Distributed Feedback

TDM Time-division Multiplexing

FDM Frequency Division Multiplexing

SNR signal-to-noise ratio (SNR)

CFD computational fluid dynamics

DAS Direct absorption technology

WMS Wavelength modulation technology

BPNN Backpropagation Neural Network

HAB Height Above Burner

USB Universal Serial Bus

CPCI Compact Peripheral Component Interconnect

FPGA Field Programmable Gate Array

PD Photo Diode Detector

ADC Analog-to-Digital Converter

ROI Region of Interest

Appendix

Near-Field Prediction in Complex Environment Based on Phaseless Scanned Fields and Machine Learning

The project seen in the appendix was completed in cooperation with Haoxuan ZHENG (ID:10672492).

Research purposes:

Modern electronic devices need to meet the requirements of multi-function, miniaturization, high speed and low power consumption to the greatest extent to carry the rapid development of the Internet of Things, mobile phones and wearable devices, automotive electronics, driverless, mobile medical and other industries. As electronic devices become more and more complex and products become more and more miniaturized, their own electromagnetic compatibility problems will become more and more serious. The increase in the operating frequency of electronic devices means that the conversion time between high and low levels is shortened. From a frequency domain perspective, it means that the signal has more abundant high frequency components. The size of the electronic device is comparable to the wavelength of high frequency component, and the "antenna effect" of the device will become obvious. The device will be more likely to generate electromagnetic radiation or receive external electromagnetic noise. On the other hand, the improvement of integration means that the device spacing becomes smaller, the distance between the interference source and the victim is shortened, which makes some EMI problems that are not considered in the traditional design become more prominent.

How to quantify complex radiation interference sources efficiently and accurately has always been the core part of the entire radiation interference problem. Quantitative electromagnetic interference is very important in the research and design process of electronic products. For complex interference source devices, constructing an equivalent radiation source model is an effective solution.

In the flat and near-field scanning, the positioning error of the scanning surface height has a great influence on the phase measurement result. The classical reconstruction source algorithm is more sensitive to the phase error than to the amplitude error. Therefore, although the phase information is very important for the interference source reconstruction algorithm, considering the difficulty of actually scanning the phase, we are more inclined to use the interference source reconstruction algorithm based on amplitude scanning. Due to the influence of measurement noise, the equivalent radiation source reconstruction algorithm based on near-field amplitude and phase scanning belongs to the solution of linear ill-conditioned problems. Once the phase information is lost, the problem will become nonlinear, which brings a lot of difficulty to the equivalent source solution. In the traditional equivalent dipole calculation method, the dipole moment information of the dipole is directly calculated by solving the related equations. Artificial neural network is developing rapidly recently, and it provides a new solution to the problem of equivalent radiation source reconstruction. In theory, no matter how complicated the mapping relationship between finite input and output is, as long as there are enough hidden layers and neurons in the artificial neural network structure and enough training data, the artificial neural network can always learn between input and output. Due to the influence of the surrounding complex environment, the matrix-vector multiplication relationship between the equivalent dipole and the free space Green's function has been inaccurate. This article uses an artificial neural network to generate a new mapping relationship to replace the original inaccurate functional relationship, and uses the near-field data obtained from near-field scanning to train ANN. However, the information of the equivalent dipole source obtained by neural network training is implicit. It is expressed by the weight, bias and activation function of the neural network, and the parameter information of each dipole cannot be refined.

Research method:

Specifically, the free space Green's formula of magnetic dipoles with known information such as position coordinates, polarization direction, amplitude, and phase are used as the input of the neural network (the position and number of magnetic dipoles are determined in advance, and what needs to be calculated is the magnetic Dipole moment). The position and the number of dipoles are all predetermined according to DUT and the scanned field pattern. The unknowns are the moments of every dipole in the array. Corresponding to the magnetic field data obtained from the near-field scanning as the output parameter of the neural network, the weight between each node of the artificial neural network after training is the unknown dipole moment. After the ANN training, if we want to obtain the magnetic field at any field point r in other new regions, we can directly input the transformation function matrix corresponding to the new region.

The magnetic dipole is defined in the form of a small loop current as $M = SI = \frac{I_0^m l}{j\omega\mu_0}$, S represents the area of the small loop, and the electric dipole is defined as $P = I_0 l$, the edge in the spherical coordinate system. The magnetic field radiation formula of the magnetic dipole M_z in the z -axis direction can be expressed as:

$$\begin{cases} H_r = M_z \frac{k_0^3}{2\pi} \left(\frac{j}{(k_0 r)^2} + \frac{1}{(k_0 r)^3} \right) \cos\theta e^{-jk_0 r} \\ H_\theta = -M_z \frac{k_0^3}{4\pi} \left(\frac{1}{(k_0 r)} + \frac{-j}{(k_0 r)^2} - \frac{1}{(k_0 r)^3} \right) \sin\theta e^{-jk_0 r} \\ H_\phi = 0 \end{cases}$$

Where $k_0 = \frac{2\pi}{\lambda} = \omega\sqrt{\varepsilon_0\mu_0}$ is the free space wave number; ε_0 and μ_0 are the permittivity and permeability of free space respectively; r represents the distance between the source point and the observation point, in rectangular coordinates. The magnetic field radiation formula of the magnetic dipole under the system can be expressed as:

$$\begin{pmatrix} H_x \\ H_y \\ H_z \end{pmatrix} = \frac{K_0}{4\pi} \begin{pmatrix} -\frac{y^2 + z^2}{r^2} g_1(r) + g_1(r) & \frac{xy}{r^2} g_1(r) & \frac{xz}{r^2} g_1(r) \\ \frac{xy}{r^2} g_1(r) & -\frac{x^2 + z^2}{r^2} g_1(r) + g_1(r) & \frac{yz}{r^2} g_1(r) \\ \frac{xz}{r^2} g_1(r) & \frac{yz}{r^2} g_1(r) & -\frac{x^2 + y^2}{r^2} g_1(r) + g_1(r) \end{pmatrix} \begin{pmatrix} K_0 M_x \\ K_0 M_y \\ K_0 M_z \end{pmatrix}$$

$g_1(r) = \left(\frac{3}{(k_0 r)^2} + \frac{j3}{k_0 r} - 1\right) \frac{e^{-jk_0 r}}{r}$, $g_2(r) = \left(\frac{2}{(k_0 r)^2} + \frac{j2}{k_0 r}\right) \frac{e^{-jk_0 r}}{r}$. Assuming that the ground plane is at $z=0$ and the equivalent source position of the dipole $z=h$, then $r = \sqrt{x^2 + y^2 + (z - h)^2}$. The above formula can be simply written:

$$Ax = H$$

For the plane approach scan, the tangential magnetic near field on the scan plane can be expressed as the sum of the fields of all equivalent dipoles, which can still be expressed by the above formula. Where $[a_{ij}] (i = 1, 2, \dots, N; j = 1, 2, \dots, M)$ is an $N \times M$ variable matrix between the equivalent dipole and the scanning magnetic field, which is determined by the free dipole. The spatial Green's function is determined. A distance variable $r = |r_i - r_j|$ is implied in this parameter. The former represents the coordinates of the scanning electron, and the latter represents the coordinates of the dipole. N represents the number of samples for the long point, and M represents the number of dipoles. Each row of the conversion matrix 3 is used as the input of a training sample, and the magnetic field data corresponding to the right side of the equal sign is used as the corresponding output. The conversion matrix d has N rows, so we have N training samples. The column vector $X_{M \times 1} = [X_x, X_y]^t$ contains the unknown dipole moments of the x and y polarization directions. The two tangential magnetic field components of the scanning plane are contained in the column vector $H_{1 \times N} = [H_x, H_y]^t$. In the training process, the least square error between the ANN output field and the actual scan length is used to control the end of the neural network training.

The calculation errors of the algorithm:

Simulation

(1) Determination of the equivalent source of electromagnetic interference between finite planes.

Two finite square metal planes, each having a side length of 400 mm, are located at $z = 0$ and $z = 100$ mm, respectively. The EMI source is an x -directional dipole located at $(0, 0, \text{ and } 50 \text{ mm})$. The origin is at the center of the lower metal plane. The source locations r_j are defined on an $8 \text{ mm} \times 8 \text{ mm}$ plane, which is 1 mm above the dipole and with the z -axis as its center. The lower scanning plane is kept as 400×400 mm. The side length of the upper scanning plane is $400 \times \delta$ mm, with $\delta \leq 100\%$.

The prediction result of the magnetic field along the z-axis: When $\delta = 100\%$, the upper and lower scanning planes have the same size. We compare the proposed ANN method with the method of cubic spline interpolation, **when $\delta = 100\%$** , when ANN is used to predict $|H_x|$, $|H_y|$, and $|H|$ on the validation plane, the error is much smaller than that of the interpolation method, especially for the fields on validation planes **above or below two scanning planes**. And it is worth noting that the near-field reconstruction error of the interpolation method is 0 when the height of the verification plane is 65mm and 80mm respectively; **when $\delta = 80\%$** , for this smaller upper scanning plane, the error of the interpolation method increases greatly, while the error of the ANN method is still smaller. Similar to $\delta = 100\%$, the interpolation method shows a large error when the observation point of the predicted field is far away from the scanning points. The interpolation method exhibits a large error in the top-left region of the validation plane, which is just below the “missing region” (nonscanning region) of the upper scanning plane. However, the ANN can accurately predict the field magnitude even in this nonscanning region. On the other hand, since the input of the ANN is Green’s function, which contains the source and observation positions, it can predict the complex field decreasing ratio from lower to upper planes, especially when there are constructive and deconstructive interference effects in the reactive near-field region. The ANN method can predict more accurately than the interpolation method. The field decreasing ratio from lower to upper scanning planes is complex since all these fields are in the reactive near-field region of the radiator. It is hard for the interpolation method to predict such a complex field decreasing ratio.

The prediction result of the magnetic field on the validation plane: The error of the predicted magnetic field magnitude on the validation plane of $z = 73$ mm is compared between the ANN and interpolation methods for different values of δ . When δ changes from 100% to 80%, it can be found that the change of ANN error with the size of the upper scanning plane is smoother than that of the interpolation method error. This validates the robustness of the ANN method.

(2) Determination of the electromagnetic interference equivalent source of two infinite plane supports and prediction of the magnetic field. In the second example, two finite metal planes in the first example are replaced by two infinite planes so that there are no edge diffractions. The size of the lower scanning plane is still $400 \text{ mm} \times 400 \text{ mm}$. The upper left corners of both scanning planes are aligned. Again, the ratio between the side

lengths of the upper scanning plane and the lower scanning plane is defined as δ . Moreover, the source location r_j is an important parameter for the ANN. It will change Green's functions inputted to the ANN. The effect of r_j on the predicted field is also analyzed in this example. And three cases of r_j are studied.

The prediction result of the magnetic field along the z-axis: For $\delta = 80\%$, when the number and location of r_j changed, ANN can still create a correct mapping relationship between the observation point and the predicted field, and the magnetic field prediction errors of the three cases are not much different, which shows the robustness of the ANN method. However, the interpolation method cannot accurately predict the field outside the scanning regions.

The prediction result of the magnetic field on the validation plane: the change in the ANN error curve is very flat and is not affected by the incomplete scanning plane. However, the interpolation error is increasing with the reduced δ .

(3) the uniform space between two infinite metal planes is replaced by lossy four-layered materials

The prediction result of the magnetic field along the z-axis: For $\delta = 80\%$, The ANN method has better prediction results on the scanning surface and outside the scanning surface than interpolation method.

The prediction result of the magnetic field on the validation plane: the proposed ANN method is still accurate for the multilayered and lossy materials.

(4) Equivalent electric dipole and neural network electric field prediction

the equivalent electric dipoles + ANN are used to predict the electric near-field from the real source, the uniform space between two infinite metal planes is replaced by lossy four-layered materials.

The prediction result of the magnetic field along the z-axis: For $\delta = 80\%$, the ANN method can be used for both electric and magnetic fields' predictions. Even the electric field error predicted at the same validation plane is smaller than the magnetic field error.

The prediction result of the magnetic field on the validation plane: In the multi-layer lossy medium, the ANN method can also accurately predict the electric field distribution on the validation plane.

Experiment (To further validate the ANN method using experimental data)

The EMI source is an unintended antenna, so a self-made patch antenna is used as the EMI source. the patch antenna is placed between two aluminum plates. A near-field scanning system is used to measure the magnetic field of the patch antenna. Two scanning planes are used for the ANN training. One is 140 mm away from the right metal plate, which is fixed as 100×100 mm. Another scanning plane 150 mm away from the right metal plate.

The prediction result of the magnetic field along the z-axis: When the center of two scanning planes aligned and the ratio between the side lengths of the two scanning planes is **0.8**, and then we reduce the size of the scanning plane, the error of the interpolation method is already large than 10%, and the DE method has a larger error than the ANN method.

The prediction result of the magnetic field on the validation plane: the interpolation method has a large error in predicting the fields on the four corners of the validation plane 145 mm away from the right metal plate. By adjusting δ , we find that ANN method is not sensitive to the size of the scanning planes.

Conclusion:

ANN reconstruction method. It can be seen as an extension of the traditional dipole method. In a complex environment where the radiation source has reflection or diffraction, the traditional dipole method is no longer accurate. We use ANN's powerful mapping capabilities to re-establish a revised equivalent source model. This new equivalent source model is represented by parameters such as ANN's weight, bias and activation function. Simulations and experimental examples show that the ANN method is more accurate than traditional methods when estimating the magnetic field distribution in other regions. This provides a new way of thinking for EMI source reconstruction and helps us analyze complex electromagnetic compatibility issues.

The source reconstruction method fully considers the multiple reflection or diffraction effects between the radiated electromagnetic wave and the surrounding environment,

effectively predicts the near-field distribution of the interference source in a complex environment, and is an analysis of the electromagnetic interference problem of the next generation of high-speed and high-density electronic equipment and diagnosis provides a new technical guarantee. The simulation and experimental examples verify the ability of the ANN algorithm to use the near-field distribution on the two scanning surfaces to calculate the near-field distribution between the scanning surfaces and outside the scanning surfaces. By adjusting the parameters and results of the neural network, the ANN method will make it possible to accurately invert the electromagnetic interference source.

In addition, we also continued to read the research paper of related authors and related fields[1-3], and found that compared with traditional methods, the use of artificial neural networks to solve electromagnetic compatibility problems such as near-field prediction is indeed better. Its accuracy and robustness can be widely applied to similar problems.

References:

[1]Wen, Jun, et al. "Development of Artificial Neural Network for Field Prediction of Unknown EM Source." 2020 IEEE International Conference on Computational Electromagnetics (ICCEM). IEEE, 2020.

[2]Shu, Yu-Fei, et al. "An equivalent dipole model hybrid with artificial neural network for electromagnetic interference prediction." IEEE Transactions on Microwave Theory and Techniques 67.5 (2019): 1790-1797.

[3]Shu, Yu-Fei, et al. "An iterative approach for EMI source reconstruction based on phaseless and single-plane near-field scanning." IEEE Transactions on Electromagnetic Compatibility 60.4 (2017): 937-944.

Bibliography

- [1] Jianxiong Mao. Clean combustion of coal. Science Press,1998.
- [2] Xinhua Chen. China should pay attention to low emission economy. Outlook, 2009, 000(046): 64–64.
- [3] Ge Qi, Zhaocang Han, Bowei Guo. Energy, combustion and environment. Metallurgical Industry Press, 1991.
- [4] Xin Zheng, Jing Yang, Lisheng Wang. Forecast of carbon dioxide emissions from fossil energy combustion in China. Hydropower and Energy Science, 2009, 27(5): 224–227.
- [5] Kui L U, Guixia Z, Xiangke W. A brief review of graphene-based material synthesis and its application in environmental pollution management. Chinese Science Bulletin, 2012(11): 1223–1234.
- [6] Chighine A, Tsekenis S A, Fisher E, et al. TDLAS using FPGA-based lock-in detection for multi-channel Chemical Species Tomography. 2015 IEEE Sensors. 2016:1-4.
- [7] Ping Zhang. Combustion Diagnostics. Ordnance Industry Press, 1988.
- [8] Ting Lin. Summary of Measuring Method of Temperature Field of Combustion Flame. China High-tech. 2009(8): 31–32.
- [9] Qi Jin, Daolong Chen. Thermocouple Temperature Measurement. Atomic Energy Press.1980.
- [10] Fei Li. Application of near-infrared absorption spectroscopy in the study of supercombustion. Graduate University of Chinese Academy of Sciences,2009.
- [11] Allen M G. Diode Laser Absorption Sensors for Gas-Dynamic and Combustion Flows. Measurement and Technology, 1998, 9(4): 545–562.
- [12] Zhou X, Jeffries J B, Hanson R K. Development of a fast temperature sensor for combustion gases using a single tunable diode laser. Applied Physics B, 2005, 81(5): 711–722.
- [13] Fei Li, Xilong Yu, Xin Lin, et al. Tomographic imaging technology based on TDLAS: TDLAT. Chinese Journal of Theoretical and Applied Mechani.2014, 46(1): 54–59.
- [14] Longjiang Zheng, Peng Li, Ruifeng Qin, et al. Research status and development trend of optical technology for gas concentration detection. Progress in Laser and Optoelectronics.2008(08): 24–32.
- [15] Hanson R K, Kuntz P A, Kruger C H. High-resolution spectroscopy of combustion gases using a tunable ir diode laser. Applied Optics, 1977, 16(8):2045.
- [16] Arroyo M P, Hanson R K. Absorption measurements of water-vapor concentration, temperature, and line-shape parameters using a tunable InGaAsP diode laser. Applied Optics, 1993, 32(30): 6104–16.
- [17] Baer D S, Nagali V, Furlong E R. Scanned- and fixed-wavelength absorption diagnostics for combustion measurements using multiplexed diode lasers. Aiaa Journal, 1996, 34(3): 489–493.
- [18] Mihalcea R M, Baer D S, Hanson R K. Diode-Laser Sensor for Measurements of CO, CO₂ and CH₄ in Combustion Flows. Applied Optics, 1997, 36(33): 8745–8752.
- [19] Zhou X, Liu X, Jeffries J B, et al. Development of a sensor for temperature and water concentration

- in combustion gases using a single tunable diode laser. *Measurement Science & Technology*, 2003, 14(8): 1459.
- [20] Iseki T. A portable remote methane detector using an InGaAsP DFB laser. *Environmental Geology*, 2004, 46(8): 1064–1069.
- [21] Farooq A, Jeffries J B, Hanson R K. CO₂ concentration and temperature sensor for combustion gases using diode-laser absorption near 2.7 μm . *Applied Physics B*, 2008, 90(3–4): 619–628.
- [22] Webber M E, Wang J, Sanders S T, et al. In situ combustion measurements of CO, CO₂, H₂O and temperature using diode laser absorption sensors. *Proceedings of the Combustion Institute*, 2000, 28(1): 407–413.
- [23] Jtc L, Jeffries J B, Hanson R K. Wavelength modulation absorption spectroscopy with 2f detection using multiplexed diode lasers for rapid temperature measurements in gaseous flows. *Applied physics. B, Lasers and optics*, 2004, 78(3–4): 503–511.
- [24] Liu C, Xu L, Member S, et al. Reconstruction of Axisymmetric Temperature and Gas Concentration Distributions by Combining Fan-Beam TDLAS With Onion-Peeling Deconvolution. *IEEE Transactions on Instrumentation & Measurement*, 2014, 63(12): 3067–3075.
- [25] Cai W, Kaminski C F. Multiplexed absorption tomography with calibration-free wavelength modulation spectroscopy. *Applied Physics Letters*, 2014, 104(15): 4788–4797.
- [26] Cai W, Kaminski C F. Tomographic absorption spectroscopy for the study of gas dynamics and reactive flows. *Progress in Energy & Combustion Science*, 2017, 59(MAR.): 1–31.
- [27] Jianqing H, Hecong L, Jinghang D, et al. Reconstruction for limited-data nonlinear tomographic absorption spectroscopy via deep learning. *Journal of Quantitative Spectroscopy and Radiative Transfer*, 2018, 218: 187-193.
- [28] Lifang Zhang. Study on Measurement of Low Concentration Multi-component Gas and Two-dimensional Temperature Concentration Distribution by Laser Absorption Spectroscopy. Zhejiang University, 2017.
- [29] Wu Q, Wang F, Li M, et al. Simultaneous In-Situ Measurement of Soot Volume Fraction, H₂O Concentration, and Temperature in an Ethylene/Air Premixed Flame Using Tunable Diode Laser Absorption Spectroscopy. *Combustion Science and Technology*, 2017, 189(7–9): 1571–1590.
- [30] Liu F, Thomson K A, Smallwood G J. Soot temperature and volume fraction retrieval from spectrally resolved flame emission measurement in laminar axisymmetric coflow diffusion flames: Effect of self-absorption. *Combustion & Flame*, 2013, 160(9): 1693–1705.
- [31] Yuquan Peng, Ruifeng Kan, Zhenyu Xu, et al. Temperature Measurement of Methane/Air Premixed Flame Furnace Based on Tunable Semiconductor Laser Absorption Spectroscopy. *Journal of Atmospheric and Environmental Optics*, 2019, 014(003): 228–234.
- [32] Sepman A, gren Y, Qu Z, et al. Real-time in situ multi-parameter TDLAS sensing in the reactor core of an entrained-flow biomass gasifier. *Proceedings of the Combustion Institute*, 2016, 36(3):4541-4548.
- [33] Sentko M M, Schulz S, Stelzner B, et al. Determination of temperature and water-concentration in fuel-rich oxy-fuel methane flames applying TDLAS. *Combustion & Flame*, 2020, 214: 336–345.
- [34] Kormann R, Fischer H, Gurk C, et al. Application of a multi-laser tunable diode laser absorption spectrometer for atmospheric trace gas measurements at sub-ppbv levels. *Spectrochimica Acta Part*

- A Molecular & Biomolecular Spectroscopy, 2002, 58(11): 2489–2498.
- [35] Lou N Z, Ning L I. In Situ Temperature Measurement by Absorption Spectroscopy Based on Time Division Multiplexing Technology. *Spectroscopy & Spectral Analysis*, 2012, 32(5): 1329–1333.
- [36] Liu J T C, Jeffries J B, Hanson R K. Large-modulation-depth 2f spectroscopy with diode lasers for rapid temperature and species measurements in gases with blended and broadened spectra. *Appl Opt*, 2004, 43(35): 6500–6509.
- [37] Huang A, Cao Z, Zhao W, et al. Frequency Division Multiplexing and Main Peak Scanning WMS Method for TDLAS Tomography in Flame Monitoring. *IEEE Transactions on Instrumentation & Measurement*, 2020, 69(11):9087-9096.
- [38] Dong L, Tittel F K, Li C, et al. Compact TDLAS based sensor design using interband cascade lasers for mid-IR trace gas sensing. *Optics Express*, 2016, 24(6): A528-A535.
- [39] Mücke R, Werle P W, Prettl W. Comparison of time and frequency multiplexing techniques in multicomponent FM spectroscopy[J]. *Proceedings of SPIE - The International Society for Optical Engineering*, 1991, 1433, 461-467.
- [40] Zhang Z R, Xia H, Dong F Z, et al. Simultaneous and on-line detection of multiple gas concentration with tunable diode laser absorption spectroscopy. *Guangxue Jingmi Gongcheng/Optics and Precision Engineering*, 2013, 21(11):2771-2777.
- [41] Zhang Z R, Dong F Z, Tu G J, et al. Selection of digital filtering techniques in trace gas concentration detection with a tunable diode laser absorption spectroscopy. *Journal of Optoelectronics.Laser*, 2010, 21(11): 1672–1676.
- [42] Kreuzer L B. Ultralow Gas Concentration Infrared Absorption Spectroscopy. *Journal of Applied Physics*, 1971, 42(7): 2934–2943.
- [43] Whiting E E. An empirical approximation to the Voigt profile. *Journal of Quantitative Spectroscopy and Radiative Transfer*, 1968, 8(6): 1379–1384.
- [44] Olivero J J, Longbothum R L. Empirical fits to the Voigt line width: A brief review. *Journal of Quantitative Spectroscopy & Radiative Transfer*, 1977, 17(2): 233–236.
- [45] Mayinger F, Feldmann O. *Optical Measurements: Techniques and Applications*. *Optical Measurements Techniques & Applications*, 2002, 2003(2): 461–468.
- [46] Weibiao Fu, Jingbin Wei. *Fundamentals of Combustion Physics*. China Machine Press. 1984.
- [47] Bilger R W, Strner S H, Kee R J. On reduced mechanisms for methane-air combustion in nonpremixed flames. *Combustion and Flame*, 1990, 80(2): 135–149.
- [48] Peters N, Kee R J. The computation of stretched laminar methane-air diffusion flames using a reduced four-step mechanism. *Combustion & Flame*, 1987, 68(1): 17–29.
- [49] Migliorini F, Iuliis S D, F. Cignoli G Z. How «flat» is the rich premixed flame produced by your McKenna burner. *Combustion & Flame*, 2008, 153(3): 384–393.
- [50] Alibert C, Vicet A, Rouillard Y, et al. GaSb-based lasers for gas monitoring[A]. *Lasers & Electro-optics Society, Leos the Meeting of the IEEE*, 2018, 4(6) :621-637.
- [51] B, Buchholz, A, et al. Rapid, optical measurement of the atmospheric pressure on a fast research aircraft using open-path TDLAS[J]. *Atmospheric Measurement Techniques*, 2014., 7, 4775-4813.
- [52] Sozykin A V. An overview of methods for deep learning in neural networks. Ural Federal University, 2017, 28-59.

- [53] Shu X W , Zhang Y J , Kan R F , et al. An Investigation of Temperature Compensation of HCL Gas Online Monitoring Based on TDLAS Method. *Guang Pu Xue Yu Guang Pu Fen XI*, 2010, 30(5):1352-1356.
- [54] Jin W, Li Z J, Wei L S, et al. The improvements of BP neural network learning algorithm[A]. *International Conference on Signal Processing*. 2002, 3:1647-1649.
- [55] Goodfellow I, Bengio Y, Courville A. *Deep Learning*. The MIT Press, 2016.
- [56] Zhihua Zhou. *Machine Learning*. Machine Learning. Tsinghua University Press,2016.